

From bioremediation to biomedicine: the potential of magnetic nanoparticles in a glance

Doctoral Thesis presented by

Soraia Fernandes



for the degree of

Doctor of Sciences by the University of Regensburg

and

Doctor in Chemistry and Materials Sciences and Technologies by the University
of Genoa

Regensburg 2016

This work was supervised by: Prof. Dr. Oliver Reiser

Graduation request filled on: 11. April 2016

Oral examination done on: 11. May 2016

Examination Committee: Chairman: PD. Dr. Sabine Amslinger (University of Regensburg)

1. Examiner / supervisor: Prof. Dr. Oliver Reiser (University of Regensburg)
2. Examiner / tutor: Dr. Teresa Pellegrino (Istituto Italiano di Tecnologia)
3. Examiner: Prof. Dr. Joachim Wegener (University of Regensburg)
4. Examiner: Prof. Dr. Sara Baldassari (University of Genova)
5. Examiner: Prof. Dr. Renata Riva (University of Genova)

This thesis was performed inside the **EU-ITN network Mag(net)icFun** in accordance to the cotutelle agreement made between the University of Regensburg and the University of Genova for a joint PhD degree programme.

The experimental work from February 2013 to March 2015 was done under the supervision of Prof. Dr. Oliver Reiser, at the *Institut für Organische Chemie der Universität Regensburg*. From April 2015 to January 2016 the experimental work was carried out at the *Nanomaterials for Biomedicine* group of the *Istituto Italiano di Tecnologia* (IIT, Genoa) under the supervision of Dr. Teresa Pellegrino.

Table of contents

Thesis abstract	1
Zusammenfassung	3
Riassunto	5
Introduction: The potential of magnetic nanoparticles in a glance	7
1. Magnetic nanoparticles: motivation and overview	7
2. Basics of magnetism for nanoparticles	8
3. Surface coating effects on the magnetic properties of nanoparticles	11
4. Applications of magnetic nanoparticles	14
4.1. Nanoparticles as potential tools in industry	14
4.1.1.(Bio)Catalytic applications	15
4.1.2.Environmental applications	17
4.2. Biomedical applications	19
5. Conclusion and future perspectives	23
6. References	23
Chapter 1: Towards the stabilization of redly recyclable carbon-coated cobalt nanoparticles via surface functionalization	29
1.1.Introduction	30
1.2.Silica-coated magnetic Co/C nanoparticles	32
1.3.Polymer-coated magnetic Co/C nanoparticles	37
1.4.Combined silica-polymer coating on magnetic Co/C nanoparticles	45
1.5.Outlook and applications	47
1.6.Experimental section	49
1.7.References	57

Chapter 2: Reversible magnetic mercury extraction from water	61
2.1 Introduction	62
2.2 Results and discussion	63
2.3 Conclusion	73
2.4 Experimental section	73
2.5 References	78
Chapter 3: Development and characterization of suitable antifouling magnetic nanocarriers for RNAi therapy	81
3.1 Introduction	82
3.2 Results and discussion	86
3.2.1 Preparation and characterization of cationic MnFe ₂ O ₄ cubes by polymer coating and further functionalization of the polymeric shell	86
3.2.2 Preparation and characterization of cationic IONCs by copolymerization of DMAEMA and OEGMEMA	90
3.2.3 Stability of the synthesized cationic nanocubes in FBS and physiological medium - interaction with serum proteins	91
3.2.4 Cell cytotoxicity and intracellular iron concentration estimation	94
3.2.5 siRNA loading onto cationic nanocubes	97
3.2.6 GFP knockdown on HeLa cells using siRNA-NCs conjugates	101
3.3 Conclusions	104
3.4 Experimental section	105
3.5 References	111
List of abbreviations	114
Curriculum Vitae	116
Acknowledgments	119

Thesis abstract

The present dissertation presents the doctoral work developed during the last three years at the University of Regensburg (UR, Regensburg, Germany) and at the Istituto Italiano di Tecnologia (IIT, Genoa, Italy). The work was focused on the development and characterization of magnetic nanoparticles for different applications, resulting in three main projects discussed herein. The first two were developed at the UR whereas the last one was carried out at the IIT.

The first chapter deals with the stabilization of carbon-coated cobalt nanoparticles (Co/C, **1**) via surface engineering in order to avoid their agglomeration in solution. In particular, different types of surface coatings were applied to these magnetic nanoparticles (MNPs) and their effect on the magnetic properties of the materials was evaluated. Silica-coated Co/C nanoparticles (Co/C@SiO₂, **4**) were successfully synthesized, revealing good dispersion in different solvents without compromising the high saturation magnetization (M_s) which was kept at 140 emu·g⁻¹. The inorganic silica shell offers a new platform for further functionalization or incorporation of other molecules of interest e.g. metal catalysts. In addition, polyethyleneimine (PEI) grafting on the nanoparticles by direct polymerization of aziridine resulted in remarkably stable nanoparticles (Co/C-PEI, **14**), which showed good dispersibility in aqueous solutions even over months of incubation. This fact is attributed to the significantly high loading of hydrophilic amino moieties which results in a M_s decrease to 39 emu·g⁻¹. Nevertheless, the MNPs could still be collected by an external magnet in less than a minute. The combined functionalization of Co/C nanoparticles using silica and PEI was also studied. For this purpose, a silica shell was first developed and then functionalized by aziridine polymerization. The resulting MNPs (Co/C@SiO₂-PEI, **15**) showed quite good dispersion in both aqueous and organic solutions, revealing a M_s comparable to Co/C-PEI. Having a multitude of surface coatings available enlarges the number potential applications given to Co/C nanoparticles e.g. as supports for catalysis, reagent scavengers and for bioremediation. Moreover, the surprising stability of Co/C-PEI dispersions in water might as well allow their application on the biotechnological field.

In the second chapter the ability of Co/C nanoparticles to remove mercury ions from water was explored. Especially Co/C-PEI (**14**) nanoparticles showed high efficiency to remove Hg²⁺ from contaminated water samples, even in the presence of competitive metal ions. These magnetic nanoparticles showed a high extraction capacity compared to other reported studies, accompanied by a selectivity character that favors the extraction of toxic mercury over other ions at relevant concentrations. Furthermore, no cobalt leaching could be observed and when using Co/C-PEI and the MNPs could be reused for at least six consecutive cycles. Moreover, the scale up of the process was effectively proved by the decontamination ($\leq 2 \mu\text{g}\cdot\text{L}^{-1} \text{Hg}^{2+}$) of 20 L of drinking water, containing $30 \mu\text{g}\cdot\text{L}^{-1} \text{Hg}^{2+}$, using just 60 mg of Co/C-PEI nanoparticles.

The third chapter discusses the preparation of suitable magnetic nanocarriers for small interfering RNA (siRNA) delivery into living cells. It elucidates the functionalization of water soluble magnetic nanocubes (NCs) with positively charged polymers for subsequent electrostatic binding of negatively-charged siRNA molecules and their *in vitro* evaluation. Two different approaches were followed. The first one consisted on the development of a polymer coating on the surface of manganese ferrite nanocubes, followed by functionalization of the polymeric shell with N’N’-dimethylethylenediamine (DMEDA) and polyethylene glycol molecules (cationic Mn-cubes, **22**). In the second approach iron oxide nanocubes were functionalized with a copolymer of (dimethylamino)ethyl methacrylate (DMAEMA) and oligoethylene glycol methyl ether methacrylate (OEGMEMA) (cationic IONCs, **25**), which revealed even higher surface charge. Therefore, cationic IONCs (**25**) proved to be more efficient for loading, protecting and delivering the siRNA while limiting the non-specific protein adsorption. In addition, no cytotoxic effects were detected, proving the potential of this nanocarrier for their usage in biological systems. At the latest stage of this work the efficiency of the nanocarriers to deliver the siRNA into living cells was assessed by measuring the expression of green fluorescent protein (GFP). Cationic IONCs (**25**) carrying anti-GFP siRNA revealed promising results, with an overall 40% downregulation on protein expression.

Zusammenfassung

Die vorliegende Dissertation gibt die Arbeit der letzten drei Jahre an der Universität Regensburg (UR, Regensburg, Deutschland) und dem Istituto Italiano di Tecnologia (IIT, Genua, Italien) wieder. Die Arbeit war fokussiert auf die Entwicklung und Charakterisierung von magnetischen Nanopartikeln für verschiedene Anwendungen, von denen die drei Hauptprojekte hier diskutiert werden. Die ersten Zwei wurden hierbei an der UR entwickelt, das Dritte am IIT durchgeführt.

Das erste Kapitel behandelt die Stabilisierung von kohlenstoffbeschichteten Cobaltnanopartikeln (Co/C, **1**) in Lösung mittels Oberflächenmodifikation. Hierfür wurden verschiedene Oberflächenbeschichtungen auf den magnetischen Nanopartikeln (MNPs) angebracht und deren Effekt auf die magnetischen Eigenschaften der Materialien untersucht. Silicabeschichtete Cobaltnanopartikel (Co/C@SiO₂, **4**) wurden erfolgreich synthetisiert und zeigten gute Dispergierbarkeit in verschiedenen Lösungsmitteln, ohne dabei die hohe Sättigungsmagnetisierung (M_s) der unbehandelten Nanopartikeln zu beeinträchtigen, welche bei 140 emu·g⁻¹ liegt. Die anorganische Silicahülle stellt eine neue Plattform für die weitere Funktionalisierung oder die Einlagerung anderer interessanter Moleküle wie z.B. Metallkatalysatoren dar. Auch durch das Anbringen von Polyethylenimin (PEI) durch direkte Polymerisation von Aziridin konnten erstaunlich stabile Nanopartikel (Co/C@PEI, **14**) gewonnen werden, welche selbst über Monate hinweg gute Dispergierbarkeit in wässrigen Lösungen zeigten. Dies wird der hohen Beladung an hydrophilen Aminogruppen zugeschrieben, welche zu einer Reduktion der M_s auf 39 emu·g⁻¹ führen. Nichtsdestotrotz können die MNPs mit Hilfe eines externen Magneten in weniger als einer Minute gesammelt werden. Die kombinierte Funktionalisierung der Co/C-Nanopartikel mit Silica und PEI wurde ebenfalls untersucht. Hierfür wurde zuerst eine Silicahülle aufgetragen und anschließend durch Aziridinpolymerisation funktionalisiert. Die so erhaltenen MNPs (Co/C@SiO₂-PEI, **15**) zeigten verhältnismäßig gute Dispergierbarkeit in sowohl wässrigen als auch organischen Lösungen, mit einer M_s vergleichbar zu Co/C-PEI. Die Verfügbarkeit einer Vielzahl an Oberflächenbeschichtungen vergrößert die Anzahl an potentiellen Anwendungsmöglichkeiten für Co/C-Nanopartikel, z.B.: als Trägermaterial für Katalysatoren, als Scavenger für Reagenzien oder zur Bioremediation. Hinzu kommt auch die erstaunliche Stabilität von Co/C-PEI-Dispersionen in Wasser, welche zusätzlich deren Einsatz in der Biotechnologie erlauben könnte.

Im zweiten Kapitel wird die Fähigkeit von Co/C-Nanopartikeln Quecksilberionen aus Wasser zu extrahieren näher untersucht. Insbesondere Co/C-PEI-Nanopartikel (**14**) zeigten hohe Effizienz in der Entfernung von Hg²⁺ aus kontaminierten Wasserproben, selbst in Anwesenheit von anderen, kompetitiven Metallionen. Diese magnetischen Nanopartikel zeigten eine hohe Extraktionskapazität im Vergleich zu anderen veröffentlichten Studien, in Verbindung mit einer Selektivität für die Extraktion von toxischem Quecksilber in relevanten Konzentrationen gegenüber anderen Ionen. Hinzu kommt, dass kein Cobaltleaching festgestellt werden konnte wenn Co/C-PEI-Nanopartikel verwendet

wurden und die MNPs in mindestens sechs aufeinanderfolgenden Zyklen wiederverwendet werden konnten. Zudem konnte die Hochskalierung des Prozesses erfolgreich am Beispiel der Dekontamination ($\leq 2 \mu\text{g}\cdot\text{L}^{-1} \text{Hg}^{2+}$) von 20 L Trinkwasser, welches $30 \mu\text{g}\cdot\text{L}^{-1} \text{Hg}^{2+}$ enthielt, gezeigt werden, wobei nur 60 mg Co/C-PEI-Nanopartikel verwendet wurden.

Das dritte Kapitel behandelt die Darstellung von geeigneten Nanocarriern als Transporter für „small interfering RNA“ (siRNA) in lebende Zellen. Es erläutert die Funktionalisierung von wasserlöslichen, magnetischen Nanocubes (NCs) mit positiv geladenen Polymeren für die elektrostatische Bindung der negativ geladenen siRNA-Moleküle, sowie deren Evaluation *in vitro*. Dabei wurden zwei verschiedene Herangehensweisen untersucht. Die Erste beinhaltete die Entwicklung einer Polymerbeschichtung der Manganferrit-Nanocubes, gefolgt von der Funktionalisierung der Polymerhülle mit N'-N'-Dimethylethylendiamin (DMAEMA) und Polyethylenglykolmolekülen (cationic Mn-cubes, **22**). Der zweite Ansatz war die Verwendung eines Copolymers aus 2-Dimethylaminoethylmethacrylat (DMAEMA) und Oligoethylenglykolmethylether (OEGMEMA) auf den Eisenoxid-Nanocubes (cationic IONCs, **25**), welche eine höhere Oberflächenladung zeigten. In der Tat zeigten (cationic IONCs, **25**) eine höhere Effizienz bei Beladung, Abschirmung und Transport, bei gleichzeitiger Verringerung von nicht-spezifischer Proteinadsorption. Zudem konnten keine zytotoxischen Eigenschaften nachgewiesen werden, was für das Potential dieses Nanotransporter und ihre zukünftige Anwendung in biologischen Systemen spricht. Auf der letzten Stufe dieser Arbeit wurde die Effektivität der Nanomaterialien als Transporter für siRNA in lebende Zellen durch Expression von grün fluoreszierendem Protein (GFP) untersucht. Mit anti-GFP siRNA-beladenes IONCs (**25**) zeigte vielversprechende Resultate, mit einer um 40% verminderten Proteinexpression.

Riassunto

La presente tesi di dottorato espone il lavoro di ricerca svolto durante gli ultimi tre anni presso l'università di Regensburg (UR, Regensburg, Germania) e l'Istituto Italiano di Tecnologia (IIT, Genova, Italia). L'attività scientifica si è focalizzata sullo sviluppo e la caratterizzazione di nanoparticelle magnetiche per differenti applicazioni, attraverso tre progetti principali qui discussi. I primi due progetti sono stati svolti all'università di Regensburg, il terzo presso l'Istituto Italiano di Tecnologia.

Il primo capitolo riporta la stabilizzazione in soluzione di nanoparticelle di cobalto rivestite di carbonio (Co/C, **1**) per mezzo di modificazioni chimico-fisiche della superficie, al fine di evitarne l'agglomerazione. In particolare, diversi tipi di rivestimento sono stati studiati e si è analizzato il loro effetto sulle proprietà magnetiche delle nanoparticelle. Nanoparticelle Co/C rivestite di silicio sono state sintetizzate con successo, dimostrando buona stabilità in diversi solventi ed il mantenimento di un valore di saturazione di magnetizzazione (M_s) pari a 140 emu.g^{-1} . Questo si presta inoltre a successive funzionalizzazioni e all'introduzione di molecole quali catalizzatori metallici. In aggiunta alla sopracitata funzionalizzazione, la sintesi diretta di un rivestimento di polietilenammina, ottenuto tramite polimerizzazione dell'aziridina, ha dimostrato essere in grado di incrementare la stabilità delle nanoparticelle (Co/C-PEI, **14**) in soluzione acquosa fino diversi mesi. Tale fenomeno può essere attribuito al significativo aumento di gruppi idrofilici, dovuti alla presenza delle amine, che tuttavia ~~ne~~ hanno determinato una diminuzione della M_s a 39 emu.g^{-1} . Ciononostante, le MNPs possono ancora essere raccolte in pochi secondi attraverso l'utilizzo di un magnete esterno. È stato inoltre affrontato lo studio dell'uso combinato di questi due materiali di rivestimenti. A tale scopo, un guscio di silicio è stato sintetizzato e successivamente funzionalizzato per mezzo della polimerizzazione dell'aziridina. Le MNPs risultanti (Co/C-@SiO₂-PEI, **15**) hanno mostrato una discreta stabilità sia in fase acquosa sia in fase organica ed una saturazione di magnetizzazione paragonabile a quella riportata per Co/C-PEI. La disponibilità di diversi rivestimenti superficiali per le nanoparticelle di Co/C ne aumenta le possibili applicazioni come supporti per catalizzatori e agenti di rimozione di inquinanti dalle acque. Inoltre, la notevole stabilità in acqua delle nanoparticelle Co/C-PEI ne può altresì permettere l'applicazione in campo biotecnologico.

Nel secondo capitolo è analizzata la capacità delle nanoparticelle di Co/C di rimuovere ioni di mercurio dalle acque. Nanoparticelle Co/C-PEI (**14**) hanno dimostrato un'elevata capacità di rimozione dei ioni Hg^{2+} da campioni di acqua contaminata, anche alla presenza di ioni metallici competitori. La capacità estrattiva e la selettività di tali nanoparticelle si sono rivelate essere molto elevate se paragonata ad altri casi oggetto studiate, favorendo l'estrazione di mercurio rispetto ad altri ioni presenti anche ad elevata concentrazione, fino ad un massimo di sei cicli di estrazione consecutivi. Nondimeno, la possibilità delle scale up del processo di estrazione è stata dimostrata

attraverso la decontaminazione di 20 L di acqua contenente $30 \mu\text{g}\cdot\text{L}^{-1}$ di Hg^{2+} fino a livelli accettabili ($\leq 2 \mu\text{g}\cdot\text{L}^{-1}$), usando solamente 60 mg di nanoparticelle Co/C-PEI.

Infine, il capitolo 3 presenta la preparazione di nanoparticelle magnetiche per il delivery di siRNA (small interfering RNA) nelle cellule. Il capitolo riguarda la funzionalizzazione di nanocubi (NCs) magnetici, solubili in acqua, con un rivestimento polimerico carico positivamente in grado di formare legami elettrostatici con molecole di siRNA che presentano invece carica negativa, e la loro successiva valutazione *in vitro*. Due diversi approcci sono studiati a tal scopo. Il primo consiste nello sviluppo di un guscio polimerico sulla superficie dei nanocubi di ferrite di manganese, seguito dalla sua funzionalizzazione con molecole di N'N'- dimetiletilediamina (DMEDA) e polietilenglicole (cationic Mn-cubes, **22**). Il secondo approccio fa uso invece di nanocubi di ossido di ferro con un copolimero composto di (dimetilamino)etile metacrilato (DMAEMA) e oligoetilene glicole metil etere metacrilato (OEGMEMA) (cationic IONCs, **25**) il quale reca una maggiore carica di superficie rispetto al primo. Infatti, IONCs (**25**) si sono dimostrati più efficienti nel caricare, proteggere e rilasciare il siRNA, limitando inoltre l'adsorbimento aspecifico di proteine che potrebbe diminuire la performance delle nanoparticelle. In aggiunta, nessun effetto citotossico è stato osservato rendendo tali particelle potenziali candidate per applicazioni biologiche. L'ultima parte di questo lavoro tratta l'efficienza di questi nanovettori nel delivery di siRNA all'interno delle cellule attraverso lo studio dell'espressione della green fluorescent protein (GFP). IONCs (**25**) recanti il siRNA anti-GFP hanno prodotto risultati promettenti, con una riduzione dell'espressione della proteina fino al 40%.

Introduction

The potential of magnetic nanoparticles in a glance

1. Magnetic nanoparticles: motivation and overview

Nanotechnology is one of the major research fields in modern science. The concept behind nanoscience started, back in 1959, with the famous statement made by physicist Richard Feynman: “There is plenty of room at the bottom”.¹ Whereas Feynman, known as the “father” of nanoscience, brought out the concept of manipulating materials with atomic precision, the term nanotechnology was first used in 1974 by Norio Taniguchi.² Although modern nanoscience is quite recent, its signs were unconsciously known for centuries. From the Lascaux cave paintings to the windows in the Notre-Dame cathedral, alternate sizes of gold and iron oxide particles created suggestive colors which animated the everyday life of people. Back then, the artists were just not aware of the underlying physicochemical principles which led to that plethora of colors. Nowadays, nanotechnology allows the controlled synthesis and functionalization of materials on the nanometer scale, providing engineers, chemists and physicists, the new “nanotechnologists”, the possibility to work on a molecular or cellular level. Such fundamental control of the materials at the nanoscale, promise a broad and revolutionary technology platform for life sciences and healthcare applications. Indeed, developments in nanoscience have provided the manufacturing of nanomaterials for industry, biomedicine, environmental engineering, safety and security, food, water resources, energy conversion, and many other areas.³

Involved in the development of this current technology, magnetic materials composed of metals such as nickel, cobalt, iron and metal oxides have been on focus of research. They can be found in a variety of devices, e.g. batteries, hard disks and videotapes, and the interest in miniaturizing these materials led to the discovery of magnetic nanoparticles (MNPs) which display different properties from the bulk.⁴ At the present time, the potential of magnetic nanoparticles is well described for applications in catalysis,⁵⁻⁸ biomedicine,⁹⁻¹¹ data storage,¹² and even environmental remediation.^{13,14} Especially in liquid systems they are very interesting as they can, with an appropriate surface chemistry, be homogeneously dispersed, highly reactive and easily separated with the aid of a magnet, due to their high response to a magnetic field.^{15,16}

There are countless methods of synthesizing different kinds of magnetic nanoparticles and their success depends highly on the chemical stability of the resultant materials.^{4,15} Moreover, once industrial applications of nanoparticles cover a broad spectrum of solvent media they need to be dispersible in various liquid phases. For instance, in water bioremediation, the MNPs need to give a stable dispersion in aqueous solutions, but also a magnetic moment high enough to allow their simple and effective recovery by an external magnet, once the purification is completed.¹⁷ Differently, for biomedical applications, they must ensure biocompatibility and colloidal stability at physiological conditions. The stability of the particles in terms of agglomeration and reactivity can be solved by coating their surface.¹⁵ These coatings can be developed from organic species such as surfactants¹⁵ or polymers^{15,18,19} or inorganic material like silica²⁰⁻²² or carbon.^{16,23} In most of the cases, the shell not only stabilizes the particles, but also acts as an anchor or additional surface for further functionalization.

Driven by the remarkable advances on magnetic nanoparticles research, this chapter revises their features and applications, pointing out relevant findings for their potential use in the industrial and biomedical fields.

2. Basics of magnetism for nanoparticles

Magnetic effects are caused by movements of particles that have both mass and electric charges. A spinning electric-charged particle creates a magnetic dipole, known as magneton. In ferromagnetic materials, magnetons are associated in groups.³ The volume of ferromagnetic material in which all magnetons are aligned in the same direction is called magnetic domain, and this distinguishes ferromagnetism from paramagnetism, being the latter one defined as a single domain state. Magnetic domains are separated by domains walls and depend on the size of the particles. Below a certain critical size, it costs more energy to create a domain wall than to support the external magnetostatic energy of the single domain. Therefore, magnetism assumes that the state of lowest energy of ferromagnetic particles has uniform magnetization for smaller particles and non-uniform magnetization for larger ones.^{3,15,24} As shown in Fig. 2, nanoparticles below a critical size are called

single domain, which means that they are uniformly magnetized with all the spins aligned in the same direction; bigger particles instead are multi-domain structured.¹⁵

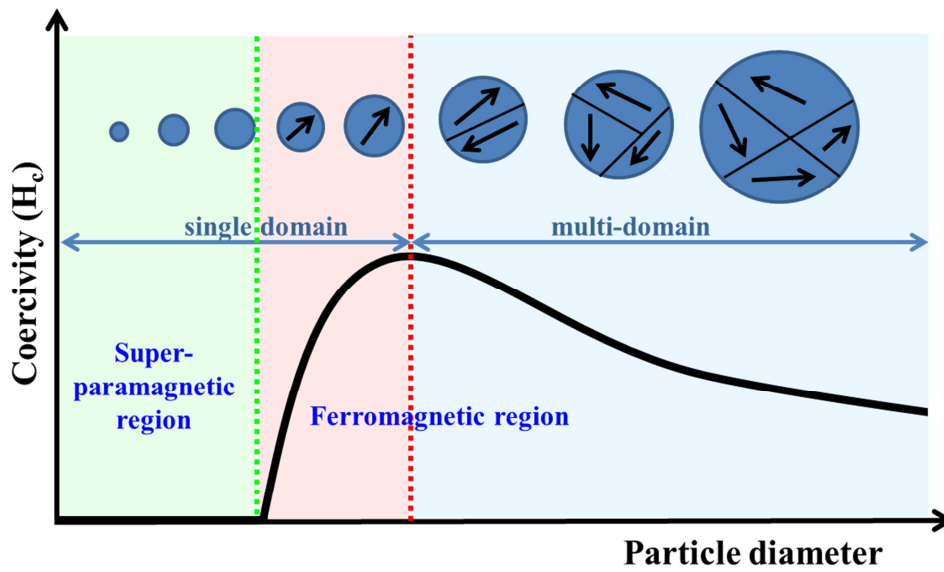


Fig. 1 Schematic illustration of the coercivity-size relations of small particles.

The reaction of ferromagnetic materials to an applied magnetic field is well described by a hysteresis loop which is characterized by coercivity and remanence (Fig. 3B left). After achieving the saturation magnetization (M_s) and removed the magnetic field applied, ferromagnetic materials, instead of retracing their original path, retain some memory known as remanence. To completely reduce the magnetization to zero, a coercive force must be applied. Thus, coercivity measures the resistance of the material to demagnetization, and is usually represented as a hysteresis curve (Fig. 3B).^{15,25}

As shown in Fig. 2, coercivity is strongly size-dependent: it increases to a maximum as the particle size is reduced until the critical value at which the transition from multi-domain to single domain is reached, and then decreases toward zero. For multi-domain particles the inversion of the magnetic moment occurs by the displacement of the magnetic domain walls (Fig. 3A); this process requires small amounts of energy and consequently leads to low coercivity values.^{3,15,25,26} Instead, for single domain particles the direction switching of the magnetic dipole occurs through the overcoming of the anisotropy energy barrier (E_A) which is defined by the following equation:

$$E_A = K_{eff}V$$

where K_{eff} is the effective anisotropy constant of the particles and V is their magnetic volume.²⁷ Therefore, the higher is the volume of single domain nanoparticles and the anisotropy constant, the higher is the value of coercivity.

When the size of the single domain particle is further decreased to another critical value at which thermal energy is high enough to easily overcome the anisotropy barrier, the magnetic moments of the particles become independent from each other and they are spontaneously and continuously reversed

resulting in absence of coercivity (Fig. 3A). This phenomenon is called superparamagnetism, because like paramagnetism is characterized by absence of coercivity, while significant saturation magnetization values are maintained (Fig. 3B right).^{3,15,26}

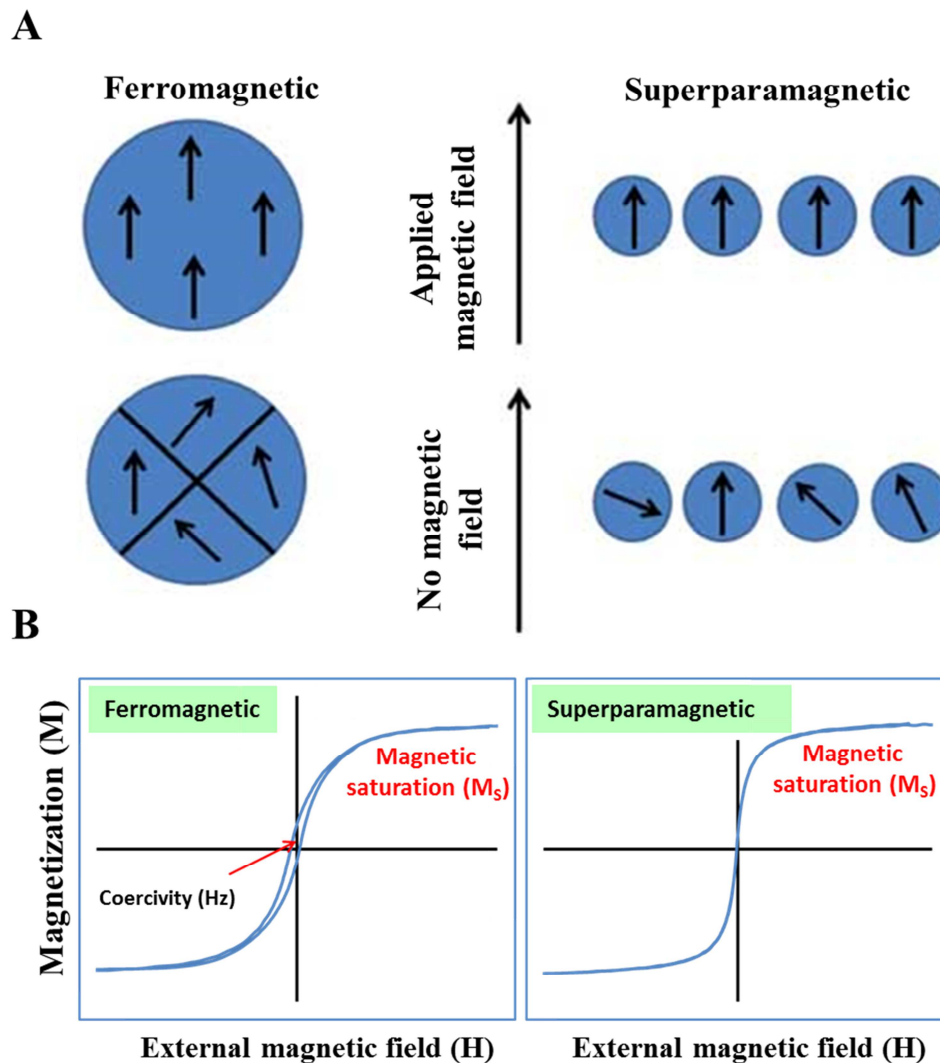


Fig. 2 A) Magnetic moment of ferromagnetic and superparamagnetic nanoparticles. Under a magnetic field the domain walls in ferromagnetic materials are removed and the spins aligned to the direction of the magnetic field, saturating the magnetization. Whereas, superparamagnetic materials which are defined as single domain structures have no domain walls to be removed, but simply the alignment of the magnetic moments to the direction of the field. The domain structure of the magnetic materials has been drawn for simplicity. Reproduced with permission from reference 3. **B)** Typical hysteresis curves obtained for ferromagnetic (left) and superparamagnetic (right) nanoparticles.

The abovementioned properties make superparamagnetic nanoparticles actually magnetic only in the presence of a magnetic field. The magnetic behavior is reverted to nonmagnetic state when the field is removed ensuring a good dispersion of the particles and avoiding the typical aggregation problems from ferromagnetic materials. For that reason, this specific type of nanoparticles is very appealing for biomedical applications.²⁸

For any application, it is usually required a surface coating of the MNPs with some organic ligands or inorganic species to stabilize them and add specific functionalities. The presence of these coatings on the surface modulates the magnetic properties by modifying the anisotropy of the metal atoms allocated on the surface. This usually leads to a decrease in the magnetic moment which is attributed to the presence of a magnetically dead layer on top of the MNPs.^{29,30} Therefore, smooth changes on size and surface coating have an impact on the coercivity and consequently on the magnetic performance of the particles. Hence, MNPs have to be carefully tailored to provide suitable nanomagnets for the diverse applications envisage.

3. Surface coating effects on the magnetic properties of nanoparticles

Despite all the significant developments on the synthesis of magnetic nanoparticles differing in shape, size and composition, their protection and stabilization in solution are crucial requirements for any application. The stability of a magnetic colloidal suspension results from the equilibrium between attractive and repulsive forces. Theoretically, four kinds of forces can contribute to the inter-particle potential in the system: (1) van-der-Waals forces, (2) dipolar forces, (3) steric repulsion and (4) electrostatic attractive forces. Controlling the strength of these forces, by applying different surface coatings, is a key parameter to obtain good dispersibility of the particles.²⁷

However, it is well known that the addition of mass on top of the magnetic nanoparticles modulates the magnetization values, limiting the potential applications of the final material. The Saturation magnetization (M_s) of magnetic particles is defined on a per gram basis ($\text{emu}\cdot\text{g}^{-1}$), thus a non-magnetic shell will necessarily decrease it. This reduction has been mainly associated to the existence of a magnetically dead layer on the particle's surface. Consequently, a commitment between stabilization of the nanoparticles dispersion in solution and preservation of high magnetic moments has to be considered when designing coating methodologies.^{15,28} More specifically, ligands such as polyethylene glycol, dextran and aminosilanes which are often used to improve the suspension of magnetic nanoparticles in liquid phase, modulate their magnetic properties by modifying the anisotropy and reducing surface magnetic moment of the metal atoms located at the surface of the particles.^{29,30}

This modulation in the magnetic properties was recently reported by Borca-Tasciuc *et al.* who demonstrated, in commercial magnetic nanoparticles, that the effect on the magnetic phase varies according to the surface functionalization as well as with the solvent used for the measurement.³¹

The different types of coatings commonly used can be roughly categorized in two groups: organic and inorganic coatings. The first one includes the use of surfactants or polymeric shells, while inorganic coatings comprise silica, carbon or precious metals.¹⁵

In order to better understand the general implications of the surface coating on the magnetic response of nanoparticles silica and polymer coatings will be further discussed here.

Silica coatings have been widely applied in iron oxide nanoparticles to prevent aggregation in the liquid phase and enhance their chemical stability. The inert silica shell inhibits particles agglomeration by two different mechanisms: (1) it shields the magnetic dipole interaction and (2) it improves the coulomb repulsion of the nanoparticles due to its negative charge. It also prevents the direct contact of the magnetic core with other molecules which might compromise their activity, as it e.g. happens for the attachment of dyes which usually leads to luminescence quenching.²⁷ These features are controlled by varying the shell thickness (Fig. 4), which can be achieved by altering the amount of silica precursor, usually tetraethyl orthosilicate (TEOS), or the amount of catalyst during synthesis.³²

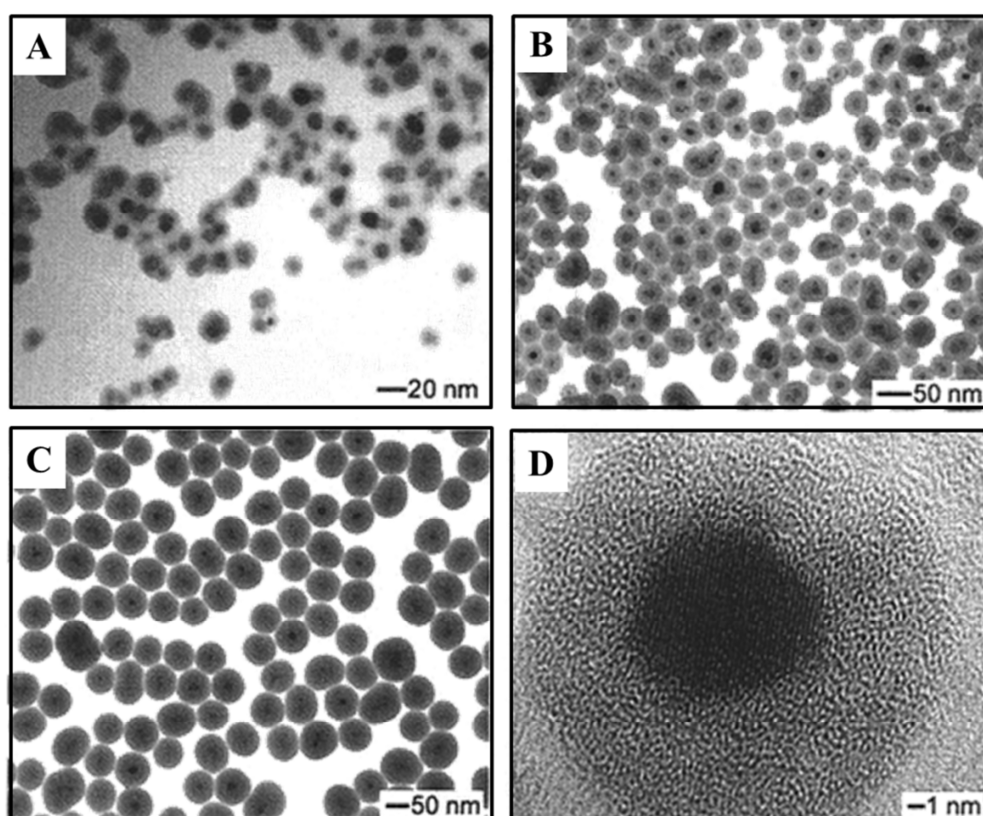


Fig. 3 (A-C) Transmission electron microscopy (TEM) images of iron oxide nanoparticles whose surfaces have been coated with silica shells of various thicknesses. In this case, the thickness of silica coating could be controlled by adjusting the amount of precursor added to the solution: (A) 10, (B) 60, and (C) 1000 mg of TEOS to 20 mL of 2-propanol. (D) A high-resolution transmission electron microscopy (HRTEM) image of the iron oxide nanoparticles whose surface has been uniformly coated with 6 nm of amorphous silica shell. Reproduced with permission from reference 39. Copyright 2002, American Chemical Society.

The preferred method to synthesize silica shells is the Ströber method also known as sol-gel process. This synthesis provides an hydrophilic, readily functionalizable additional shell on the nanoparticles surface.¹⁵ Following such a procedure, the silica is generated *in situ* by the hydrolysis and condensation of a sol-gel precursor, usually TEOS.³²⁻³⁵ This method was first applied to rod-like particles, then to micrometer-sized hematite and later to iron oxide nanoparticles.³²

For instance, Simard *et al.* synthesized multifunctional magnetic nanoparticles, involved in a silica shell doped with a dye. The authors claim comparable emission properties to the free dye molecules,

suggesting the successful hindrance of contact between dye and magnetic core offered by the presence of an outer silica shell. However, the saturation magnetization of the silica-coated iron oxide MNPs was observed to be much lower than that of the as-received MNPs. This fact is attributed to the presence of the non-magnetic silica shell (10-15 nm thick) which drops the magnetization from about 60 to 10 $\text{emu}\cdot\text{g}^{-1}$.³⁶

Another method to prepare the silica coating is by microemulsion synthesis. In this case, micelles or inverse micelles are used to confine and control the silica coating. This method requires greater effort to separate the core-shell nanoparticles from a large amount of surfactant associated with the microemulsion system.²⁷ For example, Zhang *et al.* have reported the synthesis and characterization of Mn and Co spinel ferrite silica coated nanoparticles with tunable magnetic core, by using a reverse micelle microemulsion approach. Also in this case, the authors clearly proved that both CoFe_2O_4 and MnFe_2O_4 have reduced M_S after silica coating.³⁷ More recently, the same effect was detected for NiFe_2O_4 which showed a reduced M_S after coating with silica.³⁸

Surfactants or polymers are also often employed to enhance stability, biocompatibility and functionality of MNPs. These molecules can be chemically anchored or physically adsorbed on the surface of the MNPs, to form a shell which creates repulsive forces that balance the attractive van der Waals forces acting on the nanoparticles.¹⁵ Specifically, polymers containing functional groups such as carboxylic acids, phosphates and sulfates can easily bind the surface of iron oxide nanoparticles.³⁹ In addition, a wide variety of suitable polymers were used for the coating of diverse MNPs, including polyamines,¹⁹ poly(methacrylic acid),⁴⁰ dextran (DXS) and poly(l-lysine),⁴¹ polystyrene,^{42,43} among others.

The effect of e.g. an N-isopropylacrylamide (NIPAM) coating on the magnetic properties of Fe_3O_4 MNPs was shown to decrease the magnetization of the synthesized nanoparticles from 76 to 52 $\text{emu}\cdot\text{g}^{-1}$.⁴⁴ Moreover, the magnetization of dextran-coated MNPs was evaluated to be around 7 $\text{emu}\cdot\text{g}^{-1}$. Such low value, certainly makes magnetic detection and separation by application of a magnetic field very difficult.⁴⁵ Differently, the coating of IONCs by an amphiphilic polymer, developed by Pellegrino *et al.*, resulted in no changes in coercivity and saturation magnetization. These findings indicate a bulk-like behavior of the nanocubes.⁴⁶

Another type of material which might provide better solutions considering magnetic handling of the particles are carbon-coated cobalt (Co/C) MNPs. The surface of Co/C ferromagnetic nanoparticles, first synthesized by Stark *et al.*, can be easily functionalized with different species.¹⁶ Using diazonium chemistry on the carbon outer shell allows the introduction of a multitude of functional groups. Further polymerization can be done directly from these functional sites or by click chemistry e.g. described by Reiser *et al.*¹⁹ Recently, Stark *et al.* have developed a versatile platform for click reactions of relevant tag molecules with enhanced stability in solution of the Co/C ferromagnetic nanoparticles (Fig. 5). The materials were prepared by surface initiated atom transfer radical polymerization (SI-ATRP). A reduction in M_S due to the presence of a non-magnetic layer was observed also in this case.

Nevertheless, significantly high values of magnetization are still observed (over $90 \text{ emu}\cdot\text{g}^{-1}$) when compared to the most conventional iron oxide nanoparticles.⁴⁵

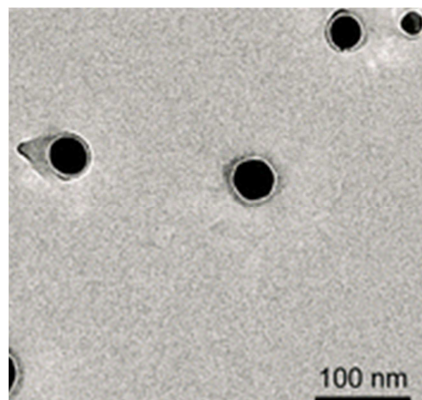


Fig. 4 TEM of stable Co/C MNPs showing the separation and the polymer layer surrounding the metal cobalt core. Adapted with permission from reference 53. Copyright 2014, Royal Society of Chemistry.

Despite the obvious tendency of the magnetization to be reduced upon the addition of nonmagnetic mass on the surface of the particles, especially polymers or silica, a clear correlation between these two parameters cannot be established and generalized for all cases. For instance, gold-coated cobalt nanoparticles have a lower magnetic anisotropy than uncoated particles, whereas gold coating of iron particles enhances the anisotropy, an effect which was attributed to alloy formation with the gold.³⁰ Similarly, magnetic coatings on top of MNPs have a dramatic effect on the final magnetic properties, since the combination of two magnetic phases will lead to new magnetic nanocomposites.¹⁵

Overall, the coercivity and hence the magnetic behavior of MNPs to an inert coating is rather complex and system specific. Therefore, the concept of magnetization reduction on addition of mass cannot be generalized, as the effects highly depend on the type of coating and its features as well on the nature of magnetic core, shape and size of the nanoparticles.

4. Applications of magnetic nanoparticles

4.1. Nanoparticles as potential tools in industry

Considering the developments on synthesis, functionalization and detailed characterization realized on magnetic nanoparticles, one can only imagine that research has resulted in thousands of potential application for these nanotools. However, how many of these applications can actually be translated to relevant industrial processes is not clear. The advantages of using magnetic nanoparticles in contrast to conventional materials are obvious: they offer the possibility of magnetic separation together with the advantageous features of nano-sized materials. Thus, potential sustainable applications where MNPs can actually replace conventional methodologies and materials are nowadays on focus of research.

At the present time, chemistry allows cost-effective manufacturing of compounds in a variety of processes. The key factor remains the separation and isolation of reagents, catalysts or intermediates. Industrial conventional processes are based on time-consuming or costly techniques such as distillation, chromatography, crystallization and filtration. A novel approach using MNPs combines provides fast and efficient magnetic separation.⁴⁷ In addition, chemical processes such as ore refining, active ingredient isolation, impurity removal and pharmaceutical manufacturing present a common problem related to the low concentration of important substances or reagents in large liquid volumes. Therefore, MNPs with high surface-to-volume ratio rise as a very attractive solution due to the possibility of capturing such reagents that are subsequently removed by magnetic separation.⁴⁷ The potential application of MNPs in different industrial processes including catalysis and bioremediation are discussed on the following paragraphs.

4.1.1. (Bio)Catalytic applications

Catalysis is a field of great importance since it provides a sustainable way to convert raw materials into valuable chemicals and fuels in an economical, efficient, and environmentally benign manner. The rationale behind it is the synthesis of compounds while minimizing the use and generation of hazardous substances and time-consuming wasteful purification techniques. In short, an ideal catalytic system must fulfil three main aspects: reactivity, easy recovery and possibility of re-use.⁴⁸⁻⁵⁰

The field of catalysis is undergoing an explosive development on the design of catalysts with excellent activity, greater selectivity and high stability. Here, MNPs have been widely applied as supports for heterogeneous catalysts. They allow the dispersion of the catalyst in solution combined with a fast and easy way to recover it from the reaction medium when isolating the product.^{47,48}

The easy and economic synthesis of magnetic nanoparticles from inexpensive raw materials in combination with the simplicity of magnetic handling might outperform and replace conventional materials such as zeolites and silica at the industrial scale in a near future. However, first, environmental implications concerning the toxicity of these nanomaterials need to be solved.^{48,49}

A broad assortment of catalytic reactions has been studied using catalysts supported on magnetic nanoparticles. They include hydrogenation, oxidation and carbon-carbon coupling reactions. Bare magnetic nanoparticles have been explored, with the catalytic activity relying solely on the magnetic material itself or other metals directly deposited on their surface. The most common nanoparticles are iron oxide, however other metal ferrites generated by partial substitution of iron by a second metal (Cu, Co, Zn, Ni, Mn) allows the expansion of scope for oxidative and coupling reactions.⁴⁹

One of the most used hybrid supports used for catalysis are silica coated magnetite particles.⁵⁰ Nazifi *et al.* prepared magnetite encapsulated in a silica shell bearing sulfonic acid groups, which can be used as a solid acid catalyst for the synthesis of 1,8-dioxo-octahydroxanthene derivatives. Such an approach avoids hazardous reagents, thus being considered as an eco-friendly alternative.⁵¹

A specific class of MNPs, the Co/C nanomagnets, have been extensively exploited for application in heterogeneous catalysis.¹⁶ Reiser *et al.* have used these nanoparticles as support for the reversible

noncovalent attachment of a pyrene-tagged Pd N-heterocyclic carbene complex. This “boomerang” catalyst was used for the hydroxycarbonylation of aryl halides in water under an atmospheric pressure of carbon monoxide, demonstrating high activity in more than 16 iterative runs.⁵² Furthermore, they reported the deposition of palladium nanoparticles on the surface of these carbon-coated MNPs for the hydrogenation of alkenes. The authors showed that the developed magnetic catalytic system compares favorably to conventional palladium catalyst in terms of activity, handling, leaching and recyclability through magnetic decantation (Fig. 5).⁵³

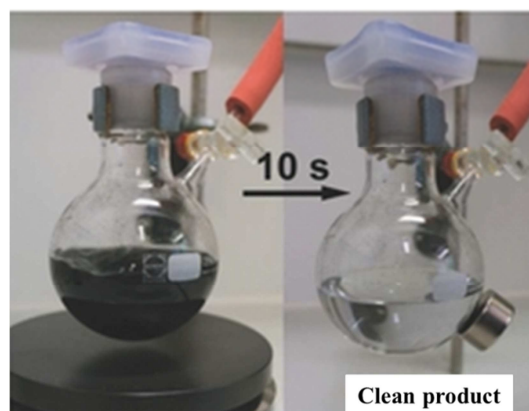


Fig. 5 Recover of catalytic Co/C nanoparticles and isolation of the product after reaction. The catalysis is performed under magnetic stirring (right picture). When the reaction is finished the magnetic catalyst is easily collected with an external magnet (left picture), giving the purified product. The nanocatalyst is then available for the next catalytic reaction. Adapted with permission from reference 25. Copyright 2013, WILEY-VCH Verlag GmbH & Co. KGaA, Weinheim.

The use of magnetic nanoparticles as supports for catalytic processes has also been extended to the field of biocatalysis. Herein, enzymes present key advantages compared to conventional chemical catalysts: (1) high activity, (2) great selectivity and (3) specificity. They are currently used in various chemical procedures such as redox reactions, (trans)esterification processes and enantioselective synthesis. However, their widespread application in many of these processes is impaired by inherent drawbacks including high costs, availability, recovery and recycling of the catalyst. For overcoming these issues, several methodologies have been reported including entrapment of the enzymes on porous materials or their immobilization on the surface of solid supports.^{54,55} The first refers to ion exchange resins whereas the second one is related with the adsorption or covalent attachment to different supports. Among these, MNPs provide the advantage of simple and fast recovery.⁴⁸

Enzymes can be attached to the surface of MNPs by EDC coupling and used for pharmaceutical and organic production, sensing and proteomics analysis. However, the immobilization of the enzyme should not impair its catalytic activity nor its selectivity.⁵⁰ Therefore, innovative approaches are necessary to prepare novel “magnetic enzymes”. Zheng *et al.* recently reported the development of a magnetic enzymatic nanosystem consisting of an iron oxide core surrounded by polydopamine and immobilized trypsin. The novel enzymatic nanohybrid proved to work efficiently for the digestion of

proteins while being conveniently separated from the reaction mixture by an external magnet.⁵⁶ Additionally, several studies have been focusing on the use of such nanocatalysts for the production of biodiesel.^{57,58} This field draws much attention as biodiesel is a renewable biodegradable, non-toxic alternative which can be generated from vegetable or waste cooking oils. For instance, Laosiripojana and co-workers have shown the efficient biocatalytic activity of immobilized lipase for the conversion of vegetable oils to fatty acid methyl ester (FAME). The biocatalyst supported on iron oxide nanoparticles could be efficiently recycled for at least 5 cycles with more than 80% activity remaining.⁵⁹ Similarly, Lee *et al.* have immobilized lipase onto MNPs and used them for biodiesel production from waste cooking oil.⁶⁰

Compared to common petrodiesel, biodiesel has a higher cetane number and does not contain hazardous aromatic compounds and almost no sulfur, thus reducing the emission of carbon monoxide, hydrocarbons, and particulate matter in the exhaust gas. This might considerably reduce air pollution while attenuating our dependence on petroleum.⁶⁰

4.1.2. Environmental applications

As mankind progress rapidly with industrialization, in modern civilization, it is natural to expect increasing contaminations. The unavailability of high quality drinking water is a critical problem across the world, especially in the so called third world countries. A significant amount of toxic compounds have been found in drinking water in large concentrations, including pesticides, heavy metals and micro-organisms, especially around industrial areas where the situation is quite severe. Hence, a number of solutions have been used for purification of drinking water, namely: sand filtration, activated carbon based adsorption, distillation and reverse osmosis. While all of them deliver great benefits, they are still far from ensuring availability of quality drinking water at an affordable price and fast time. Therefore, there is an increasing demand to discover novel materials to further improve the most conventional technologies.⁶¹

During the last decades, magnetic nanoparticles, which offer great flexibility for their *in situ* application, have been widely studied for remediation of groundwater, soil and air on both experimental and field scale.³ Indeed, magnetically assisted chemical separation (MACS) technology might provide a cost-effective solution to the most challenging environmental clean-up problems. Here, MNPs provide a convenient and simple method to remove a variety of contaminants from complicated matrices in wide range of chemical conditions. Such technology presents evident advantages when compared to conventional used adsorbents, as it requires considerably less complex equipment which in turn facilitates the scale-up processes.^{3,62}

MACS technology for the separation of radionuclides in tank-separation has been reported as a new approach to solve the critical problem of waste treatment at the US department of Energy and Department of Defense sites. This type of expertise can be used at any tank or location, including situations where remote operation is necessary. Unlike ion exchange processes, MACS does not require preliminary filtration of the solution. The effectiveness of the process has been demonstrated at

bench scale for decontamination of uranium, americium, and plutonium at the Argonne National Laboratory in Lemont, US.⁶² Additionally, also dyes or hazardous metal ions can be removed from wastewater of many industrial sectors, such as textile factories, tanneries and paint industry using MACS technology.^{3,63,64}

A successful wastewater treatment must fulfil the following criteria: treatment flexibility and efficiency, reuse of the treatment agents, environmental safety and low cost.⁶⁵ Magnetic scavengers or nanosorbents have been specifically explored for the removal of heavy metals ions from water, which is an issue of great concern due to their imminent danger to health and environment and their tendency for bioaccumulation even at low concentrations.

For instance, Nassar has shown that iron oxide nanoparticles have a maximum adsorption capacity for Pb(II) of 36 milligrams per gram of nanomaterial which is considerably higher than the previously reported low cost sorbents.⁶⁶ The small size of the nanoparticles allows the diffusion of metal ions from solution to the active sites of the adsorbent, making them very effective and economic. Moreover, *Pang et al.* demonstrated the efficiency of functionalized iron oxide MNPs for removal of Hg(II), revealing an extraction capacity as high as 380 milligrams of mercury per gram of nanosorbents. However, no selectivity tests in combination with other metals were reported.⁶⁷

The mechanisms of decontamination can involve adsorption by surface site binding or electrostatic interaction.⁶⁵ An overview of magnetic nanoparticles used as scavengers or nanosorbents for metal removal in polluted water is given in Table 1.

Table 1. Magnetic scavengers for decontamination of different metal ions in polluted water.

Scavenger	Functional group	Heavy metal	Maximum extraction capacity
Mesostructured silica magnetite ⁶⁸	-NH ₂	Cu(II)	0.5 mmol·g ⁻¹
δ-FeOOH-coated-γ-Fe ₂ O ₃ ⁶⁹	-	Cr(VI)	25.8 mg·g ⁻¹
Magnetic iron-nickel oxide ⁷⁰	-	Cr(VI)	30 mg·g ⁻¹
Montmorillonite-supported MNPs ⁷¹	-AlO; -SiO	Cr(VI)	15.3 mg·g ⁻¹
Hydrous iron oxide MNPs ⁶¹	-	As(V), Cr(VI)	As(V): 8 mg·g ⁻¹
Amino-modified Fe ₃ O ₄ MNPs ⁷²	-NH ₂	Cu(II), Cr(VI)	Cu(II): 12.43 mg·g ⁻¹ Cr(VI): 11.24 mg·g ⁻¹
Poly-L-cysteine coated Fe ₃ O ₄ MNPs ⁷³	-Si-O; -NH ₂	Ni(II), Pb(II), Zn(II), As(III), Cu(II), Cd(II)	Over 50% recovery for all metals. The best performance was found for Ni(II) to be 89%.
m-PAA-Na-coated MNPs ⁷⁴	-COO	Cu(II), Pb(II), Cd(II), Ni(II)	Cu(II): 30 mg·g ⁻¹ ; Pb(II): 40 mg·g ⁻¹ ; Cd(II): 5 mg·g ⁻¹ ; Ni(II): 27 mg·g ⁻¹

Fe ₃ O ₄ -silica coated MNPs ⁷⁵	-Si-OH	Pb(II), Hg(II)	Over 90% extraction for both elements.
PEI-coated Fe ₃ O ₄ MNPs ⁷⁶	-NH ₂	Cr(VI)	83.3 mg·g ⁻¹
Dimercaptosuccinic acid-coated Fe ₃ O ₄ MNPs ⁷⁷	-SH	Hg(II) Ag(I), Pb(II), Cd(II),	Hg(II): 220 mg·g ⁻¹
Salicylic acid functionalized silica-coated Fe ₃ O ₄ MNPs ⁶⁴	-COOH	Cu(II), Cr(III), Cd(II), Ni(II)	Cu(II): 39.9 mg·g ⁻¹ ; Cr(III): 39.8 mg·g ⁻¹ ; Cd(II): 27.8 mg·g ⁻¹ ; Ni(II):17.3 mg·g ⁻¹
PEI-coated Co/C MNPs ¹⁷	-NH ₂	Hg(II)	550 mg·g ⁻¹
Amino-functionalized silica materials with a magnetic core ⁷⁸	-NH ₂	Cu(II)	0.7 mmol·g ⁻¹

The application of such materials for decontamination processes in real situations must circumvent aggregation of the MNPs as well as undesired interaction with other substances. For instance, phosphates might compete with the heavy metals for active sites, thus limiting the effectiveness of the scavenger. For resolving this constraint, again the strategy is to apply different coatings or functional groups on the surface of the MNPs.^{75,79,80}

Similarly, a vast amount of work has been done on the removal of organic pollutants from water using MNPs as sorbents. Liu *et al.* showed iron oxide hollow nanospheres could efficiently remove red dyes from water and be collected using an external magnet.⁸¹ Similarly to heavy metal adsorption, the adsorption of contaminants takes place via surface exchange reaction until the surface functional sites are fully occupied. Furthermore, different modified-MNPs have been studied for the removal of polycyclic aromatic hydrocarbon (PAH) pollutants from water, allowing the elution of analytes after extraction and recycling of the adsorbent.^{82,83}

Considering the advances achieved in MNPs research, this technology might provide opportunities for developing next-generation nanosorbents for the decontamination of polluted water. Such novel scavengers compare well to conventional technologies, showing higher specificity and capacity, easier separation and extended lifecycles.⁶⁵

4.2. Biomedical applications

MNPs have also been explored for their potential medical application in clinic. In biomedicine or biotechnology, the applications of such nanomagnets might be classified as *in vitro* or *in vivo* according to their use outside or inside the body, respectively. *In vitro* applications are related with magnetic separation, selection or diagnosis whereas *in vivo* applications include therapeutic areas as hyperthermia, drug delivery and procedures like magnetic resonance imaging (MRI).³

Most particles currently used in the biomedical field are superparamagnetic iron oxide nanoparticles (SPIONs). They receive great interest as they can be magnetized with an external magnetic field and

immediately re-dispersed once the magnet is removed. For that reason they provide enhanced colloidal stability which is required for any application in biological systems.^{15,47}

Magnetic separation can also be used as a fast and efficient method for the capture of specific proteins, cells, DNAs or bacteria often required for analysis.¹⁵ For instance, Pawar *et al.* developed a suitable magnetic scavenger, comprising iron oxide nanoparticles coated with silica and an additional shell of chitosan, for the separation of DNA from biological samples.⁸⁴ The isolation results of genomic DNA achieved from saliva indicated that the functionalized magnetic nanoparticles have outstanding advantages in operation, selectivity, and capacity over the present existing isolation protocols (phenol–chloroform extraction).

Berensmeier *et al.* have shown an efficient high-gradient magnetic separation for technical scale protein recovery using low cost magnetic nanoparticles. The authors claim that using 100 grams of functionalized nanomagnets containing a pentadentate chelate ligand, a purification performance of around 12 grams of His-GFP per hour is achieved, with an eluate purity of 96% and a yield of 93% for the whole process.⁸⁵ Actually, the successful performance of such nanomaterials for *in vitro* applications made their translation into commercialized products possible e.g. Dynabeads®, which can be used for cell separation, protein isolation and exosome analysis.

In a typical bioseparation application, the biological entities are tagged with MNPs and then collected with an external magnetic field. Due to their high surface-to-volume ratio, magnetic nanoparticles have superior performance on the bioseparation of molecules in large volumes of fluids. Additionally, the attachment of antibodies to the MNPs can be used for highly specific binding of the target molecules.³

Another application in which the use of magnetic nanoparticles has received attention is cancer treatment. Most pharmaceutical approaches used to treat cancer nowadays are based on chemotherapeutic agents, which generally exhibit high cytotoxic effects but poor specificity for the intended biological target. This practice often results in systemic distribution of the antitumor drug causing severe side effects in healthy tissues.⁴ Therefore, it is important to find different type of therapies with improved performances to reduce size effects for the patient. Encouraged by these facts, researchers have been focus on the development of potential drug targeting magnetic nanocarriers. This concept was first introduced in 1970 by Widder *et al.* and to the present time the possibility of suitable applications for magnetic nanocarriers has drastically increased.⁸⁶ Magnetic targeting is defined as the guidance of drug-loaded MNPs to the desired site of action using a localized magnetic field, holding them there during the treatment and then removing them once the therapy is completed.¹⁵ Significant advantages can be achieved performing such a therapy, as it allows the reduction of the drug dosage, diminishing the adverse side effects due to the high local concentration of the drug at the desired part of the organism.^{3,15}

Despite the very promising *in vitro* results, first clinical trials have revealed poor effective response. Consequently, magnetic nanocarriers have not been approved and used in clinic yet.⁴ To accomplish a

successful performance, the magnetic carrier, has to be carefully tailored with specific chemical properties. As described before, the stabilization of the nanomagnets must be ensured. This can be achieved by the development of polymeric or silica shells on the surface of the MNPs. The additional use of protein repellent species (e.g. PEG) is often the strategy followed to avoid interaction with opsonins, increasing the circulation of the nanomaterials in the blood stream. At any stage of this synthetic route, different types of therapeutic molecules can be physically adsorbed or covalently attached. Among them, doxorubicin (DOXO) and paclitaxel (PTX) have been widely studied.⁴ Pellegrino *et al.* have shown the efficiency of magnetic nanocubes covered with a shell of thermo-responsive polymer to load DOXO and release it under an alternating magnetic field. Such material might be used in future for the combined cancer therapy using hyperthermia and chemotherapy, while circumventing the side effects of conventional chemotherapy.⁸⁷ In another study, Xu and co-workers developed a PTX encapsulated magnetic nanocarrier using thermoresponsive molecules as coating agent. High encapsulation efficiency and tumor inhibition reflected the great potential of the carriers for specific binding and targeting release of the antitumor drug.⁸⁸

Similarly, the concept of magnetic delivery has been extended to gene transfection, commonly known as magnetofection. In the last few years, due to the importance of nucleic acid delivery for producing proteins or shutting down the production of endogenous genes, magnetofection has attracted considerable attention. The delivery is based on the magnetic force exerted upon the magnetic vectors to direct them into the target cells both *in vitro* and *in vivo*.⁴ Compared to conventional gene delivery strategies, magnetofection has shown to significantly increase gene delivery to human xenograft tumor models.²⁸ Plank *et al.* have brought together gene vectors with magnetic nanoparticles, showing the potentiated efficacy of the vector up to several hundred-fold, allowed the reduction of the duration of gene delivery to minutes.⁸⁹

In addition, Chen *et al.* used modified-SPIONs coated with polyethyleneimine (PEI) as a multiple gene delivery system for transfection of porcine kidney cells. The PEI-coated SPIONS showed strong binding affinity for DNA plasmids expressing the genes encoding a green (DNAGFP) or red (DNADsRed) fluorescent protein. As a result, stable and efficient co-expressed of GFP and DsRed in porcine kidney PK-15 cells was achieved by magnetofection.⁹⁰

More recently, RNA interference (RNAi) technology has been in the focus of research since siRNAs or miRNAs can target and inhibits the expression of almost any gene.^{91,92} The use of magnetic nanoparticles as carries offer the mentioned advantages of reducing time of therapy and minimize vector dosage.²⁸ Currently, *in vitro* magnetofection products using cationic polymer coated MNPs are commercially available. For instance, Magnetofection™ offers a variety of products which cover a wide range of cell as well as cargo type (siRNA, DNA, oligonucleotides). RNAi will be described in Chapter 3.

Additional to drug delivery and gene transfection the so-called hyperthermia therapy is also being explored as an alternative approach for cancer treatment. Hyperthermia is considered a supplementary

treatment to chemotherapy, radiotherapy and also surgical interventions.¹⁵ The rationale behind this therapeutic approach is the capacity of SPIONs to produce heat when exposed to an alternating magnetic field. This feature can be used *in vivo* for destroying pathological cells in tumors, since they are much more sensitive to temperature increase (over 41°C) than normal cells.^{3,15,27}

The key advantage of hyperthermia relies on the possibility to heat the restricted area of the tumor. Specifically, when exposed to an alternating magnetic field the magnetization of the SPIONs flips randomly from the parallel to the antiparallel orientations. This causes the transfer of magnetic energy to the particles in the form of heat. The use of subdomain magnetic nanoparticles is preferred to multi-domain microparticles due to their higher absorption of power at tolerable magnetic fields.³ The hyperthermia capacity of SPIONs strongly depends on their properties: e.g. size, chemical composition, shape, etc. Consequently, well-defined synthetic routes for SPIONs are required in order to enhance their heating performance and reduce the dose to a minimum level.¹⁵

Pastor *et al.* evaluated the effect of SiO₂ coating on Fe₃O₄ MNPs. Unfortunately, they confirmed a reduced M_s and a lower coercivity, and consequently a lower heating capacity, for SiO₂-coated Fe₃O₄ MNPs as compared to analogous uncoated Fe₃O₄ nanoparticles.⁹³ Depending on the severity of this reduction, the ability of the materials for being using for example in hyperthermia therapy might be compromised.

Nevertheless, several *in vitro* studies for the selective remote inactivation of cancer cells by oscillating magnetic fields have been reported. For instance, Pellegrino *et al.* have recently proved the potential of superparamagnetic nanocubes for efficiently perform hyperthermia therapy. This study revealed more than 50% of cancerous cell mortality over an hour of treatment.⁴⁶

The establishment of hyperthermia in clinical routine had encouraged the industrial sector to develop suitable MNPs capable of generating heat when exposed to an oscillating magnetic field. The German company MagForce for example, developed suitable products (NanoTherm, NanoPlan and NanoActivator) for the local treatment of glioblastoma multiform, prostate and pancreatic cancer.⁴

SPIONs also proved to be a novel class of materials for cellular and molecular imaging. As contrast agents they have the advantage of inducing an enhanced contrast in MRI in comparison to paramagnetic ones. Consequently, fewer amounts of particles are needed to dose the human body.³ Most of the multimodal MRI studies include the conjugation of MNPs with organic fluorophores. This conjugates provide high anatomical resolution and sensitivity. The optical component can be detected by a variety of techniques both *in vivo* and *in vitro*, such as fluorescent microscopy, flow cytometry, spectrophotometry, clinical endoscopy, etc.⁴ For example, Hwang *et al.* have developed a non-invasive multimodal magnetic particle (labelled with fluorescent, radioisotopic substances) as a potential tool for *in vivo* imaging. MicroPET and MRI images showed intense radioactivity and ferromagnetic intensities with MFBR-laden cells. Their imaging approach provide time-course imaging analysis to track cellular localization and distribution by using optical, radionuclide, and magnetic resonance agents in living subjects.⁹⁴ A lot of other studies have been reported using MNPs for bio-imaging,

including the monitoring of stem cell migration and clearance mechanisms of nanoparticles in humans.⁴

Thanks to the great advances on the synthesis and functionalization of MNPs, these nanomaterials are a strong candidate to set up an acceptable platform for diagnosis and therapy. However, their application in clinic, avoiding any collateral effect to the patient, requires further work which is being accomplished cooperatively by researchers of different scientific areas.

5. Conclusions and future perspectives

This review shows the remarkable progress on MNPs research for the development of suitable solutions on both industrial and medical fields. The possibility of magnetic separation or accumulation represents the major advantage of MNPs when compared to most conventional technologies currently used. In addition, other advantages can be pointed out: (1) they can be easily synthesized and (2) conjugated with other molecules in a straightforward way, expanding to a great extent their potential applications.

One of the features which might compromise the application of MNPs is their stability in solution. Circumventing magnetic collapse between particles is absolutely necessary to ensure functionality and good performance of the materials. Therefore, different type of coatings can be applied including carbon shells, inorganic coatings e.g. silica, or organic molecules like surfactants or polymers. Nevertheless, when applying a surface coating caution should be taken in order to minimize the effects on the magnetic properties of the pristine nanoparticles safeguarding their easy magnetic recovery or guidance.

With all the advances achieved on this field, there was a boost on the amount of suitable applications found for MNPs. Properly tailored they can be used for diverse functions. From bioremediation of water,¹⁷ passing through catalytic systems, until biomedical materials, magnetic nanoparticles have covered a broad range of applications, resulting already in the commercialization of some products. Even though few limitations have still to be overcome, considering the speed at which research is evolving it can simply be expected that in the near future MNPs will substitute conventional methodologies, modernizing both the chemical and biomedical industries.

6. References

1. Toumey, C. *Nature Nanotechnology* **2009**, 4, (12), 781-781.
2. Webster, T. J. *International Journal of Nanomedicine* **2007**, 2, (1), 1-2.
3. Akbarzadeh, A.; Samiei, M.; Davaran, S. *Nanoscale Research Letters* **2012**, 7, (1), 1-13.

4. Colombo, M.; Carregal-Romero, S.; Casula, M. F.; Gutierrez, L.; Morales, M. P.; Bohm, I. B.; Heverhagen, J. T.; Prosperi, D.; Parak, W. J. *Chemical Society Reviews* **2012**, 41, (11), 4306-4334.
5. Schätz, A.; Long, T. R.; Grass, R. N.; Stark, W. J.; Hanson, P. R.; Reiser, O. *Advanced Functional Materials* **2010**, 20, (24), 4323-4328.
6. Schätz, A.; Reiser, O.; Stark, W. J. *Chemistry – A European Journal* **2010**, 16, (30), 8950-8967.
7. Wittmann, S.; Schätz, A.; Grass, R. N.; Stark, W. J.; Reiser, O. *Angewandte Chemie International Edition* **2010**, 49, (10), 1867-1870.
8. Linhardt, R.; Kainz, Q. M.; Grass, R. N.; Stark, W. J.; Reiser, O. *RSC Advances* **2014**, 4, (17), 8541-8549.
9. Herrmann, I. K.; Schlegel, A.; Graf, R.; Schumacher, C. M.; Senn, N.; Hasler, M.; Gschwind, S.; Hirt, A.-M.; Gunther, D.; Clavien, P.-A.; Stark, W. J.; Beck-Schimmer, B. *Nanoscale* **2013**, 5, (18), 8718-8723.
10. Byrne, J. M.; Coker, V. S.; Moise, S.; Wincott, P. L.; Vaughan, D. J.; Tuna, F.; Arenholz, E.; van der Laan, G.; Patrick, R. A. D.; Lloyd, J. R.; Telling, N. D. *Journal of The Royal Society Interface* **2013**, 10, (83).
11. Herrmann, I. K.; Urner, M.; Graf, S.; Schumacher, C. M.; Roth-Z'graggen, B.; Hasler, M.; Stark, W. J.; Beck-Schimmer, B. *Advanced Healthcare Materials* **2013**, 2, (6), 829-835.
12. Singamaneni, S.; Bliznyuk, V. N.; Binek, C.; Tsymbal, E. Y. *Journal of Materials Chemistry* **2011**, 21, (42), 16819-16845.
13. Zeltner, M.; Toedtli, L. M.; Hild, N.; Fuhrer, R.; Rossier, M.; Gerber, L. C.; Raso, R. A.; Grass, R. N.; Stark, W. J. *Langmuir* **2013**, 29, (16), 5093-5098.
14. Koehler, F. M.; Rossier, M.; Waelle, M.; Athanassiou, E. K.; Limbach, L. K.; Grass, R. N.; Gunther, D.; Stark, W. J. *Chemical Communications* **2009**, (32), 4862-4864.
15. Lu, A.-H.; Salabas, E. L.; Schüth, F. *Angewandte Chemie International Edition* **2007**, 46, (8), 1222-1244.
16. Grass, R. N.; Athanassiou, E. K.; Stark, W. J. *Angewandte Chemie International Edition* **2007**, 46, (26), 4909-4912.
17. Fernandes, S.; Eichenseer, C. M.; Kreitmeier, P.; Rewitzer, J.; Zlateski, V.; Grass, R. N.; Stark, W. J.; Reiser, O. *RSC Advances* **2015**, 5, (58), 46430-46436.
18. Quarta, A.; Curcio, A.; Kakwere, H.; Pellegrino, T. *Nanoscale* **2012**, 4, (11), 3319-3334.
19. Kainz, Q. M.; Reiser, O. *Accounts of Chemical Research* **2014**, 47, (2), 667-677.
20. Singh, R. K.; Kim, T.-H.; Patel, K. D.; Knowles, J. C.; Kim, H.-W. *Journal of Biomedical Materials Research Part A* **2012**, 100A, (7), 1734-1742.
21. Quy, D. V.; Hieu, N. M.; Tra, P. T.; Nam, N. H.; Hai, N. H.; Thai Son, N.; Nghia, P. T.; Anh, N. T. V.; Hong, T. T.; Luong, N. H. *Journal of Nanomaterials* **2013**, 2013, 6.

22. Bahadur, N. M.; Furusawa, T.; Sato, M.; Kurayama, F.; Siddiquey, I. A.; Suzuki, N. *Journal of Colloid and Interface Science* **2011**, 355, (2), 312-320.
23. Seo, W. S.; Lee, J. H.; Sun, X. M.; Suzuki, Y.; Mann, D.; Liu, Z.; Terashima, M.; Yang, P. C.; Mc Connell, M. V.; Nishimura, D. G.; Dai, H. J. *Nature Material* **2006**, 5, 971.
24. Koksharov, Y. A., Magnetism of Nanoparticles: Effects of Size, Shape, and Interactions. In *Magnetic Nanoparticles*, Wiley-VCH Verlag GmbH & Co. KGaA: 2009; pp 197-254.
25. Mody Vicky, V.; Singh, A.; Wesley, B., Basics of magnetic nanoparticles for their application in the field of magnetic fluid hyperthermia. In *European Journal of Nanomedicine*, 2013; Vol. 5, p 11.
26. Jun, Y.-w.; Choi, J.-s.; Cheon, J. *Chemical Communications* **2007**, (12), 1203-1214.
27. Laurent, S.; Forge, D.; Port, M.; Roch, A.; Robic, C.; Vander Elst, L.; Muller, R. N. *Chemical Reviews* **2008**, 108, 2064.
28. Mody, V. V.; Cox, A.; Shah, S.; Singh, A.; Bevins, W.; Parihar, H. *Applied Nanoscience* **2013**, 4, (4), 385-392.
29. van Leeuwen, D. A.; van Ruitenbeek, J. M.; de Jongh, L. J.; Ceriotti, A.; Pacchioni, G.; Häberlen, O. D.; Rösch, N. *Physical Review Letters* **1994**, 73, (10), 1432-1435.
30. Paulus, P. M.; Bönnemann, H.; van der Kraan, A. M.; Luis, F.; Sinzig, J.; de Jongh, L. J. *The European Physical Journal D - Atomic, Molecular, Optical and Plasma Physics* 9, (1), 501-504.
31. Yuan, Y.; Rende, D.; Altan, C. L.; Bucak, S.; Ozisik, R.; Borca-Tasciuc, D.-A. *Langmuir* **2012**, 28, (36), 13051-13059.
32. Lu, Y.; Yin, Y.; Mayers, B. T.; Xia, Y. *Nano Letters* **2002**, 2, (3), 183-186.
33. Stöber, W.; Fink, A.; Bohn, E. *Journal of Colloid and Interface Science* **1968**, 26, (1), 62-69.
34. Philipse, A. P.; van Bruggen, M. P. B.; Pathmamanoharan, C. *Langmuir* **1994**, 10, (1), 92-99.
35. Zolfigol, M. A.; Yarie, M. *RSC Advances* **2015**, 5, (125), 103617-103624.
36. Ma, D.; Guan, J.; Dénommée, S.; Enright, G.; Veres, T.; Simard, B. *Chemistry of Materials* **2006**, 18, (7), 1920-1927.
37. Vestal, C. R.; Zhang, Z. J. *Nano Letters* **2003**, 3, (12), 1739-1743.
38. Larumbe, S.; Pérez-Landazábal, J. I.; Pastor, J. M.; Gómez-Polo, C. *Journal of Applied Physics* **2012**, 111, (10), 103911.
39. Cornell, R.; Schwertmann, U., The Iron Oxides: Structure, Properties, Reactions, Occurrence and Uses. VCH Verlagsgesellschaft GMBH Weinheim, Germany: 1996.
40. Griffete, N.; Lamouri, A.; Herbst, F.; Felidj, N.; Ammar, S.; Mangeney, C. *RSC Advances* **2012**, 2, (3), 826-830.
41. Mancarella, S.; Greco, V.; Baldassarre, F.; Vergara, D.; Maffia, M.; Leporatti, S. *Macromolecular Bioscience* **2015**, 15, (10), 1365-1374.

42. Vestal, C. R.; Zhang, Z. J. *Journal of the American Chemical Society* **2002**, 124, (48), 14312-14313.
43. Kainz, Q. M.; Späth, A.; Weiss, S.; Michl, T. D.; Schätz, A.; Stark, W. J.; König, B.; Reiser, O. *ChemistryOpen* **2012**, 1, (3), 125-129.
44. Shamim, N.; Hong, L.; Hidajat, K.; Uddin, M. S. *Colloids and Surfaces B: Biointerfaces* **2007**, 55, (1), 51-58.
45. Hofer, C. J.; Zlateski, V.; Stoessel, P. R.; Paunescu, D.; Schneider, E. M.; Grass, R. N.; Zeltner, M.; Stark, W. J. *Chemical Communications* **2015**, 51, (10), 1826-1829.
46. Guardia, P.; Di Corato, R.; Lartigue, L.; Wilhelm, C.; Espinosa, A.; Garcia-Hernandez, M.; Gazeau, F.; Manna, L.; Pellegrino, T. *ACS Nano* **2012**, 6, (4), 3080-3091.
47. Stark, W. J.; Stoessel, P. R.; Wohlleben, W.; Hafner, A. *Chemical Society Reviews* **2015**, 44, (16), 5793-5805.
48. Polshettiwar, V.; Luque, R.; Fihri, A.; Zhu, H.; Bouhrara, M.; Basset, J.-M. *Chemical Reviews* **2011**, 111, (5), 3036-3075.
49. Hudson, R.; Feng, Y.; Varma, R. S.; Moores, A. *Green Chemistry* **2014**, 16, (10), 4493-4505.
50. Govan, J.; Gun'ko, Y. K. *Nanomaterials* **2014**, 4, (2), 222.
51. Naeimi, H.; Nazifi, Z. S. *Journal of Nanoparticle Research* **2013**, 15, (11), 1-11.
52. Wittmann, S.; Schätz, A.; Grass, R. N.; Stark, W. J.; Reiser, O. *Angewandte Chemie International Edition* **2010**, 49, (10), 1867-1870.
53. Kainz, Q. M.; Linhardt, R.; Grass, R. N.; Vilé, G.; Pérez-Ramírez, J.; Stark, W. J.; Reiser, O. *Advanced Functional Materials* **2014**, 24, (14), 2020-2027.
54. Zlateski, V.; Fuhrer, R.; Koehler, F. M.; Wharry, S.; Zeltner, M.; Stark, W. J.; Moody, T. S.; Grass, R. N. *Bioconjugate Chemistry* **2014**, 25, (4), 677-684.
55. Kim, J.; Grate, J. W.; Wang, P. *Chemical Engineering Science* **2006**, 61, (3), 1017-1026.
56. Cheng, G.; Zheng, S.-Y. *Scientific Reports* **2014**, 4, 6947.
57. Korman, T. P.; Sahachartsiri, B.; Charbonneau, D. M.; Huang, G. L.; Beaugard, M.; Bowie, J. U. *Biotechnology for Biofuels* **2013**, 6, (1), 1-13.
58. Jeong, G.-T.; Park, D.-H. *Applied biochemistry and biotechnology* **2008**, 148, (1-3), 131-139.
59. Raita, M.; Arnthong, J.; Champreda, V.; Laosiripojana, N. *Fuel Processing Technology* **2015**, 134, 189-197.
60. Yu, C.-Y.; Huang, L.-Y.; Kuan, I. C.; Lee, S.-L. *International Journal of Molecular Sciences* **2013**, 14, (12), 24074-24086.
61. Pradeep, T.; Anshup. *Thin Solid Films* **2009**, 517, (24), 6441-6478.
62. Nuñez, L.; Kaminski, M. D. *Journal of Magnetism and Magnetic Materials* **1999**, 194, (1-3), 102-107.
63. Tang, S. C. N.; Lo, I. M. C. *Water Research* **2013**, 47, (8), 2613-2632.
64. Shishehbore, M. R.; Afkhami, A.; Bagheri, H. *Chemistry Central Journal* **2011**, 5, (1), 1-10.

65. Xu, P.; Zeng, G. M.; Huang, D. L.; Feng, C. L.; Hu, S.; Zhao, M. H.; Lai, C.; Wei, Z.; Huang, C.; Xie, G. X.; Liu, Z. F. *Science of The Total Environment* **2012**, 424, 1-10.
66. Nassar, N. N. *Journal of Hazardous Materials* **2010**, 184, (1–3), 538-546.
67. Shen, X.; Wang, Q.; Chen, W.; Pang, Y. *Applied Surface Science* **2014**, 317, 1028-1034.
68. Kim, Y.; Lee, B.; Yi, J. *Separation Science and Technology* **2003**, 38, (11), 2533-2548.
69. Hu, J.; Lo, I. M. C.; Chen, G. *Separation and Purification Technology* **2007**, 58, (1), 76-82.
70. Wei, L.; Yang, G.; Wang, R.; Ma, W. *Journal of Hazardous Materials* **2009**, 164, (2–3), 1159-1163.
71. Yuan, P.; Fan, M.; Yang, D.; He, H.; Liu, D.; Yuan, A.; Zhu, J.; Chen, T. *Journal of Hazardous Materials* **2009**, 166, (2–3), 821-829.
72. Huang, S.-H.; Chen, D.-H. *Journal of Hazardous Materials* **2009**, 163, (1), 174-179.
73. White, B. R.; Stackhouse, B. T.; Holcombe, J. A. *Journal of Hazardous Materials* **2009**, 161, (2–3), 848-853.
74. Mahdavian, A. R.; Mirrahimi, M. A.-S. *Chemical Engineering Journal* **2010**, 159, (1–3), 264-271.
75. Ambashta, R. D.; Sillanpää, M. *Journal of Hazardous Materials* **2010**, 180, (1–3), 38-49.
76. Pang, Y.; Zeng, G.; Tang, L.; Zhang, Y.; Liu, Y.; Lei, X.; Li, Z.; Zhang, J.; Xie, G. *Desalination* **2011**, 281, 278-284.
77. Yantasee, W.; Warner, C. L.; Sangvanich, T.; Addleman, R. S.; Carter, T. G.; Wiacek, R. J.; Fryxell, G. E.; Timchalk, C.; Warner, M. G. *Environmental Science & Technology* **2007**, 41, (14), 5114-5119.
78. Melnyk, I. V.; Gdula, K.; Dąbrowski, A.; Zub, Y. L. *Nanoscale Research Letters* **2016**, 11, 61.
79. Feng, Y.; Gong, J.-L.; Zeng, G.-M.; Niu, Q.-Y.; Zhang, H.-Y.; Niu, C.-G.; Deng, J.-H.; Yan, M. *Chemical Engineering Journal* **2010**, 162, (2), 487-494.
80. Girginova, P. I.; Daniel-da-Silva, A. L.; Lopes, C. B.; Figueira, P.; Otero, M.; Amaral, V. S.; Pereira, E.; Trindade, T. *Journal of Colloid and Interface Science* **2010**, 345, (2), 234-240.
81. Iram, M.; Guo, C.; Guan, Y.; Ishfaq, A.; Liu, H. *Journal of Hazardous Materials* **2010**, 181, (1–3), 1039-1050.
82. Li, Y.; Qi, L.; Shen, Y.; Ma, H. *Analytica Chimica Acta* **2014**, 811, 36-42.
83. Yan, Z.; Yuan, J.; Zhu, G.; Zou, Y.; Chen, C.; Yang, S.; Yao, S. *Analytica Chimica Acta* **2013**, 780, 28-35.
84. Tiwari, A. P.; Satvekar, R. K.; Rohiwal, S. S.; Karande, V. A.; Raut, A. V.; Patil, P. G.; Shete, P. B.; Ghosh, S. J.; Pawar, S. H. *RSC Advances* **2015**, 5, (11), 8463-8470.
85. Fraga García, P.; Brammen, M.; Wolf, M.; Reinlein, S.; Freiherr von Roman, M.; Berensmeier, S. *Separation and Purification Technology* **2015**, 150, 29-36.
86. Widder, K. J.; Senyei, A. E.; Ranney, D. F. *Advances in Pharmacology and Chemotherapy* **1979**, 16, 213-271.

87. Kakwere, H.; Leal, M. P.; Materia, M. E.; Curcio, A.; Guardia, P.; Niculaes, D.; Marotta, R.; Falqui, A.; Pellegrino, T. *ACS Applied Materials & Interfaces* **2015**, 7, (19), 10132-10145.
88. Shen, J.-M.; Yin, T.; Tian, X.-Z.; Gao, F.-Y.; Xu, S. *ACS Applied Materials & Interfaces* **2013**, 5, (15), 7014-7024.
89. Scherer, F.; Anton, M.; Schillinger, U.; Henke, J.; Bergemann, C.; Kruger, A.; Gansbacher, B.; Plank, C. *Gene therapy* **2002**, 9, (2), 102-109.
90. Wang, Y.; Cui, H.; Li, K.; Sun, C.; Du, W.; Cui, J.; Zhao, X.; Chen, W. *PLoS ONE* **2014**, 9, (7), e102886.
91. Kanasty, R.; Dorkin, J. R.; Vegas, A.; Anderson, D. *Nature Materials* **2013**, 12, (11), 967-977.
92. Bumcrot, D.; Manoharan, M.; Kotliansky, V.; Sah, D. W. Y. *Nature Chemical Biology* **2006**, 2, (12), 711-719.
93. Larumbe, S.; Gómez-Polo, C.; Pérez-Landazábal, J. I.; Pastor, J. M. *Journal of Physics: Condensed Matter* **2012**, 24, (26), 266007.
94. Hwang, D. W.; Ko, H. Y.; Kim, S.-K.; Kim, D.; Lee, D. S.; Kim, S. *Chemistry – A European Journal* **2009**, 15, (37), 9387-9393.

Chapter 1

Towards the stabilization of readily recyclable carbon-coated cobalt nanoparticles via surface functionalization

Highly magnetic carbon-coated cobalt (Co/C) nanoparticles were engineered via surface functionalization for meeting different dispersibility requirements. Such nanoparticles are very attractive due to their particularly easy magnetic collection, being widely used in different chemical processes e.g. synthesis or catalysis. However, better dispersion of these nanoparticles in a variety of reaction media is desirable in order to avoid strong stirring or continuous sonication. Circumventing magnetic collapse of the particles in solution certainly help to maximize their performance for any envisage application. Therefore, here I report the development of different surface coatings, more specifically silica or polymeric shells, on Co/C nanoparticles rendering them dispersible in organic solvents and most importantly in aqueous phase, without compromising their facile magnetic separation.

Parts of this chapter are published in:

- Kainz, Q. M.; Fernandes, S.; Eichenseer, C. M.; Besostri, F.; Korner, H.; Muller, R.; Reiser, O. *Faraday Discussions* **2014**, 175, 27-40. Reproduced with permission of The Royal Society of Chemistry. (<http://pubs.rsc.org/en/Content/ArticleLanding/2014/FD/C4FD00108G>).
- Fernandes, S.; Eichenseer, C. M.; Kreitmeier, P.; Rewitzer, J.; Zlateski, V.; Grass, R. N.; Stark, W. J.; Reiser, O. *RSC Advances* **2015**, 5, (58), 46430-46436. Reproduced with permission of The Royal Society of Chemistry. (<http://pubs.rsc.org/en/Content/ArticleLanding/2015/RA/C5RA04348D>).

1.1 Introduction

Magnetic nanoparticles (MNPs) are of great interest for researchers in a variety of fields including catalysis,¹⁻³ magnetic resonance imaging (MRI),^{4,5} biotechnology/biomedicine⁶⁻¹¹ and environmental remediation.¹²⁻¹⁶ Many suitable methods for the synthesis of nanoparticles, applicable in the aforementioned disciplines have been developed. However, the performance of magnetic materials is highly dependent on their stability at the different surrounding conditions to which they are exposed.¹⁷ Generally, the as-synthesized MNPs are chemically unstable, being easily oxidized and prone to agglomeration. Therefore, it is crucial to develop suitable surface coatings to protect and stabilize the nanoparticles while simultaneously ensuring high magnetization and dispersibility in solution.¹⁷ Coating strategies include surface grafting using organic species (e.g. surfactant¹⁷ and/or polymers¹⁷⁻¹⁹) or inorganic layers (e.g. silica²⁰⁻²² or carbon^{23,24}). In most cases the surface coating does not only provide protection and stabilization but also offers an additional platform for further functionalization with catalytic active species, various drugs or specific binding sites. Functionalized MNPs are particularly promising for application in catalysis,¹⁻³ bioseparation²⁵ and biolabeling²⁶ due to the possibility of magnetic separation from solution. Especially in liquid-phase catalysis, one can combine the high dispersion and reactivity of the nanoparticles with an easy and fast recovery.^{27,28} In fact, magnetically driven separation makes the recovery of catalysts much simpler than tedious cross-flow filtration and centrifugation methods allowing the recycling and reusability of expensive catalysts or ligands.¹

Despite the significant advances on the synthesis of MNPs the possibility to scale up the production process, as well as the need to ensure the stability and recycling of the resulting magnetic materials are still challenging. Not meeting these requirements can significantly limit their applicability especially when considering the industrial sector.¹⁷

For instance metallic nanoparticles, having a much higher magnetization than their oxide counterparts have attracted much attention. However, high reactivity and undesired toxicity of the metal core of these MNPs are two additional problems contributing for limiting their application. Silica, polymers or surfactants are commonly used as a primary coating for metallic MNPs to reduce the impact of the mentioned issues. Nevertheless, instability in basic environments and high temperatures of these coatings still need to be overcome. Differently, carbon-coated MNPs are remarkably stable under harsh conditions.¹⁷ For instance, Johnson *et al.* have reported a direct salt-conversion approach for large-scale synthesis of carbon-encapsulated magnetic Fe and Fe₃C nanoparticles, by direct pyrolysis.²⁹ The authors proved the potential for scaling up the synthesis as well as the stability of the materials at temperatures up to 400°C. Unfortunately, there was a broad size distribution of the nanoparticles ranging from 20-200 nm was observed. In addition, Lu and co-workers have shown the fabrication of carbon shell protected cobalt nanoparticles, via pyrolysis, proving the high

stability under acidic and basic conditions.³⁰ The graphitic-shell provides a barrier against oxidation and prevents metal leaching from the core while preserving its high magnetic moment.³¹ However maintaining the particles in an isolated, dispersible state has proven to be very challenging, especially in aqueous phase.¹⁷

Over the past few years ferromagnetic cobalt nanoparticles containing graphene-like carbon layers (Co/C MNPs) have been investigated.¹⁸ Such commercially available nanoparticles, firstly synthesized by Stark *et al.*, have a number of attractive features. First of all, the metal core of these particles (20–50 nm in size) renders them highly magnetic with a saturation magnetization (M_s) of 130–160 emu.g⁻¹.²³ This allows an easy recovery even if heavy molecules are attached to the particle surface, condition which generally decreases the magnetization to levels of unfunctionalized superparamagnetic iron oxide particles (30–50 emu.g⁻¹).¹⁷ Additionally, the carbon shell, having a thickness of only 1–3 nm, provides high stability against oxygen as well as acidic and basic pH. Last but not least, the carbon shell offers the possibility for covalent surface attachment via diazonium chemistry or simple adsorption by Π - Π stacking.³² Nevertheless, due to their high magnetization and hydrophobic surface these particles are prone to agglomeration (see Fig. 1), especially in aqueous phase.

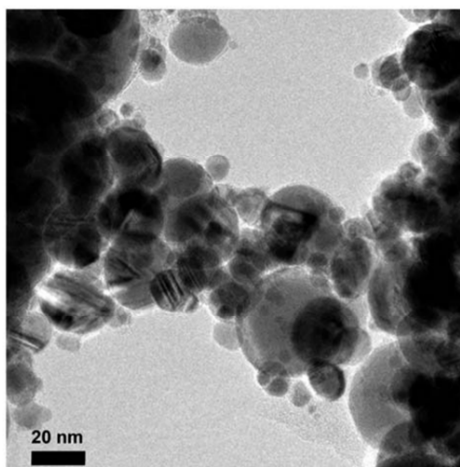


Fig. 1. Transmission electron microscopy (TEM) picture showing the clear tendency for agglomeration of ferromagnetic Co/C nanoparticles. Figure adapted with permission from reference 33. Copyright 2012, Royal Society of Chemistry.

Envisioning a real industrial application for such materials it is demanding to improve their dispersibility in solution since most of the automated industrial reactors allow simply shaking and not stirring or sonication, usually needed to disperse these MNPs. Indeed, even in our laboratories dispersibility issues might impair the use of the nanoparticles e.g. in catalytic reactions in water. Stark *et al.* recently showed that carbon-coated nanoparticles covalently functionalized with highly charged polymers, allow the formation of stable dispersions in aqueous media.³³ Additionally, Hongjie Dai and co-workers, have shown the use of water-

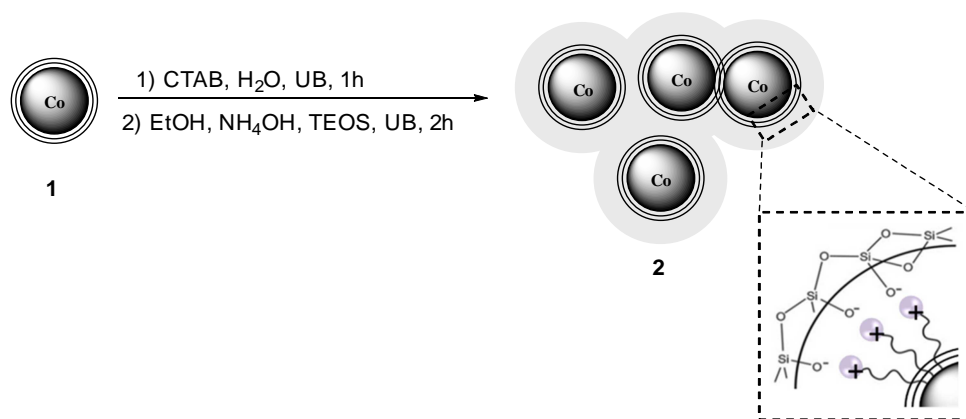
soluble FeCo/graphitic shell nanocrystals as contrast agents by capping them with a phospholipidic-poly(ethylene glycol) (PL-PEG).²⁴

Therefore the feasibility to attenuate the properties of Co/C MNPs by applying different coatings was studied, aiming to achieve good dispersibility while keeping high magnetization values. Herein, the comparison of various complementary synthetic strategies for functionalizing Co/C nanoparticles is reported. This includes organic and inorganic coatings, and the extensive evaluation of such materials with respect to their dispersibility in various solvents. Furthermore, the magnetic performance of the MNPs, regarding recovery and recyclability, was also assessed and compared for the different type of coatings applied.

1.2 Silica-coated magnetic Co/C nanoparticles

Inorganic silica coating offers a biologically inert and chemically reactive shell which has been intensively studied during the last decades for applications in chemistry and biomedicine. The hydrophilicity and biocompatibility of silica makes it very attractive for biotechnological applications such as protein separation³⁴ or photothermal cancer therapy.²¹ Likewise, studies on silica-coated supports for catalysis^{21,35} or peptide synthesis³⁶ have been reported. Commonly, the direct coating of silica on different physical supports is done by ammonia-catalyzed hydrolysis and condensation of tetraethyl orthosilicate (TEOS).^{21,22,37,38} This low cost sol-gel process usually offers good homogeneity of the formed shell.

In this subsection, the development of a silica shell starting from the pristine Co/C (**1**), as shown in Scheme 1, is discussed. Firstly, the cationic surfactant cetyltrimethylammonium bromide (here referred as CTAB) is adsorbed on the outer graphene-like layer of the MNPs (**1**) by hydrophobic interaction of its alkyl chain exposing the ammonium group on the surface of the MNPs. In this manner, it forms a positive wrapping around the nanoparticles in aqueous solution. Subsequently, the injection of TEOS under basic conditions leads to its hydrolysis and condensation into silicate polyanions. These can interact with the positively exposed charges from the CTAB simply by electrostatic interaction or hydrogen-bonding (see Scheme 1). Therefore, the presence of CTAB should facilitate the growth of a silica shell around the nanoparticles while preventing TEOS own nucleation process.³⁴



Scheme 1 Synthesis of Co/C@SiO₂ (**2**) from pristine Co/C (**1**), using CTAB as the surfactant for the silica growth on the nanoparticle's surface.

In a study reporting silica grafting onto carbon nanotubes, Zhang and co-authors claim that one of the parameters affecting the morphology of the silica-coated MNPs is the ratio (w/w) CTAB/MNPs used.³⁴ Thus, the variation of CTAB added to the MNPs was studied for the following ratios: 2:1; 20:1; 60:1. The presence of silica was immediately confirmed by attenuated total reflection infrared spectroscopy (ATR-IR) in confront with the pristine Co/C MNPs (**1**) which have no detectable peaks. According to the spectra obtained for all the three samples (Fig. 2) a strong band at 1100 cm⁻¹ is assigned to the Si-O-Si asymmetric stretching. Other bands at 950 and 800 cm⁻¹ are recognized as the Si-OH stretching and Si-O-Si symmetric vibration,³⁸ confirming the silica coating on the nanoparticles.

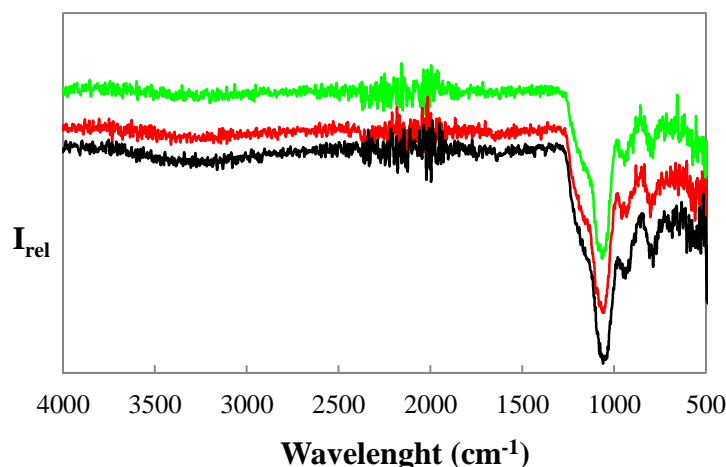


Fig. 2 ATR-IR spectra of Co/C@SiO₂ (**2**) prepared from pristine Co/C (**1**) using different ratios (w/w) of CTAB/MNPs. Green line: ratio 2:1; red line: ratio 20:1; black line: ratio 60:1.

Indeed, TEM analysis confirmed the presence of silica for all three samples. Despite slight differences between each ratio CTAB/MNPs tested, the results still show significant aggregation of the beads. For the lowest amount of CTAB used (Fig. 3A), very thick shells are formed and the homogeneous nucleation process of TEOS is favored, most likely due to the insufficient amount of CTAB on the

surface of the particles. In contrast, using higher ratios of CTAB to MNPs (see Fig. 3B and 3C) one can reduce the formation of silica nanoparticles as well as the thickness of the silica-coated nanobeads. However, defined silica shells around the beads are not obtained in any of these samples, as considerable agglomeration of the initial magnetic materials is detected.

Accordingly, a significant decrease in the saturation magnetization of the MNPs was detected. As shown in Fig. 4, the M_S values are similar and approximated to 55 emu.g^{-1} . This value is much lower than the one registered for the pristine MNPs (1) which have a M_S around 150 emu.g^{-1} .²³ This phenomenon is directly related to the huge increase in silica mass around the nanomaterials, as seen in the TEM pictures (Fig. 3).

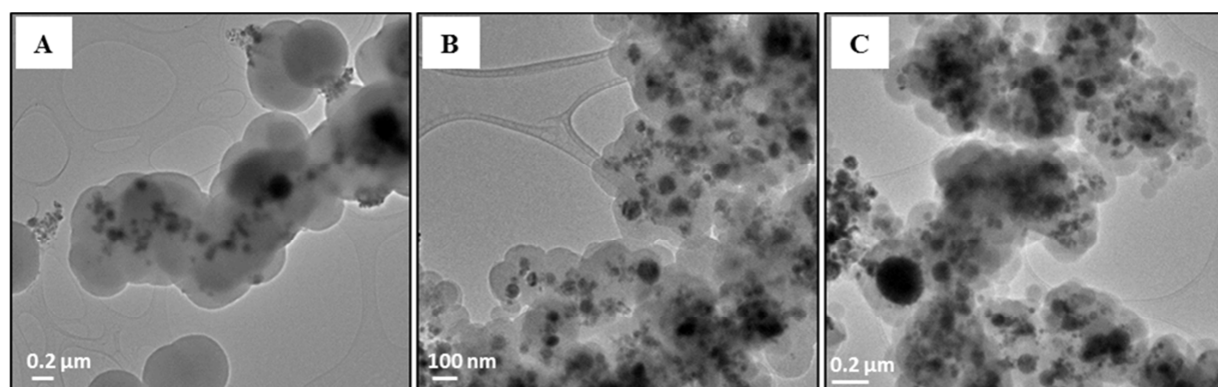


Fig. 3 TEM pictures of Co/C@SiO_2 (2) prepared from pristine Co/C (1) using different ratios (w/w) of CTAB/MNPs: A) 2:1; B) 20:1; C) 60:1.

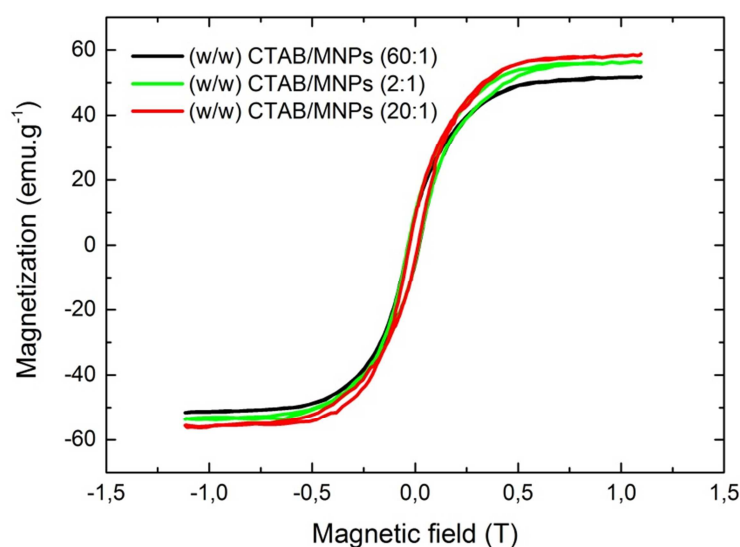
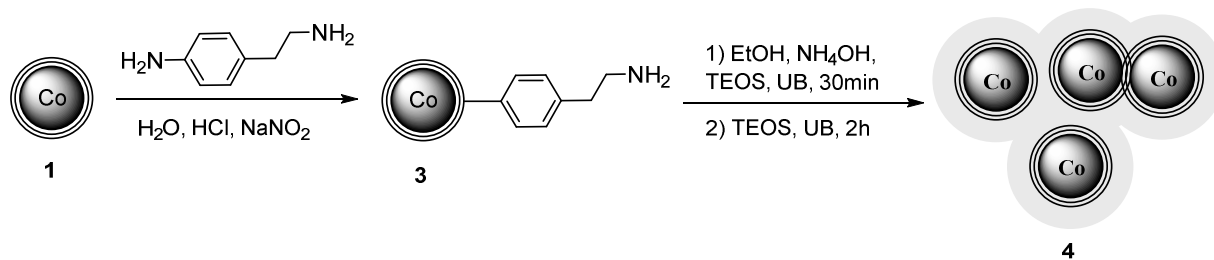


Fig. 4 Saturation magnetization of the different synthesized Co/C@SiO_2 (2). Green line: ratio (w/w) CTAB/MNPs 2:1; red line: ratio CTAB/MNPs 20:1; black -line: ratio CTAB/MNPs 60:1.

In order to avoid the decrease in magnetization of Co/C MNPs, a strategy for the synthesis of a thinner and more defined silica shell around the nanoparticles was developed. Here, the silica was grown from the exposed amine groups on the surface of functionalized nanoparticles (3)²³ as illustrated in Scheme 2.



Scheme 2 Synthesis of Co/C@SiO₂ (4) from Co/C-NH₂ (3). The volume ratio TEOS:EtOH for the growth of silica was varied as: 0.05, 0.2 and 2%.

The functionalized nanoparticles were obtained by covalently attaching linkers bearing amine groups to the surface of Co/C (1). To do this, 4-(2-aminoethyl)aniline was converted to the corresponding diazonium salt which subsequently reacts with the carbon surface of pristine nanobeads (1) upon sonication (Scheme 2). The loading with amino groups was determined by elemental microanalysis to be 0.1 mmol.g⁻¹. To grow the silica on the surface of Co/C-NH₂ (3), the MNPs were dispersed in ethanol with catalytic amounts of ammonia while a solution of TEOS was added dropwise to promote a controlled shell formation.

In this case, the volume ratio TEOS to EtOH was varied from 0.05, 0.2 up to 2% in order to check the impact on the morphology of the silica shell. Again, the formation of silica was confirmed by ATR-IR spectroscopy showing the most pronounced band of Si-O-Si asymmetric stretching at 1100cm⁻¹ and 950-800cm⁻¹ (Fig. 5).

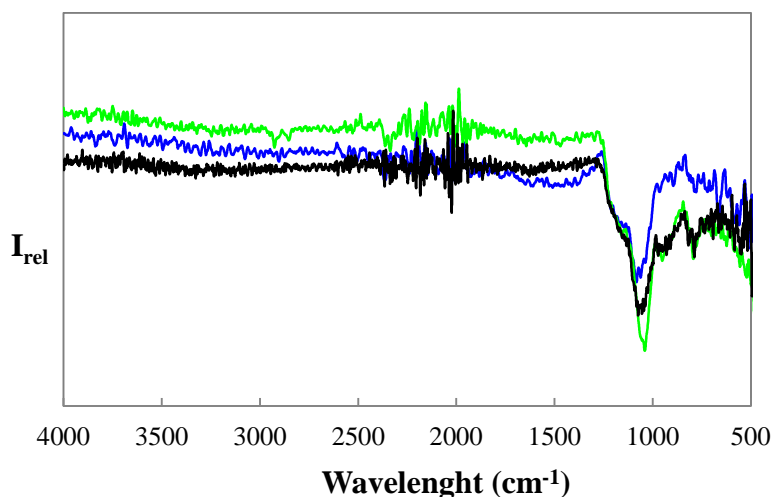


Fig. 5 ATR-IR spectra of Co/C@SiO₂ (4) prepared from Co/C-NH₂ (3) using different volume ratios of TEOS/EtOH. Blue line: 0.05% TEOS; green line: 0.2% TEOS; black line: 2% TEOS.

Generally, according to the TEM pictures in Fig. 6, this synthesis gives much nicer coated nanobeads than the one described for the previous methodology. Increasing the amount of TEOS leads to the formation of less defined shells, much thicker and randomly distributed (Fig. 6C). On the contrary, using 0.2 and 0.05% of TEOS (Fig. 6B or 6A, respectively) results in fine encapsulated magnetic

beads surrounded by a much thinner shell. Moreover, sample aggregation, which was detected by TEM in Fig. 3 for the previous reported materials, is much less pronounced here. These facts are in good agreement with the values measured for the magnetization of the MNPs (see Fig. 7) which were found to be higher when the silica shell around the NPs was smaller. Usually the M_S is lowered with the gain of mass as detected for the sample prepared with 2% TEOS in which the silica coating is considerably bigger. By adjusting the parameters of the synthesis it is possible to keep the magnetic properties of the nanoparticles in the range of the non-functionalized ones (150 emu.g^{-1}).²³ In fact, from Fig. 7, one can see that for nanobeads prepared with 0.05% of TEOS the saturation magnetization of the material is practically unchanged (140 emu.g^{-1}) and decreases as the amount of TEOS used for the reaction increases (114 emu.g^{-1} for TEOS 0.2% and 60 emu.g^{-1} for TEOS 2%). Such properties evidence Co/C nanoparticles to be highly attractive when compared even to the most common unfunctionalized magnetite nanoparticles, with a maximum M_S value measured at 92 emu.g^{-1} .

123

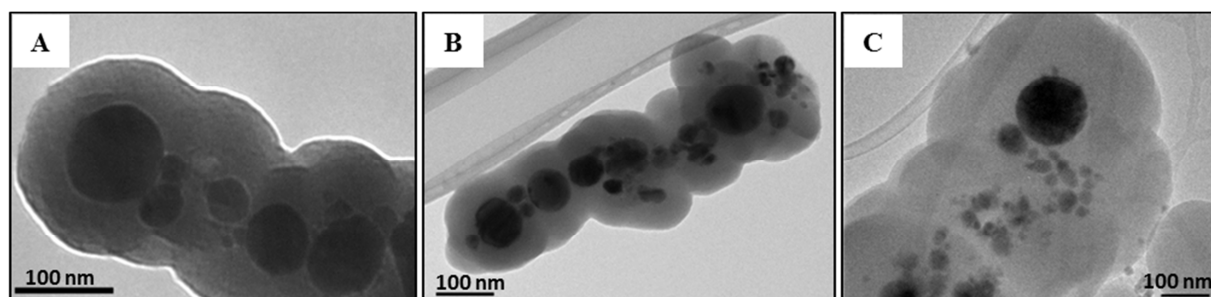


Fig. 6 TEM pictures of Co/C@SiO₂ (4) prepared from Co/C-NH₂ (3) using different volume ratios of TEOS/EtOH. A) 0.05% TEOS; B) 0.2% TEOS; C) 2% TEOS.

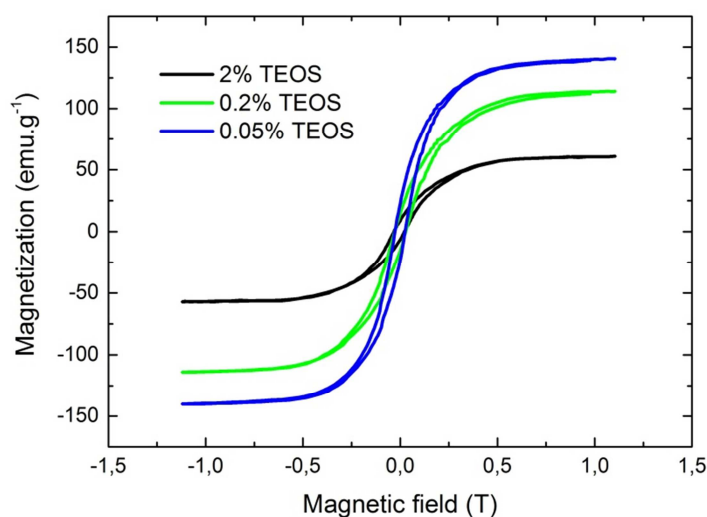


Fig. 7 Saturation magnetization of the synthesized Co/C@SiO₂ (4) using different volume ratios of TEOS/EtOH. Blue line: 0.05% TEOS; green line: 0.2% TEOS; black line: 2% TEOS.

In confront to the saturation magnetization stated for silica coated-magnetite nanoparticles, which drops usually to values as low as 15 emu.g^{-1} ,³⁹ the impact of these results becomes even greater. Kim *et al.* reported an excellent magnetization of silica-coated magnetite nanoparticles to be about 64.1

emu.g^{-1} ,²⁰ which is still 2 times lower than the values obtained for the best synthesis conditions of silica-coated ferromagnetic Co/C nanobeads (140emu.g^{-1}).

As shown in Fig. 8, the developed coating, improves the stability of the nanoparticles in different solvents (water, ethanol and DCM) while allowing a fast recovery from solution within a few seconds (Fig. 8D). Despite their high magnetization, it is possible to keep such materials in solution with a simple continuous shaking mechanism which is definitely not enough for the pristine Co/C nanomagnets. Even after collection or deposition, a simple hand shaking is enough as depicted in Fig. 8C for dispersing them again in the respective solvent.

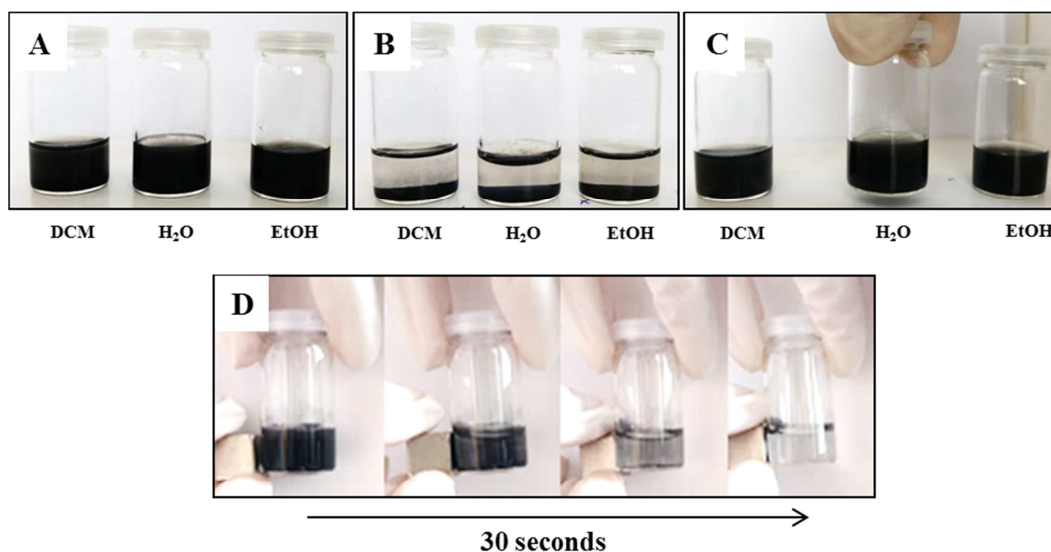


Fig. 8 Co/C@SiO₂ (4) dispersion in DCM, H₂O and EtOH after 5 minutes of sonication (A), deposition / precipitation over time (B), re-dispersion with hand shaking (C). Fast recovery of the nanobeads with an external magnet (D).

The improvement in dispersibility of the beads obtained by applying a silica coating on the surface allows for the possibility to explore the potential of these nanomagnets for example in catalysis as it will be discussed further in this chapter. Additionally, the presence of silanol groups on the surface can easily react with various coupling agents to covalently attach molecules to the Co/C MNPs. 3-(aminopropyl)triethoxysilane (known as APTES) has been commonly used to introduce amine groups on the surface of silica coated magnetite nanoparticles.⁴⁰ Later in this chapter another approach will be discussed for the attachment of amine-rich polymers on silica-coated Co/C MNPs.

1.3 Polymer-coated magnetic Co/C nanoparticles

Bearing in mind the stabilization of Co/C MNPs in aqueous phase, polymer coatings comprising high number of polar groups arise as a promising strategy to be explored. Highly ramified dendrimeric-like molecules are very attractive since they offer the possibility of changing charge, functionality, and

reactivity of magnetic supports, enhancing their stability and dispersibility.^{41,42} Two different methodologies, shown in Fig. 9, can be adopted for the synthesis of these polymers: a convergent or a divergent growth. The convergent pathway starts from peripheral molecules and proceeds inward building dendrons which are then coupled together at the focal point. On the other hand, the divergent approach starts from a reactive core molecule which is expanded giving rise to different generations of the dendrimer. The resultant molecules contain much higher number of functional terminal groups in contrast to linear polymers.^{41,43,44}

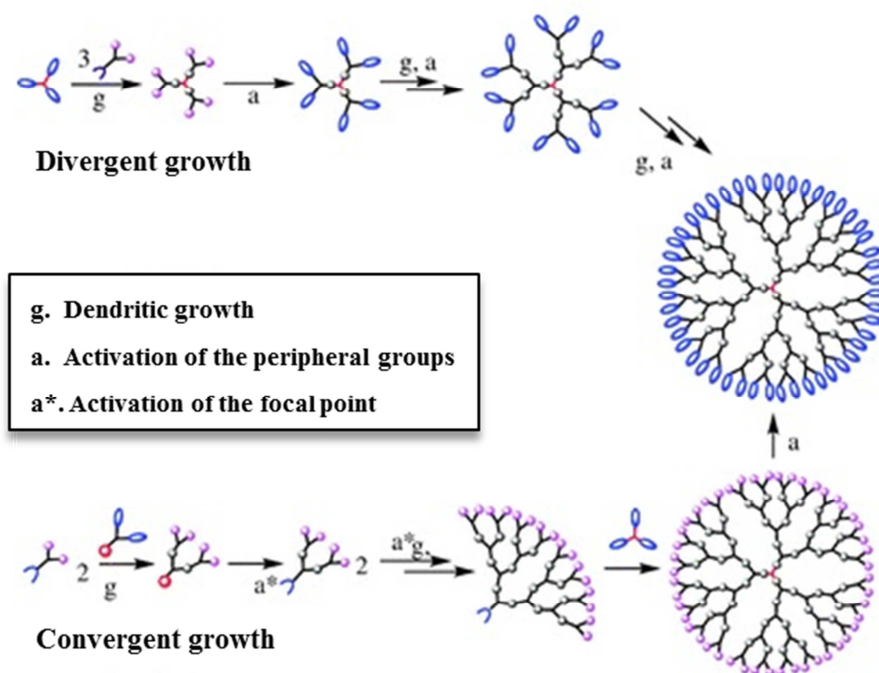
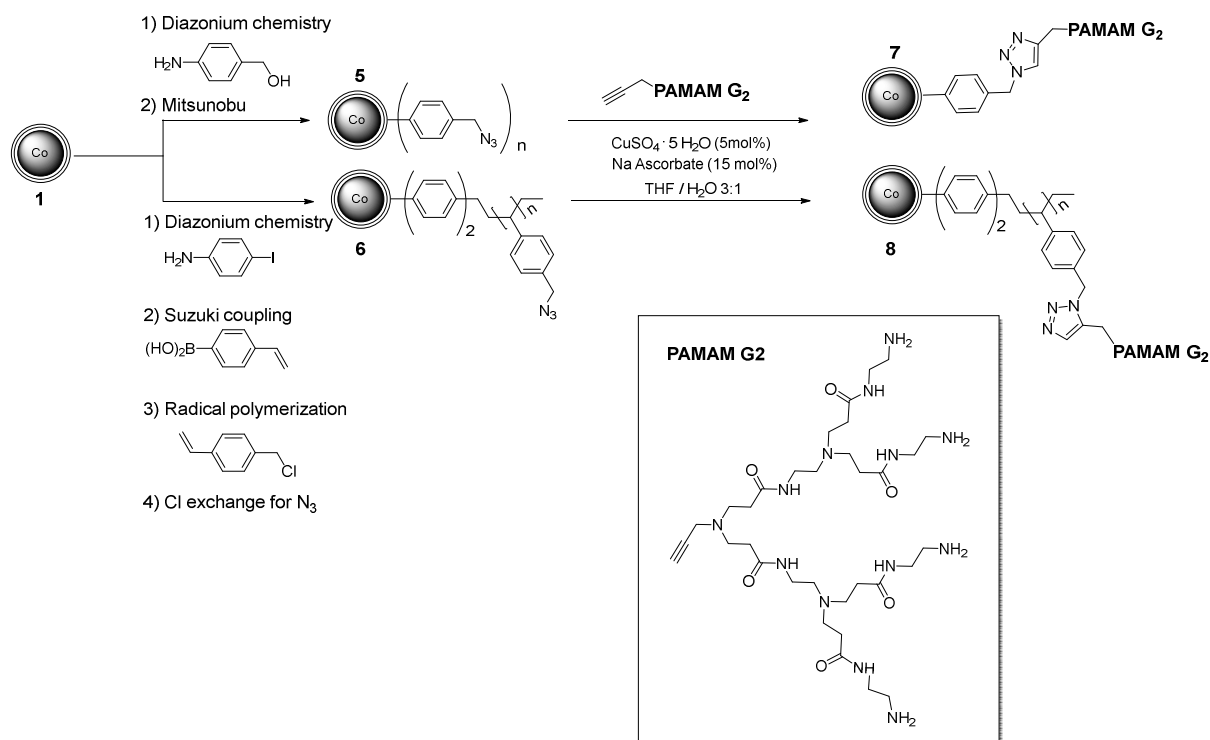


Fig. 9 Schematic representation of convergent and divergent synthesis of dendrimers. Adapted with permission from reference 44. Copyright 2012, Royal Society of Chemistry

The preparation of dendron-functionalized MNPs can be done by directly synthesizing the dendrons on the surface of the nanoparticles⁴⁵ or by attaching the previously synthesized molecules using e.g. click-chemistry.^{18, 46} Either way, the nanomaterials can be functionalized with different generations of the desired dendrons. On one hand, the direct synthesis from the surface, a “grafting from” approach, of the nanoparticles leads to higher loadings but compromises the control on the synthesis due to the difficulty of analysis on the MNPs. On the other hand, the synthesis of the dendrons followed by “clicking” on the surface, here referred as “grafting to” strategy, provides a much better control on its purity but decreases the loadings of polymer achieved.¹⁸

A grafting to methodology for the covalent attachment of poly(amidoamine) PAMAM dendrons on the surface of Co/C MNPs was performed and the results discussed here. Second generation (G2) of PAMAM dendrons were synthesized according to a procedure described in literature.⁴⁷

Briefly, propargyl amine is successively reacted with methyl acrylate and ethylenediamine via conventional divergent growth, giving consecutive generations of the dendrons with duplicated number of functional groups, after each complete generation (2 steps). The propargyl group on the focal point allows the dendrons to be easily clicked to the surface of the Co/C nanoparticles previously functionalized with azide moieties (Scheme 3).¹²



Scheme 3 Covalent immobilization of PAMAM dendron G2 on Co/C MNPs via click chemistry.¹² Benzyl azide-functionalized nanoparticles (**5**) and nanoparticles enwrapped in a Wang type resin with azide moieties (**6**) were used to click the dendrons under similar reaction conditions.

Two different routes were followed to link PAMAM G2 to Co/C nanoparticles: benzyl azide-functionalized Co/C nanoparticles (Co/C-N₃, **5**)^{46, 48} or a Wang type resin having azide end groups covalently attached to Co/C nanoparticles (Co/C-PS-N₃, **6**),^{25, 49, 50} were found to be suitable platforms to accommodate PAMAM dendrons via ligation by a copper catalyzed azide/alkyne cycloaddition using conditions previously described.^{46, 48} Co/C-PS-N₃ (**6**) generally offer higher loading of azide groups, up to 2.4 mmol azide per gram of nanoparticles, compared to Co/C-N₃ (**5**) which have loadings in the range of 0.1 mmol azide per gram of MNPs.¹²

The click reaction was conveniently followed and confirmed by IR spectroscopy, monitoring the attenuation of the azide band at 2100 cm⁻¹ before and after reaction (see Fig. 10).

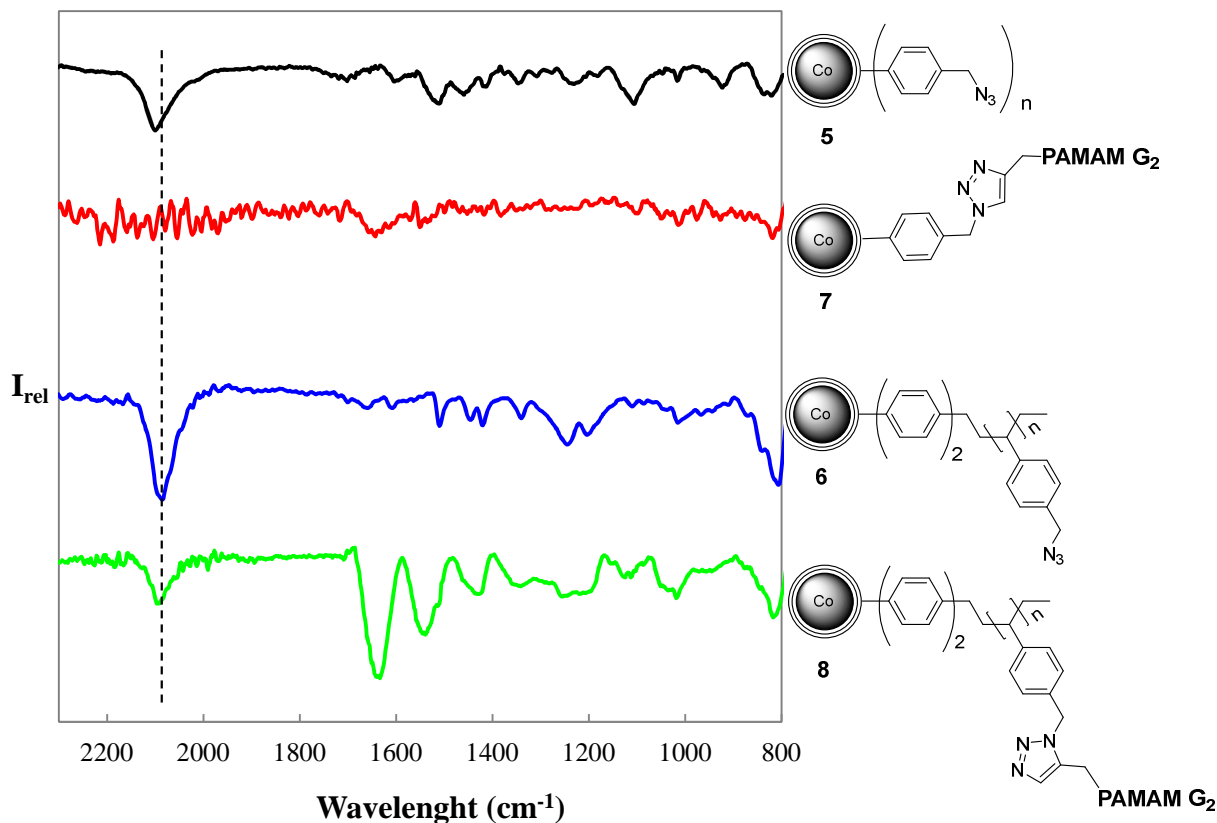


Fig. 10 ATR-IR spectra of azide-functionalized nanoparticles: Co/C-N₃ (**5**) (black line) and Co/C-PS-N₃ (**6**) (blue line); and the respective PAMAM-functionalized nanoparticles after click reaction: Co/C-PAMAM G₂ (**7**) (red line) and Co/C-PS-PAMAM G₂ (**8**) (green line).

The loading of dendrons on the surface of the nanoparticles (**7**) and (**8**) was estimated by thermogravimetric analysis (TGA) analysis to be 0.02 and 0.6 mmol of PAMAM molecules per gram of nanomaterial, respectively. Both the loadings are considerably low in view of the loadings of the initial azide-tagged MNPs (**5**) and (**6**). This might be easily explained by the steric hindrance of such ramified dendrons which cannot fit more than a certain amount of molecules due to a limitation on space organization. From Fig. 11, one can confirm that the higher gain in mass for NPs (**8**) results in a lower saturation magnetization (50 emu.g⁻¹) when compared to the nanomaterials (**7**) (105 emu.g⁻¹). However, both types of PAMAM-functionalized MNPs are still quite easily recovered from solutions simply by applying an external magnet. Unfortunately, despite the presence of the polar groups on the surface, none of the materials (**7**) or (**8**) is well dispersible in aqueous solutions most likely due to the low loadings of PAMAM obtained.

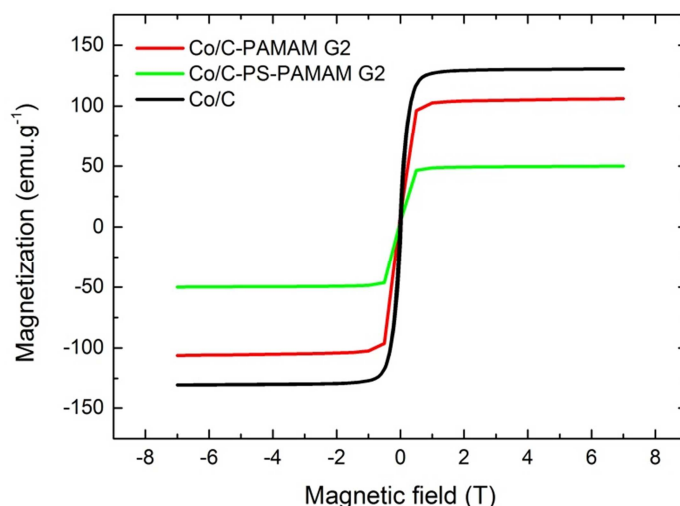
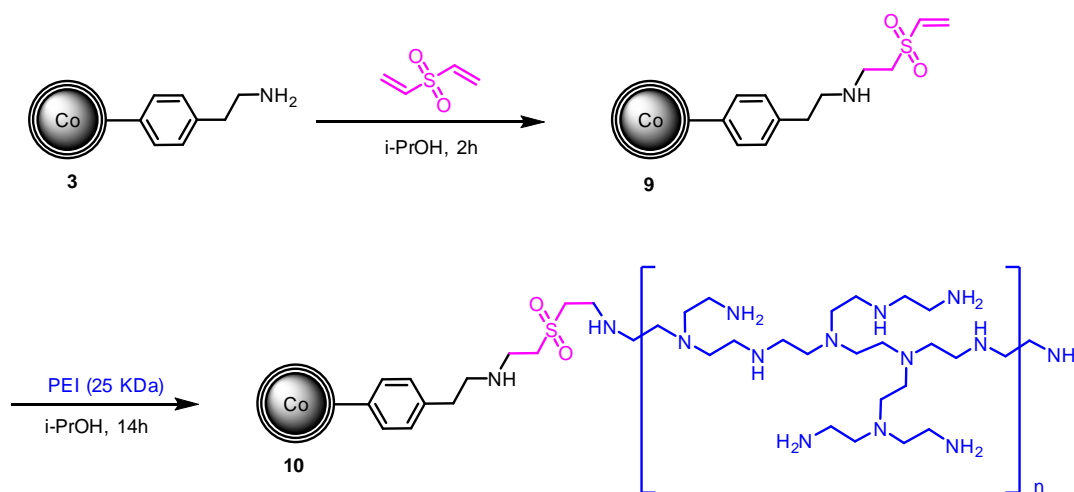


Fig. 11 Saturation magnetization of the synthesized Co/C-PAMAM G2 (**7**) (red line) and Co/C-PS-PAMAM G2 (**8**) (green line) in comparison to pristine Co/C (**1**).

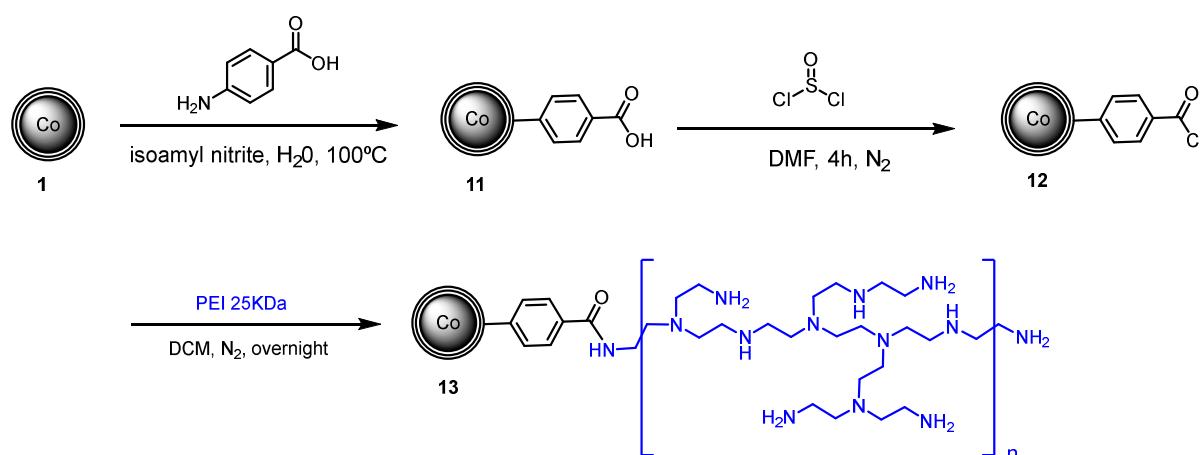
Polyethylenimine (PEI) has been used to functionalize magnetic nanoparticles making them water stable through its high density of amine groups. Several studies describe the grafting of commercially available PEI with different molecular weights to the surface of different nanoparticles.⁵¹⁻⁵³

Following a “grafting to” strategy reported by Lellouche *et al.*,⁵¹ commercial PEI (25 KDa) was attached on divinyl sulfone (DVS) functionalized nanoparticles (Scheme 4). For this purpose, DVS, which is a homobifunctional molecule, was used to react with the amine groups of Co/C-NH₂ (**3**) by rapid Michael additions. The subsequent addition of branched PEI to the readily prepared Co/C-DVS (**9**) resulted in PEI-coated MNPs (**10**). The total content of nitrogen for Co/C-PEI (**10**) was estimated to be 0.36 mmol per gram of nanomaterial by elemental microanalysis. Repeating both steps, an increase in the nitrogen loading to 0.64 mmol per gram was achieved. Unfortunately, even at such loadings the dispersibility of the nanoparticles in aqueous phase was not improved.



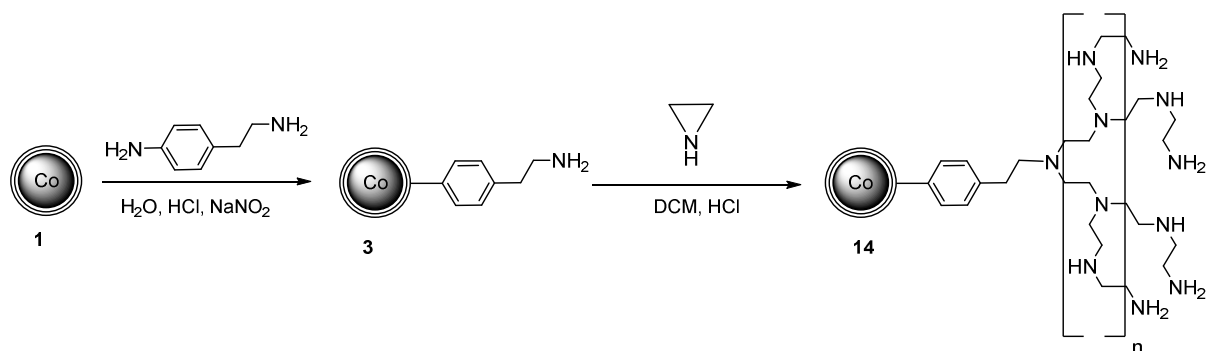
Scheme 4 Synthesis of Co/C-PEI (**10**) by Michael addition of DVS and subsequent reaction of CO/C-DVS (**9**) with branched PEI (25 KDa).

Another approach reported by Adronov *et al.*⁵³ for the PEI functionalization of carbon nanotubes (CNTs), revealing impressive solubility in aqueous solution, was tested for the Co/C MNPs (Scheme 5). Here, benzoic acid was first attached to the pristine Co/C nanoparticles (**1**) by diazonium chemistry. This step was carried out using two different reaction conditions: (1) the one described in Scheme 4 and (2) the conditions usually described for the diazonium chemistry applied to these Co/C nanobeads described e.g. in Scheme 2 for the synthesis of Co/C-NH₂ (**3**). As a result it was found that route (1) resulted in 10 times higher loadings of benzoic acid than route (2). Thus, Co/C-COOH (**11**) from route (1) were used to react with thionyl chloride producing chloride acid functionalized nanoparticles (Co/C-COCl) (**12**). The last step consisted on the reaction of Co/C-COCl (**12**) with a large excess of branched PEI resulting in PEI-coated Co/C nanoparticles (**13**) with a total content of nitrogen estimated to be 0.7 mmol per gram of nanomaterial. However, once more the developed polymer coating revealed to be insufficient to enhance the dispersibility of the MNPs (**13**) in aqueous phase. Together with the results showed for the “clicking” of PAMAM on Co/C-N₃ MNPs these findings confirm the unsatisfactory polymer loading to the nanoparticles following a “grafting to” methodology.



Scheme 5 Grafting of PEI (25 KDa) to Co/C-COCl nanoparticles (**12**). First benzoic acid is attached to the nanoparticles via diazonium chemistry giving Co/C-COOH (**11**). Subsequently (**11**) are reacted with thionyl chloride to produce Co/C-COCl (**12**) which are subsequently reacted with branched PEI resulting on Co/C-PEI (**13**).

In contrast, Leong *et al.*, have shown that the direct polymerization of aziridine under acidic conditions leads to higher amounts of polymer covalently attached to the surface of CNTs.⁵⁴ Therefore, a “grafting from” approach of the PEI onto the MNPs by aziridine polymerization on the surface of Co/C-NH₂ (**3**) was attempted. Using 1000 equivalents of aziridine, Co/C-PEI nanoparticles (**14**) were obtained (Scheme 6) with a loading of 10-14 mmol amino functionalities per gram of nanomaterial based on the nitrogen content determined by elemental analysis or by TGA measurements.³²



Scheme 6 Synthesis of Co/C-PEI (**14**) by aziridine polymerization on the surface of Co/C-NH₂ (**3**), under acidic conditions.³²

The chemical structure of PEI-coated MNPs (**14**) was identified by infrared spectroscopy. As shown in Fig. 12, the recorded spectrum reveals the characteristic peaks of PEI at 3417 cm⁻¹ (N-H stretching), 2934-2812 cm⁻¹ (C-H stretching), 1604 cm⁻¹ (N-H bending), 1458 cm⁻¹ (C-H bending) and 1350-1000 cm⁻¹ (C-N stretching).⁵⁵

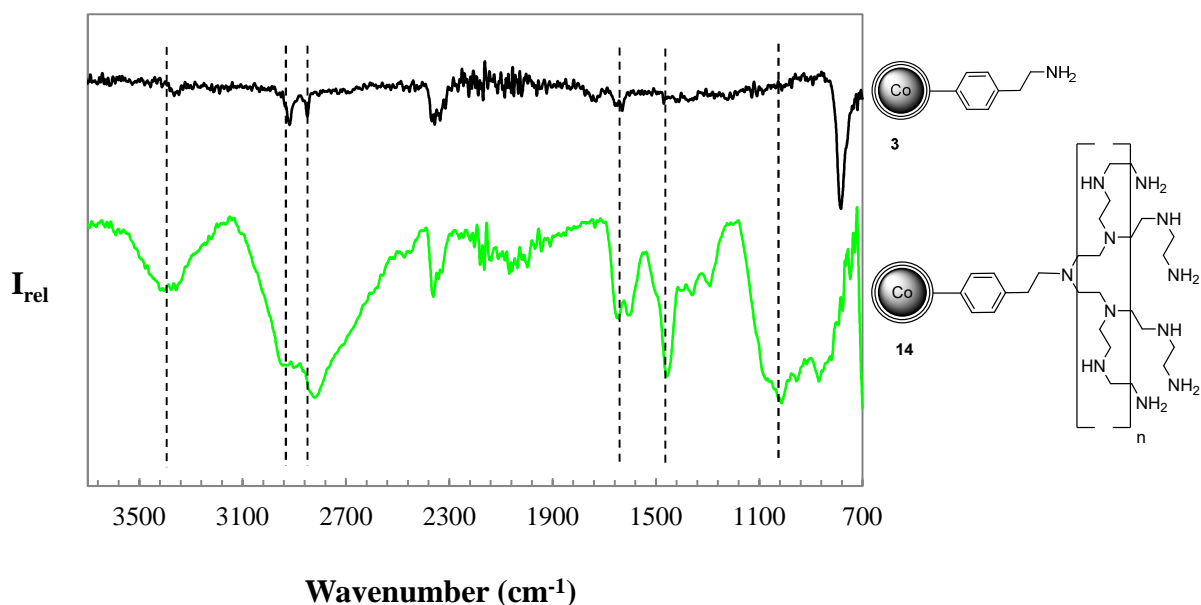


Fig. 12 Characteristic ATR-IR spectra of Co/C-NH₂ (**3**) (black line) and Co/C-PEI (**14**) (green line).

Moreover, as shown in Fig. 13, TEM analysis indicated that Co/C-PEI (**14**) consisted of discrete particles contrasting the pristine Co/C nanoparticles showed in Fig. 1 where major agglomeration can be observed. The magnetization of Co/C-PEI was considerably decreased to 39 emu.g⁻¹ (Fig. 14). This reduction is consistent with the significant gain in mass of the PEI-polymer (60 wt% by TGA). Indeed, this nanomaterial proved to form stable dispersions in water over days with no tendency for agglomeration or sedimentation. Interestingly, this tendency was also observed in a biphasic systems with dichloromethane present as a second layer (see Fig. 14 right flask), contrasting the Co/C-PAMAM particles (**7**) and (**8**), as well as the PEI-coated nanoparticles (**10**) and (**13**) described above.

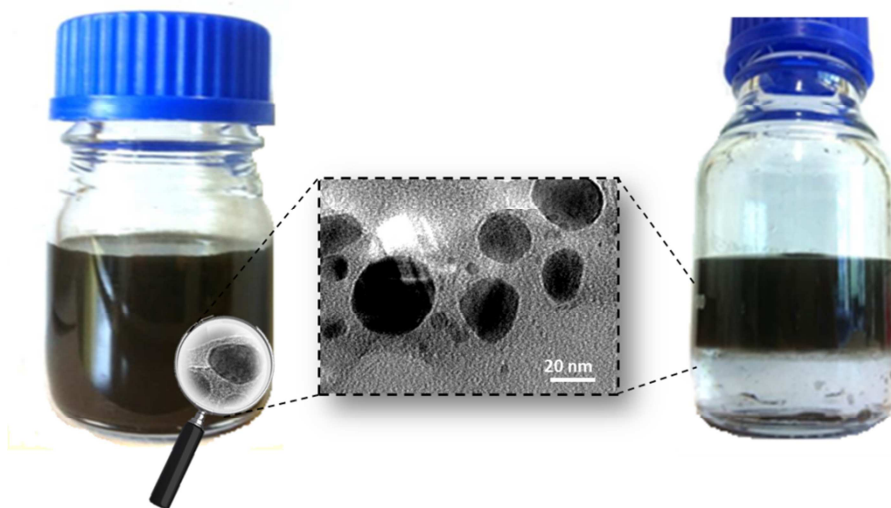


Fig. 13 Stability of Co/C-PEI (**14**) in water (left flask) and in biphasic system (Water/DCM – right flask). The stability is also confirmed from the TEM micrograph where single MNPs can be distinguished. The scale bar is 20 nm.

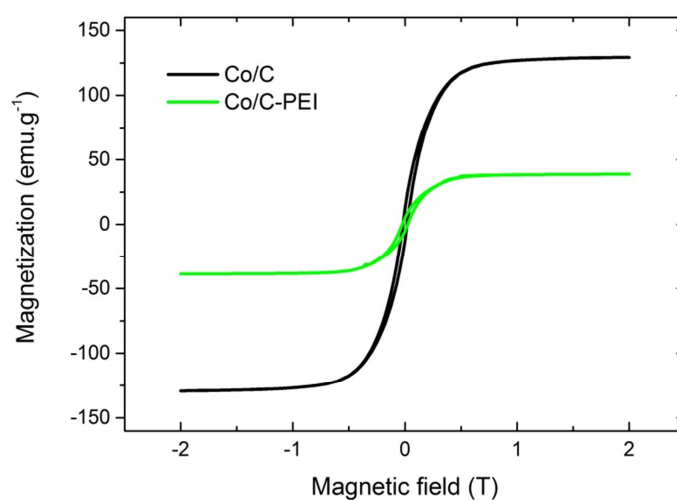


Fig. 11 Saturation magnetization of Co/C-PEI (**14**) (green line) in comparison to pristine Co/C (**1**) (black line).

These nanoparticles proved their stability over months in aqueous solution, opening the possibility their use in biotechnological applications. On the contrary if freeze-dried, the particles can be well re-dispersed in water or polar solvents and collected by an external magnet, as shown in Fig. 15. This makes them also interesting for applications in chemical processes where water is used as the solvent or in water bioremediation as it is discussed later in chapter 2.

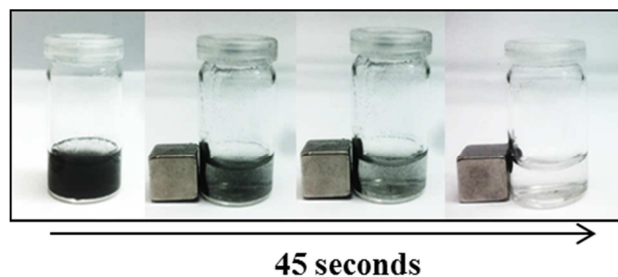
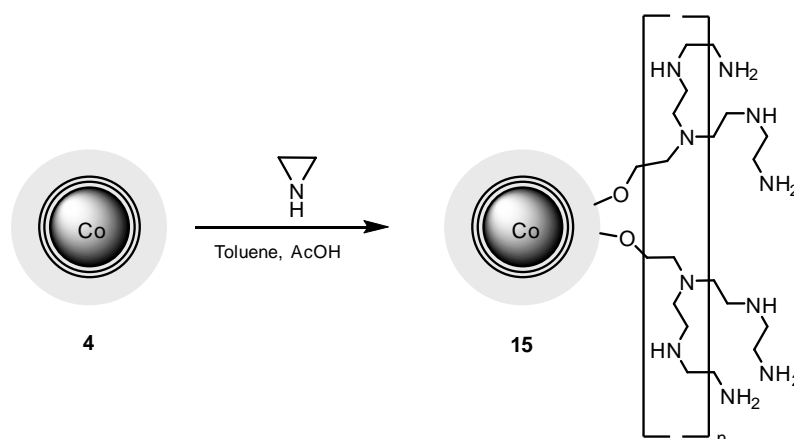


Fig. 15 Lyophilized Co/C-PEI (**14**) re-dispersion by sonication (5 minutes) and collection with an external magnet. The recovery is done in a few seconds after putting the magnet on the side of the flask.

1.4 Combined silica-polymer coating on magnetic Co/C nanoparticles

Once optimized the synthesis and development of polymeric and inorganic silica coatings on top of Co/C MNPs, the combination of both strategies was studied and the stability in solution for different solvents was evaluated. PEI-coated MNPs (**14**) showed very good stability in water, but not in organic solvents. For instance, in DCM these MNPs are not dispersible even using sonication. Aiming to produce a more versatile material, containing a high density of NH_2 reactive groups while being dispersible also in organic solvents, the combination of both types of coatings was studied. To achieve this purpose, first the silica shell was implemented as described in Scheme 2. Then, aziridine polymerization was carried out using the conditions described by Lindén *et al.* for grafting PEI on the surface of silica materials (Scheme 7).⁵⁶



Scheme 7 Synthesis of Co/C@SiO₂-PEI (**15**) from Co/C@SiO₂ (**4**) by polymerization of aziridine under acidic conditions.

The presence of hyperbranched PEI, which was grown from the free hydroxyl groups on the outer silica shell, was confirmed by IR spectroscopy. From Fig. 16 one can see that the starting material **4** exhibit only the bands for silica, at 1100cm^{-1} and $950\text{-}800\text{cm}^{-1}$, while the spectra of Co/C@SiO₂-PEI (**15**) matches also with minor shifts the peaks assigned to Co/C-PEI (**14**) at 3417 cm^{-1} (N-H stretching), $2934\text{-}2812\text{ cm}^{-1}$ (C-H stretching), 1604 cm^{-1} (N-H bending), 1458 cm^{-1} (C-H bending) and $1350\text{-}1000\text{ cm}^{-1}$ (C-N stretching).

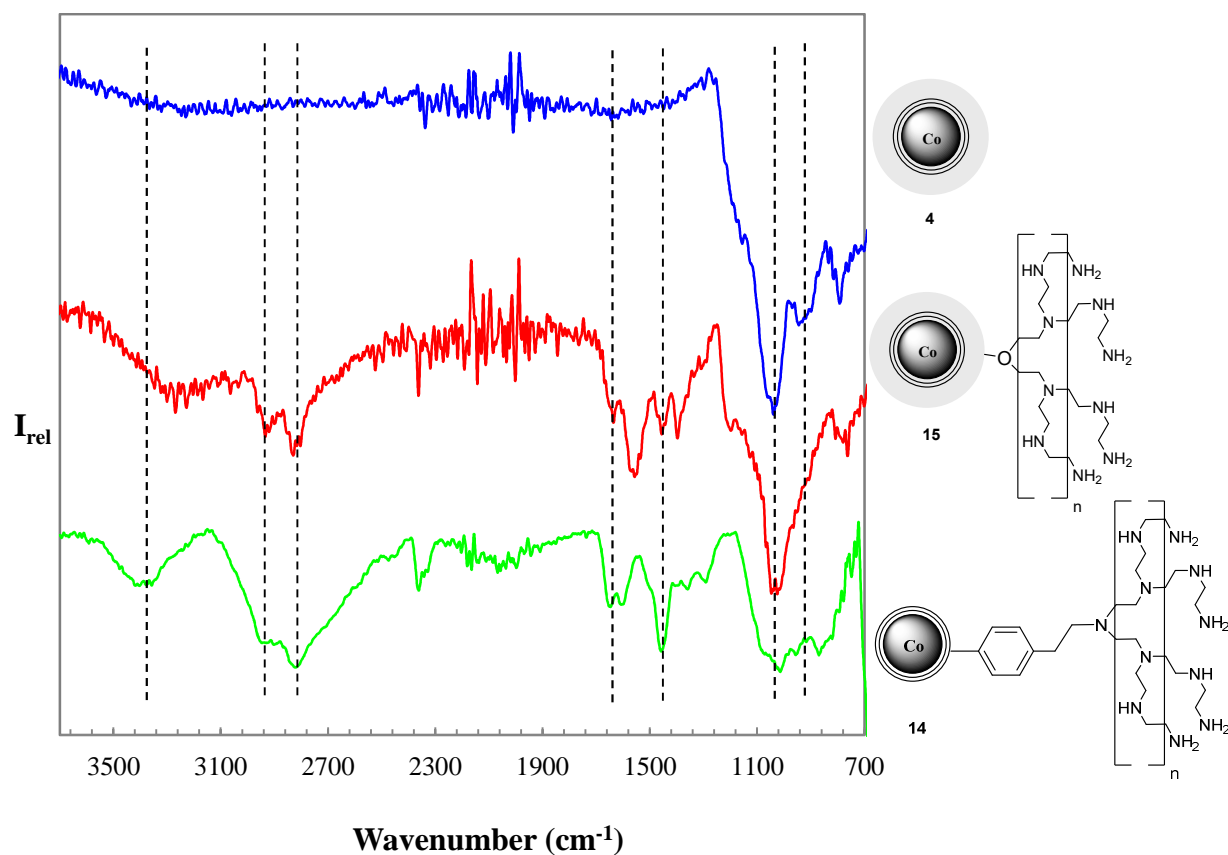


Fig. 16 Characteristic ATR-IR spectra for Co/C@SiO₂ (**4**) (blue line), Co/C-PEI (**14**) (green line) and Co/C@SiO₂-PEI (**15**) (red line).

As expected, the saturation magnetization measured for Co/C@SiO₂-PEI (**15**) (45 $\text{emu}\cdot\text{g}^{-1}$) drops to comparable values of those found for Co/C-PEI (**14**) due to the gain in mass during the polymerization (see Fig. 17).

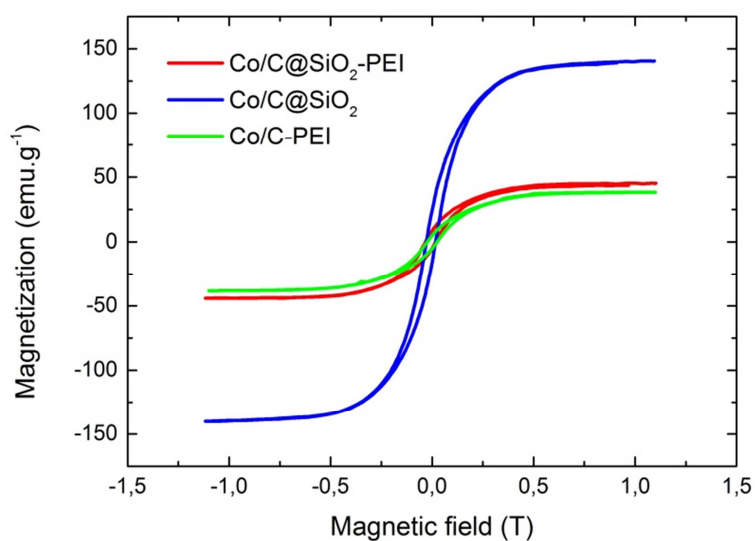


Fig. 17 Saturation magnetization for Co/C@SiO₂ (**4**) (blue line), Co/C-PEI (**11**) (green line) and Co/C@SiO₂-PEI (**12**) (red line).

Regarding the dispersibility in solution of these MNPs it was found that the combination of silica and PEI indeed result in a nanomaterial, highly loaded with amino groups, which can be easily dispersed in both aqueous and organic systems. Fig. 18A shows, the dispersion of Co/C@SiO₂-PEI (**15**) in water, DCM and ethanol, proving the improvement achieved when comparing with the Co/C-PEI (**14**) which revealed a great stability in water systems but not in organic media. The stability of the beads was also confirmed for other organic solvents such as: NMP, DMA and DMF. Moreover, the materials can be collected, using a magnet, within less than a minute as depicted in Fig. 18B. This outcome enlarges the range of applications suitable to Co/C nanoparticles especially as supports for catalysis and scavengers for intermediate reagents.

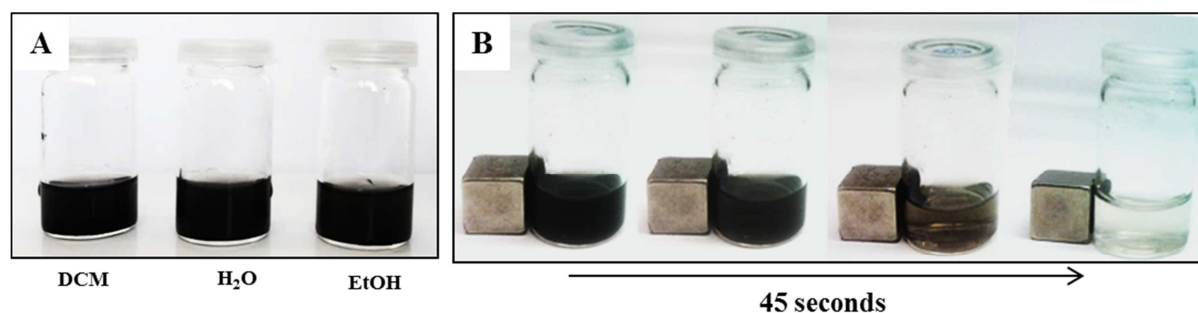


Fig. 18 Co/C@SiO₂-PEI (**15**) dispersibility in water, DCM and ethanol (A) and recovery from solution applying an external magnet (B).

1.5 Outlook and applications

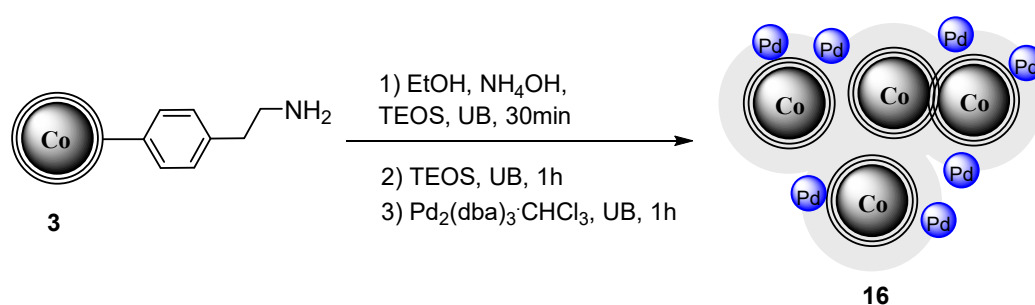
As described along this chapter, Co/C MNPs offer the advantage of easy and fast collection applying an external magnet due to their extremely high magnetic moment. However, this feature brings also disadvantages considering their dispersibility in solution. Typically continuous sonication or strong stirring are applied to ensure the dispersion of such nanoparticles. Unfortunately, for industrial applications this is not always possible. Rather than sonication or stirring, industrial reactors usually offer the possibility of simple shaking. For this reason better dispersion of the nanobeads in diverse solvents is required. Therefore, the aim of this project was to develop different surface coatings to stabilize the dispersion of Co/C MNPs in solution, improving their performance and increasing the range of applications possibly given to these nanobeads. Both silica and polymers were grafted on the surface and the obtained magnetic materials fully characterized and compared in terms of dispersibility and easiness of recovery. Similarly the combination of the two coatings was tested giving promising results for developing a more versatile material dispersible both in aqueous and organic phase.

Silica coated magnetic nanoparticles, showed much better dispersibility in solution than the pristine MNPs (**1**) without compromising the high magnetization of the materials, which are easily and fast collected with a magnet. Bringing and maintaining them dispersed in solution requires a simple

shaking of the flask. On the other hand, PEI-coated MNPs (**14**) showed a surprising stability in water which might be interesting for using these materials in biotechnological applications. If kept in solution these materials seem to be stable over months of incubation. Once lyophilized, despite the significant decrease in the magnetization mass of these samples, they could still be recovered from solution within few seconds of collection with an external magnet.

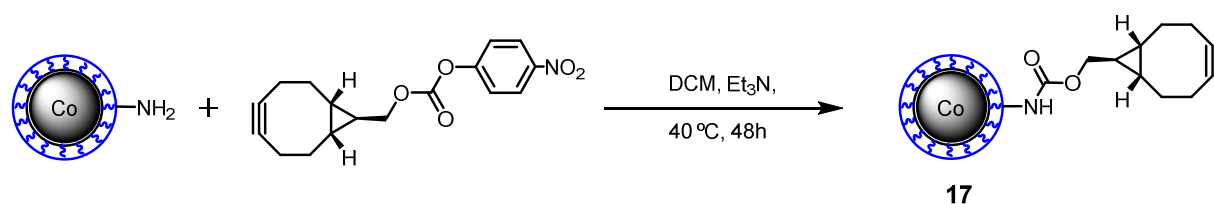
Different applications have been explored for the developed magnetic supports. Generally it was found that a “grafting from” approach leads to higher polymeric functionalization of the nanoparticles and consequently better dispersions than a “grafting to” methodology. Polymer coated-MNPs have been used as scavengers for metal recovery from contaminated water samples proving the great recyclability and potential of Co/C-PEI nanomagnets (**14**) to be used in a real upscale process (described in detail in chapter 2). PEI-coated nanomaterials show a much better performance than the PAMAM-coated ones specifically due to the improvement in aqueous dispersion and the higher amount of amine groups available on the surface. Their potential in catalysis was also explored by incorporating Pd nanoparticles and testing them for hydrogenation reactions. Additionally, other metals such as Ru, Pt and Au have been successfully incorporated and are very promising for being used in catalytic reactions having water as the solvent, which is not possible for Co/C MNPs (**1**).

Similarly, Co/C@SiO₂ were used as a platform for incorporating metals and their use in catalysis was explored. Fe, Ru and Pd were successfully incorporated with loadings of: 0.06, 0.11 and 0.17 mmol of catalyst per gram of material. The amount of catalyst incorporated can be tuned by changing the initial amount of the respective precursor added to the synthesis. Given the work which has been done on Co/C nanoparticles for catalytic applications using Pd as the active catalyst,^{1,3} Pd-doped silica-coated magnetic nanoparticles (Co/C@SiO₂@Pd) were also prepared and their performance compared to the previous developed systems. The synthesis of these nanobeads was done according to Scheme 8. The procedure is adapted from the synthesis of Co/C@SiO₂ (**4**) adding Pd₂(dba)₃·CHCl₃ complex while growing the silica shell. These catalysts have shown promising results for Suzuki-Miyaura coupling reactions between phenyl boronic acid and aryl halide (iodide and bromide), using very low amounts of catalyst (0.1 and 0.3, respectively) and short reaction times in the microwave, allowing the recyclability of the catalyst for at least 6 cycles.



Scheme 8 Synthesis of Pd-incorporated Co/C@SiO₂ MNPs (**13**). The same procedure was followed to incorporate ruthenium and iron.

Moreover, the potential of Co/C-PEI (**14**) and Co/C@SiO₂-PEI (**15**) MNPs for being used as reagent scavengers has been studied in collaboration with Dr. Peter Meier from NOVARTIS (Basel, Switzerland). ((1R,8S,9s)-bicyclo[6.1.0]non-4-yn-9-yl)methyl 4-nitrophenyl carbonate (here referred as BCN ligand) was attached on the surface of the amine-functionalized magnetic beads following the synthesis depicted in Scheme 9. The resulting Co/C-BCN nanoparticles exposing the triple bond were explored for scavenging a variety of azide-tagged molecules revealing very promising results. The high loading of amino groups on nanoparticles (**14**) and (**15**) allows higher loadings of the BCN ligand thus reducing the amount of nanoparticles needed for the copper-free click reaction of different azide-labeled molecules.



Scheme 9 Synthesis of BCN-functionalized particles (**17**) from PEI-functionalized nanomaterials (**14**) and (**15**).

1.6 Experimental section

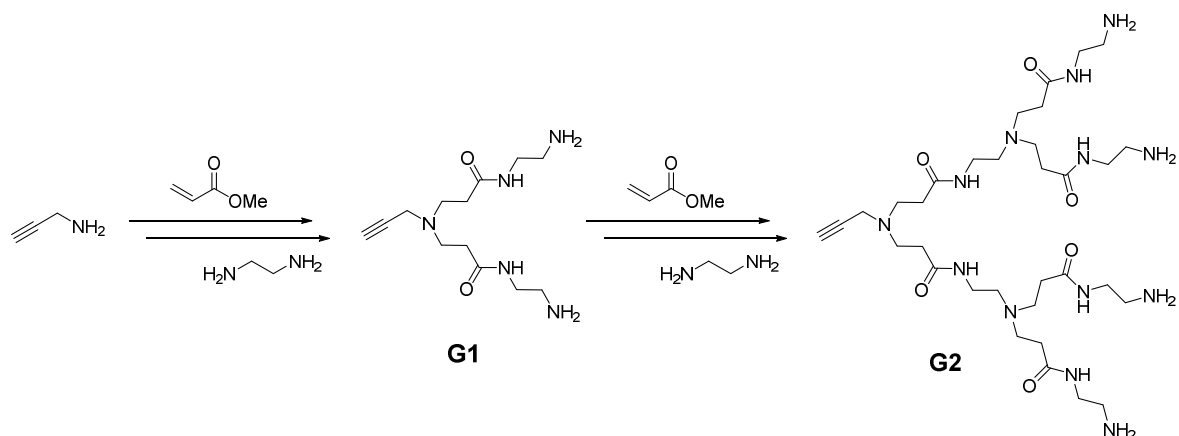
Materials and methods

The Co/C nanomagnets (**1**) were purchased from Turbobeads Llc, Switzerland. Prior to use, they were washed in a concentrated HCl / water mixture (1:1) 5 times for 24 h. Acid residuals were removed by washing with Millipore water (5x) and the particles were dried at 50°C in a vacuum oven.⁵⁷ The magnetic nanobeads were dispersed using an ultrasonic bath and recovered with the aid of a neodymium based magnet (15 x 30 mm). ATR-IR was carried out on a Biorad Excalibur FTS 3000, equipped with a Specac Golden Gate Diamond Single Reflection ATR-System or a Varian FTS 1000 spectrometer. Elemental microanalysis was carried out by the micro analytical department of the University of Regensburg using a Vario EL III or Mikro-Rapid CHN apparatus (Heraeus).

The ICP-OES was measured on a Spectroflame EOP (Spectro) at the University of Regensburg. Thermogravimetric analysis (TGA) was done on a TGA 7 (Perkin Elmer). The magnetization measurements and TEM pictures of all silica-encapsulated nanoparticles was done at the Trinity College of Dublin, while for all the other samples both characterizations were performed at the Physics Faculty of the University of Regensburg.

Amine-functionalized nanoparticles (**3**)³³, azide-functionalized nanoparticles (**5**)^{58,59} and azide-functionalized polystyrene-coated nanoparticles (**6**)²⁵ were prepared on the gram scale following previously reported procedures.

Synthesis of PAMAM dendrons



Scheme 7 Divergent synthesis of clickable PAMAM dendrons with propargyl amine at the focal point.

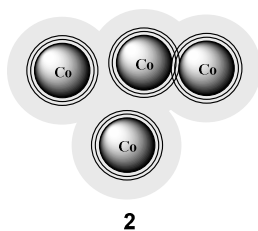
The synthesis of PAMAM dendrons was done according to a procedure described elsewhere.⁴⁷ Herein, propargyl amine (1.0 equiv.) was reacted with methyl acrylate (83 equiv.) under N_2 at room temperature giving rise to the dendron G0.5 (95%). Then, ethylenediamine (60 equiv.) was added (1.0 equiv.) to yield dendron G1 with two amino functional groups (98%). After repetition of these two steps, second generation dendrons could be obtained in good yields (88%). For every half-generation dendron purification by silica column chromatography was performed. NMR and EI-MS are in accordance with the literature values.⁴⁷

Nomenclature of the magnetic nanoparticles

The nomenclature of the beads is done as follows:

Co/C	Carbon-coated cobalt nanoparticles
Co/C@SiO ₂	Silica-encapsulated carbon-coated cobalt nanoparticles
Co/-NH ₂	Amine -functionalized carbon-coated cobalt nanoparticles
Co/C -N ₃	Azide-tagged carbon-coated cobalt nanoparticles
Co/C-PAMAM G2	Second generation PAMAM-functionalized carbon-coated cobalt nanoparticles
Co/C-PS-N ₃	Azide-tagged polystyrene-coated carbon-coated cobalt nanoparticles
Co/C-PS-PAMAM G2	Second generation PAMAM-functionalized polystyrene-coated carbon-coated cobalt nanoparticles
Co/C-DVS	Divinyl sulfone functionalized carbon-coated cobalt nanoparticles
Co/C-COOH	Benzoic acid functionalized carbon-coated cobalt nanoparticles
Co/C-COCl	Chloride acid functionalized carbon-coated cobalt nanoparticles
Co/C-PEI	PEI-functionalized carbon-coated cobalt nanoparticles
Co/C@SiO ₂ -PEI	PEI-functionalized silica-encapsulated carbon-coated cobalt nanoparticles
Co/C@ SiO ₂ @Pd	Palladium doped silica-encapsulated carbon-coated cobalt nanoparticles
Co/C-BCN	BCN ligand-functionalized carbon-coated cobalt nanoparticles

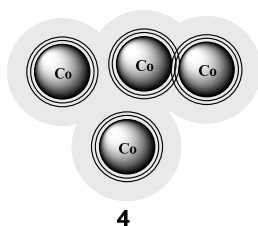
Synthesis of Co/C@SiO₂ (2)



The synthesis of Co/C@SiO₂ (2) was adapted from a procedure described in the literature for silica coating of CNTs.³⁴ Typically, 50 mg of Co/C (1) were dispersed in 50 mL of EtOH together with the desired amount of CTAB (0.1, 1 or 3 g) and sonicated for 1h. Then, the NPs were decanted in order to remove non-attached CTAB and re-dispersed in 20 mL of EtOH for 30 minutes. When a stable dispersion is obtained, 2mL of NH₄.OH (32%) is added to the solution and sonicated for 2 minutes, followed by the addition of a TEOS solution (0.5 mL in 20 mL of EtOH) in a dropwise manner. Sonication was done for 90 minutes and then the reaction was left to stir overnight. In the end the MNPs (2) were magnetically decanted, intensively washed with EtOH and dried under vacuum.

IR (v/cm⁻¹) (0.1 g CTAB): 1067, 943, 789; (1 g CTAB): 1057, 957, 802; (3 g CTAB): 1058, 937, 787.

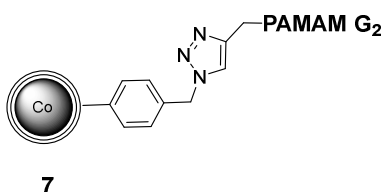
Synthesis of Co/C@SiO₂ (4)



In a typical synthesis, 50 mg of Co/C-NH₂ (3) were sonicated in 100 mL of EtOH and 8 mL of NH₄.OH (32%) for 30 minutes. Then, TEOS (2, 0.2 or 0.05 mL) was added into the solution reacted for 2 hours. After completion of the reaction time, the obtained MNPs (4) were intensively washed with EtOH and dried under vacuum.

IR (v/cm⁻¹) (2%TEOS): 1074, 929, 786; (0.2%TEOS): 1039, 987, 779; (0.05%TEOS): 1080, 777.

Synthesis of Co/C-PAMAM G2 (7)



In a typical experiment, 100 mg of azide functionalized nanoparticles (0.019 mmol (N_3) per gram nanoparticles, 0.007 mmol) (**5**) and 5 equivalents (70 mg, 0.095 mmol) of the second generation PAMAM dendron, containing 4 functional groups, were used. The PAMAM was previously dissolved in 5 mL of degassed THF/ H_2O (3:1) mixture followed by the successive addition of Co/C- N_3 (**5**), Na-ascorbate (30 mol%, 0.029 mmol, 5.75 mg) and $CuSO_4$ (10 mol%, 0.0095 mmol, 2.37 mg). Afterwards the reaction mixture was sonicated for 15 minutes and stirred for 48 hours at room temperature. The magnetic nanoparticles were separated applying an external magnet and washed with acetone (5x 5 mL), H_2O (5x 5 mL) and acetone (3x 5 mL). In the end, the nanobeads were dried under vacuum. The reactions were monitored by ATR-IR, evaluating the attenuation of the azide peak (Fig. 10) and the loadings estimated by TGA (Fig. 19).

Co/C-PAMAM (**7**): TGA (N_2): 0.02 mmol.g⁻¹; 1.4 % mass loss.

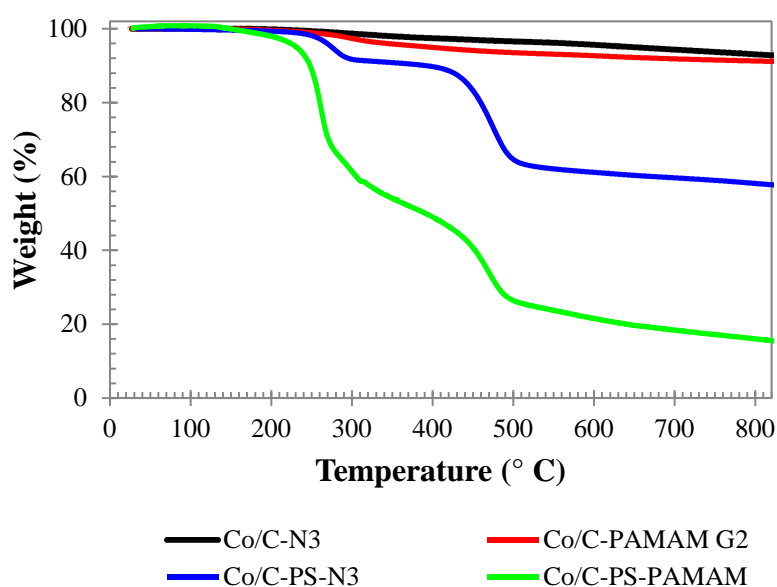
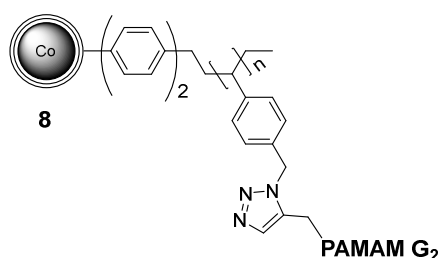


Fig. 19 TGA spectra of the azide tagged nanoparticles (**5**) (black) and (**6**) (blue) and the subsequent PAMAM-clicked magnetic beads (**7**) (red) and (**8**) (green). The loadings can be estimated from the weight loss % of the materials.

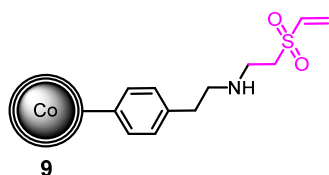
Synthesis of Co/C-PS-PAMAM G2 (**8**)



In a typical experiment, 100 mg of azide functionalized nanoparticles (**8**) (2.42 mmol (N₃) per gram nanoparticles, 0.242 mmol) (**5**) and 5 equivalents (894 mg, 1.21 mmol) of the second generation PAMAM dendron, containing 4 functional groups, were used. The PAMAM was previously dissolved in 5 mL of degassed THF/H₂O (3:1) mixture followed by the successive addition of Co/C-PS-N₃ (**8**), Na-ascorbate (30 mol%, 0.363 mmol, 72 mg) and CuSO₄ (10 mol%, 0.121 mmol, 30 mg). Afterwards the reaction mixture was sonicated for 15 minutes and stirred for 48 hours at room temperature. The magnetic nanoparticles were separated applying an external magnet and washed with acetone (5x 5 mL), H₂O (5x 5 mL) and acetone (3x 5 mL). In the end, the nanobeads were dried under vacuum. The reactions were monitored by ATR-IR, evaluating the attenuation of the azide peak (Fig. 10) and the loadings estimated by TGA (Fig. 19).

Co/C-PS-PAMAM (**8**): TGA (N₂): 0.6 mmol.g⁻¹; 42 % mass loss.

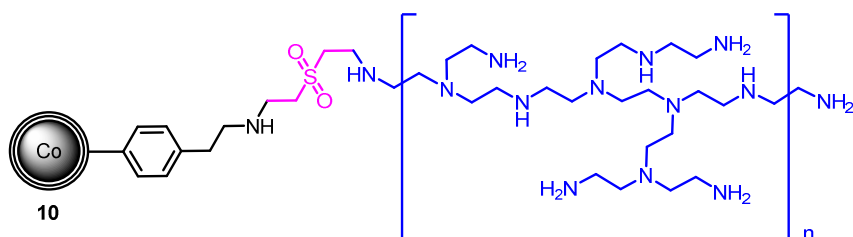
Synthesis of Co/C-DVS (**9**)



Co/C-NH₂ (**3**) (500 mg, 0.05 mmol, 1.0 equiv.) were dispersed in 20 mL of *i*-PrOH in the ultrasonic bath for 5 minutes. A solution of DVS (10 μL, 0.15 mmol, 3 equiv.) in 5 mL of *i*-PrOH was added to the reaction and the mixture sonicated for 5 minutes more followed by vigorously stirring for 2 hours. Finally Co/C-DVS (**9**) were washed three times with *i*-PrOH and dried under vacuum.

Elemental microanalysis [%]: Co/C (**3**): C, 10.5; H, 0.2; N, 0.14; Co/C-DVS (**9**): C, 10.6; H, 0.2; N, 0.14; Loading (C): 0.02 mmol.g⁻¹.

Synthesis of Co/C-PEI (**10**)

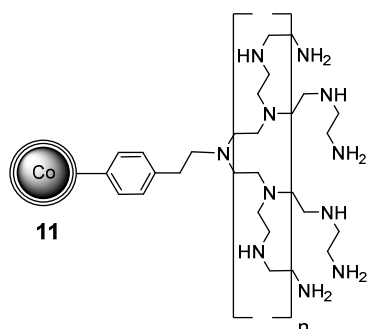


Co/C-DVS (**9**) (500 mg, 0.01 mmol) were dispersed in 20 mL of *i*-PrOH in the ultrasonic bath during 5 minutes. 500 mg of branched PEI (25 KDa) was dissolved in 5 mL of *i*-PrOH and the solution added to the nanoparticles dispersion. The reaction was left in ultrasonic bath for 5 minutes and after stirred

55°C over a period of 4 hours. The resulting PEI-coated nanoparticles (**13**) were washed with DMF (3x), water (3x) and diethyl ether (2x) and freeze dried for elemental microanalysis.

Elemental microanalysis [%]: C, 14.18; H, 0.89; N, 1.87; Loading (N): 0.7 mmol·g⁻¹.

Synthesis of Co/C-PEI (**14**)³²



In a typical experiment, amine-functionalized Co/C MNPs (**3**)²³ (100 mg, 0.015 mmol, 1.0 equiv.), were pre-dispersed in 10 mL DCM using an ultrasonic bath for 15 min. Under stirring, aziridine (778 μL, 15 mmol, 1000 equiv.) and catalytic amounts of conc. HCl (15 μL, 15 M) were added to the reaction mixture which was heated up to 80 °C for 24 h. Afterwards, the NPs were collected using an external magnet, washed with DCM (2x 50 mL), H₂O (5x 50 mL) and again DCM (3x 50 mL). In the end, the beads were re-dispersed in water or freeze-dried. The extent of polymerization was estimated by TGA (59 wt%), as depicted in Fig. 20.

IR (v/cm⁻¹): 3417, 2934, 2821, 2362, 1648, 1604, 1458, 1351, 1298, 1014.

Elemental microanalysis [%]: C, 28.69; H, 5.30; N, 13.27; Loading (N): 9.5 mmol·g⁻¹.

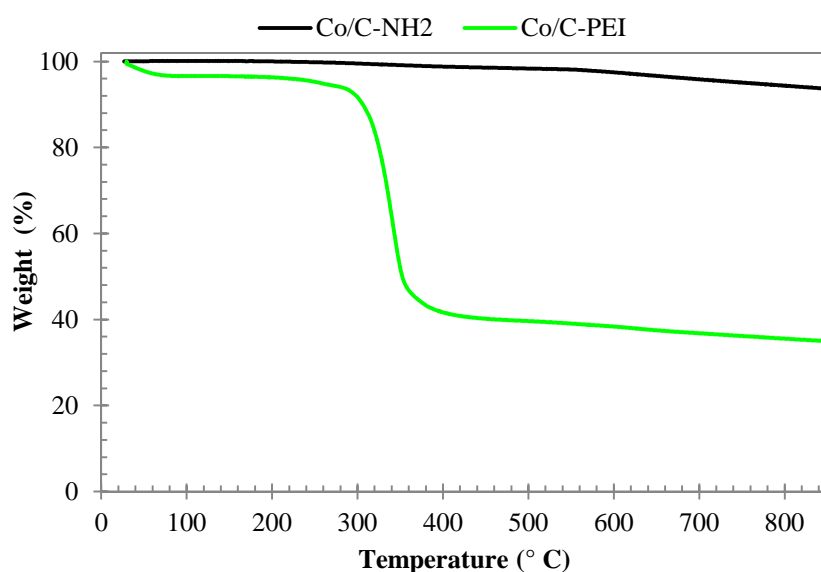
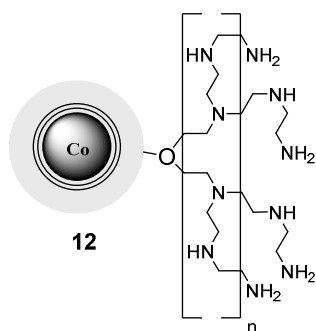


Fig. 20 TGA analysis of the amine-coated Co/C nanoparticles (**3**) (black) and PEI-coated MNPs (**14**) (green) to estimate % of polymerization.

Synthesis of Co/C@SiO₂-PEI (15)



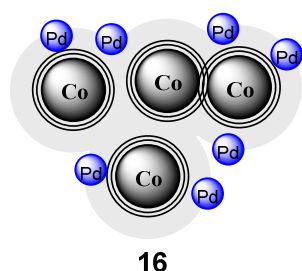
Adapted from a procedure described in literature.⁵⁶ Under a nitrogen controlled atmosphere, 60 mg of Co/C@SiO₂ (**4**) were dispersed in 3 mL of toluene together with 6 μ L of acetic acid, for 5 minutes by sonication. Then, 360 μ L of aziridine were added and the reaction refluxed under N₂ for 24 hours.

The washing was performed 5 times with toluene and the obtained Co/C@SiO₂-PEI (**15**) freeze-dried.

IR (v/cm⁻¹): 3408, 2926, 2844, 1631, 1524, 1485, 1419, 1051, 771.

Elemental microanalysis [%]: C, 10.38; H, 2.03; N, 3.35; Loading (N): 1.5 mmol N /g.nanoparticles

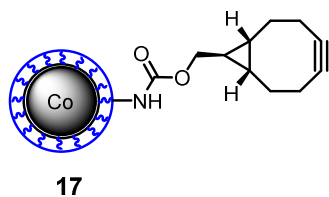
Synthesis of Co/C@SiO₂@Pd (16)



250 mg of Co/C-NH₂ (**3**) were sonicated in 500 mL of EtOH and 40 mL of NH₄.OH (32%) for 30 minutes. TEOS (2, 0.2 or 0.05 mL) was added into the solution and reacted for 1 hour, after which Pd₂(dba)₃·CHCl₃ (50 mg, 0.048 mmol) was added. The mixture was sonicated for 1 hour more. After completion of the reaction time, the obtained Co/C@SiO₂@Pd (**16**) were intensively washed with EtOH and dried under vacuum.

The amount of incorporated metal per nanoparticles was estimated by ICP to be 0.107 mmol.g⁻¹.

Synthesis of Co/C-BCN (17)



In a typical experiment, 100 mg of Co/C-PEI (**14**) (0.177 mmol N) were dispersed in 4 mL anhydrous DCM in the ultrasonic bath for 10 minutes, under nitrogen atmosphere. After, Et₃N (740 μL, 5.31 mmol, 30 equiv.) and BCN ligand (111 mg, 0.354 mmol, 2 equiv.) are added to the mixture which is left to stir at 40°C during 48h. In the end of the reaction, the resulting BCN-functionalized nanoparticles (**17**) were washed with DCM (5x) and freeze-dried.

1.7 References

1. Kainz, Q. M.; Linhardt, R.; Grass, R. N.; Vilé, G.; Pérez-Ramírez, J.; Stark, W. J.; Reiser, O. *Advanced Functional Materials* **2014**, 24, (14), 2020-2027.
2. Lu, A.-H.; Schmidt, W.; Matoussevitch, N.; Bönemann, H.; Spliethoff, B.; Tesche, B.; Bill, E.; Kiefer, W.; Schüth, F. *Angewandte Chemie International Edition* **2004**, 43, (33), 4303-4306.
3. Wittmann, S.; Schätz, A.; Grass, R. N.; Stark, W. J.; Reiser, O. *Angewandte Chemie International Edition* **2010**, 49, (10), 1867-1870.
4. Bruns, O. T.; Itrich, H.; Peldschus, K.; Kaul, M. G.; Tromsdorf, U. I.; Lauterwasser, J.; Nikolic, M. S.; Mollwitz, B.; Merkel, M.; Bigall, N. C.; Sapra, S.; Reimer, R.; Hohenberg, H.; Weller, H.; Eychmüller, A.; Adam, G.; Beisiegel, U.; Heeren, J. *Nature Nanotechnology* **2009**, 4, (3), 193-201.
5. Fang, C.; Zhang, M. *Journal of Materials Chemistry* **2009**, 19, (35), 6258-6266.
6. Sokolova, V.; Epple, M. *Angewandte Chemie International Edition* **2008**, 47, (8), 1382-1395.
7. Guardia, P.; Di Corato, R.; Lartigue, L.; Wilhelm, C.; Espinosa, A.; Garcia-Hernandez, M.; Gazeau, F.; Manna, L.; Pellegrino, T. *ACS Nano* **2012**, 6, (4), 3080-3091.
8. Guardia, P.; Riedinger, A.; Nitti, S.; Pugliese, G.; Marras, S.; Genovese, A.; Matera, M. E.; Lefevre, C.; Manna, L.; Pellegrino, T. *Journal of Materials Chemistry B* **2014**, 2, (28), 4426-4434.
9. Deka, S. R.; Quarta, A.; Di Corato, R.; Riedinger, A.; Cingolani, R.; Pellegrino, T. *Nanoscale* **2011**, 3, (2), 619-629.
10. Chomoucka, J.; Drbohlavova, J.; Huska, D.; Adam, V.; Kizek, R.; Hubalek, J. *Pharmacological Research* **2010**, 62, (2), 144-149.
11. Mattingly, S. J.; O'Toole, M. G.; James, K. T.; Clark, G. J.; Nantz, M. H. *Langmuir* **2015**, 31, (11), 3326-3332.
12. Fernandes, S.; Eichenseer, C. M.; Kreitmeyer, P.; Rewitzer, J.; Zlateski, V.; Grass, R. N.; Stark, W. J.; Reiser, O. *RSC Advances* **2015**, 5, (58), 46430-46436.
13. Elliott, D. W.; Zhang, W.-x. *Environmental Science & Technology* **2001**, 35, (24), 4922-4926.
14. Takafuji, M.; Ide, S.; Ihara, H.; Xu, Z. *Chemistry of Materials* **2004**, 16, (10), 1977-1983.

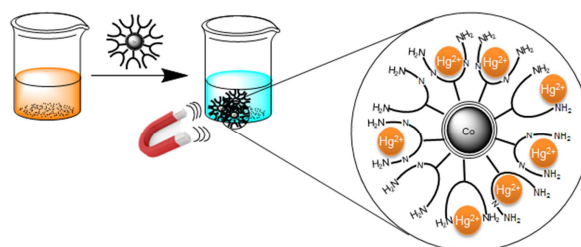
15. Liu, J.-f.; Zhao, Z.-s.; Jiang, G.-b. *Environmental Science & Technology* **2008**, 42, (18), 6949-6954.
16. Rofouei, M. K.; Rezaei, A.; Masteri-Farahani, M.; Khani, H. *Analytical Methods* **2012**, 4, (4), 959-966.
17. Lu, A.-H.; Salabas, E. L.; Schüth, F. *Angewandte Chemie International Edition* **2007**, 46, (8), 1222-1244.
18. Kainz, Q. M.; Reiser, O. *Accounts of Chemical Research* **2014**, 47, (2), 667-677.
19. Quarta, A.; Curcio, A.; Kakwere, H.; Pellegrino, T. *Nanoscale* **2012**, 4, (11), 3319-3334.
20. Singh, R. K.; Kim, T.-H.; Patel, K. D.; Knowles, J. C.; Kim, H.-W. *Journal of Biomedical Materials Research Part A* **2012**, 100A, (7), 1734-1742.
21. Liu, S.; Han, M.-Y. *Chemistry – An Asian Journal* **2010**, 5, (1), 36-45.
22. Bahadur, N. M.; Furusawa, T.; Sato, M.; Kurayama, F.; Siddiquey, I. A.; Suzuki, N. *Journal of Colloid and Interface Science* **2011**, 355, (2), 312-320.
23. Grass, R. N.; Athanassiou, E. K.; Stark, W. J. *Angewandte Chemie International Edition* **2007**, 46, (26), 4909-4912.
24. Seo, W. S.; Lee, J. H.; Sun, X. M.; Suzuki, Y.; Mann, D.; Liu, Z.; Terashima, M.; Yang, P. C.; Mc Connell, M. V.; Nishimura, D. G.; Dai, H. J. *Nature Materials* **2006**, 5, 971.
25. Kainz, Q. M.; Späth, A.; Weiss, S.; Michl, T. D.; Schätz, A.; Stark, W. J.; König, B.; Reiser, O. *ChemistryOpen* **2012**, 1, (3), 125-129.
26. Freitas, M.; Viswanathan, S.; Nouws, H. P. A.; Oliveira, M. B. P. P.; Delerue-Matos, C. *Biosensors and Bioelectronics* **2014**, 51, 195-200.
27. Zhang, L.; Li, P.; Li, H.; Wang, L. *Catalysis Science & Technology* **2012**, 2, (9), 1859-1864.
28. Shokouhimehr, M. *Catalysts* **2015**, 5, (2), 534.
29. Geng, J.; Jefferson, D. A.; Johnson, B. F. G. *Chemical Communications* **2004**, (21), 2442-2443.
30. Lu, A.-H.; Li, W.-C.; Matoussevitch, N.; Spliethoff, B.; Bonnemann, H.; Schuth, F. *Chemical Communications* **2005**, (1), 98-100.
31. Chan, H. B. S.; Ellis, B. L.; Sharma, H. L.; Frost, W.; Caps, V.; Shields, R. A.; Tsang, S. C. *Advanced Materials* **2004**, 16, (2), 144-149.
32. Kainz, Q. M.; Fernandes, S.; Eichenseer, C. M.; Besostri, F.; Korner, H.; Muller, R.; Reiser, O. *Faraday Discussions* **2014**, 175, 27-40.
33. Zeltner, M.; Grass, R. N.; Schätz, A.; Bubenhofer, S. B.; Luechinger, N. A.; Stark, W. J. *Journal of Materials Chemistry* **2012**, 22, (24), 12064-12071.
34. Zhang, M.; Wu, Y.; Feng, X.; He, X.; Chen, L.; Zhang, Y. *Journal of Materials Chemistry* **2010**, 20, (28), 5835-5842.
35. Baig, R. B. N.; Varma, R. S. *Chemical Communications* **2012**, 48, (50), 6220-6222.

36. Stutz, C.; Bilecka, I.; Thunemann, A. F.; Niederberger, M.; Borner, H. G. *Chemical Communications* **2012**, 48, (57), 7176-7178.
37. McCarthy, S. A.; Davies, G.-L.; Gun'ko, Y. K. *Nature Protocols* **2012**, 7, (9), 1677-1693.
38. Yang, Y.; Qiu, S.; Cui, W.; Zhao, Q.; Cheng, X.; Li, R. K. Y.; Xie, X.; Mai, Y.-W. *Journal of Materials Science* **2009**, 44, (17), 4539-4545.
39. Setyawan, H.; Fajaroh, F.; Widiyastuti, W.; Winardi, S.; Lenggoro, I. W.; Mufti, N. *Journal of Nanoparticle Research* **2012**, 14, (4), 1-9.
40. Laurent, S.; Forge, D.; Port, M.; Roch, A.; Robic, C.; Vander Elst, L.; Muller, R. N. *Chemical Reviews* **2008**, 108, 2064.
41. Dykes, G. M. *Journal of Chemical Technology & Biotechnology* **2001**, 76, (9), 903-918.
42. Pan, B.; Cui, D.; Sheng, Y.; Ozkan, C.; Gao, F.; He, R.; Li, Q.; Xu, P.; Huang, T. *Cancer Research* **2007**, 67, (17), 8156-8163.
43. Tomalia, D. A.; Fréchet, J. M. J. *Journal of Polymer Science Part A: Polymer Chemistry* **2002**, 40, (16), 2719-2728.
44. Tomalia, D. A.; Naylor, A. M.; Goddard, W. A. *Angewandte Chemie International Edition in English* **1990**, 29, (2), 138-175.
45. Liu, W.-M.; Xue, Y.-N.; Peng, N.; He, W.-T.; Zhuo, R.-X.; Huang, S.-W. *Journal of Materials Chemistry* **2011**, 21, (35), 13306-13315.
46. Kainz, Q. M.; Schätz, A.; Zöpfl, A.; Stark, W. J.; Reiser, O. *Chemistry of Materials* **2011**, 23, (16), 3606-3613.
47. Lin, Y.-J.; Tsai, B.-K.; Tu, C.-J.; Jeng, J.; Chu, C.-C. *Tetrahedron* **2013**, 69, (7), 1801-1807.
48. Schätz, A.; Grass, R. N.; Stark, W. J.; Reiser, O. *Chemistry – A European Journal* **2008**, 14, (27), 8262-8266.
49. Kainz, Q. M.; Zeltner, M.; Rossier, M.; Stark, W. J.; Reiser, O. *Chemistry – A European Journal* **2013**, 19, (30), 10038-10045.
50. Keller, M.; Perrier, A.; Linhardt, R.; Travers, L.; Wittmann, S.; Caminade, A.-M.; Majoral, J.-P.; Reiser, O.; Ouali, A. *Advanced Synthesis & Catalysis* **2013**, 355, (9), 1748-1754.
51. Buchman, Y. K.; Lellouche, E.; Zigdon, S.; Bechor, M.; Michaeli, S.; Lellouche, J.-P. *Bioconjugate Chemistry* **2013**, 24, (12), 2076-2087.
52. Liao, K.-S.; Wan, A.; Batteas, J. D.; Bergbreiter, D. E. *Langmuir* **2008**, 24, (8), 4245-4253.
53. Lawson, G.; Gonzaga, F.; Huang, J.; de Silveira, G.; Brook, M. A.; Adronov, A. *Journal of Materials Chemistry* **2008**, 18, (14), 1694-1702.
54. Liu, Y.; Wu, D.-C.; Zhang, W.-D.; Jiang, X.; He, C.-B.; Chung, T. S.; Goh, S. H.; Leong, K. W. *Angewandte Chemie International Edition* **2005**, 44, (30), 4782-4785.
55. Wang, F.; Liu, P.; Nie, T.; Wei, H.; Cui, Z. *International Journal of Molecular Sciences* **2013**, 14, (1), 17.

56. Rosenholm, J. M.; Duchanoy, A.; Lindén, M. *Chemistry of Materials* **2008**, 20, (3), 1126-1133.
57. Rossier, M.; Koehler, F. M.; Athanassiou, E. K.; Grass, R. N.; Aeschlimann, B.; Gunther, D.; Stark, W. J. *Journal of Materials Chemistry* **2009**, 19, (43), 8239-8243.
58. Schätz, A.; Long, T. R.; Grass, R. N.; Stark, W. J.; Hanson, P. R.; Reiser, O. *Advanced Functional Materials* **2010**, 20, 4323-4328.
59. Schätz, A.; Grass, R. N.; Stark, W. J.; Reiser, O. *Chemistry - A European Journal* **2008**, 14, 8262-8266.

Chapter 2

Reversible magnetic mercury extraction from waterⁱ



A facile and efficient way to decontaminate Hg^{2+} polluted water with the aid of magnetic, highly stable and recyclable carbon-coated cobalt (Co/C) nanoparticles is reported. Comparing non-functionalized Co/C nanomagnets with particles that were functionalized with amino moieties, the latter one proved to be more effective for scavenging mercury with respect to extraction capacity and recyclability. A novel nanoparticle–polyethyleneimine hybrid (Co/C-PEI) prepared by direct ring opening polymerization of aziridine initiated by an amine functionalized nanoparticle surface led to a high capacity material (10 mmol amino groups per gram nanomaterial) and thus proved to be the best material for scavenging toxic mercury at relevant concentrations ($\text{mg}\cdot\text{L}^{-1}$ / $\mu\text{g}\cdot\text{L}^{-1}$) for at least 6 consecutive cycles. On a large-scale, 20 liters of drinking water with an initial Hg^{2+} concentration of $30\ \mu\text{g}\cdot\text{L}^{-1}$ can be decontaminated to the level acceptable for drinking water ($\leq 2\ \mu\text{g}\cdot\text{L}^{-1}$) with just 60 mg of Co/C-PEI particles.ⁱⁱ

ⁱ Reproduced with permission from The Royal Society of Chemistry: S. Fernandes, C. M. Eichenseer, P. Kreitmeier, J. Rewitzer, V. Zlateski, R.N. Grass, W.J. Stark, O. Reiser, *RSC Advances* 2015, 5, 46430-46436. This manuscript was jointly written by S. Fernandes and C. M. Eichenseer. (<http://pubs.rsc.org/en/Content/ArticleLanding/2015/RA/C5RA04348D>).

ⁱⁱ The synthesis and characterization of Co/C-PAMAM G2 (**7**) and Co/C-PS-PAMAM G2 (**8**) were done by S. Fernandes. The synthesis of NOVA PEG Amino Resin PEI (**18**) was performed by C. Eichenseer. The large scale experiment was carried out by S. Fernandes and V. Zlateski at the ETH, Zurich. All other experiments were carried out by S. Fernandes and C. Eichenseer at the University of Regensburg.

2.1 Introduction

Removal of organic and inorganic waste from water has become an issue of major interest for the last few decades. In particular, the decontamination of heavy metals is still a matter of great concern, since these harmful substances can cause severe threats to human health. In this context, mercury is considered one of the most toxic pollutants to the environment and public health, being involved in several disasters of food poisoning in different countries around the world.^{1,2} The cumulative character of this metal leads to an enrichment in the environment and the food chain,^{3,4} which in turn may cause permanent adverse effects in the liver, lung, brain or kidney of living organisms, even at very low doses.^{1,4} Furthermore, its solubility in water brings along additional problems concerning the toxicity, especially for the aquatic system.⁵ Indeed, in its divalent form mercury is often found in fresh water, seawater, ground water and soil in considerable amounts.^{1,4} Therefore, mercury and its derivatives are considered as priority hazardous substances (PHSs)^{1,6} by several environmental associations that have started mercury monitoring programs worldwide.¹

Facing the above-mentioned harms, different methodologies have been used for water treatment such as centrifugation, ultrafiltration, crystallization, sedimentation, solid-phase extraction and chemical precipitation.^{1,2} Usually, the extraction of particular heavy metals is performed by using insoluble adsorbents.⁷⁻⁹ However, this method requires further filtration which involves energy-intensive pumping and tedious recovery of the materials.¹⁰

In an attempt to develop more sensitive, simple and cost-effective materials, nanotechnology has attracted much attention in this field.^{2,5} Magnetic nanoparticles in particular might contribute to such applications due to their distinct advantages like high surface area-to-volume ratio and therefore higher extraction capacities compared to micrometer-sized particles. Another major advantage is the facile and convenient separation of the nanoparticles by applying an external magnetic field, enabling an easy recovery and recycling of the scavenger,^{1,4,6} potentially even in the open environment.

Additionally, materials that selectively bind Hg^{2+} in the presence of other metals are needed in order to prove feasibility in a real water decontamination situation. For instance, studies with 1-naphthylthiourea–methyl isobutyl ketone¹¹ or mesoporous crystalline material functionalized with mercaptopropyl¹² showed that these selectively extract Hg(II) from aqueous samples. Nevertheless, recovery and regeneration of the chelating agent proved to be impractical. Considering this, a selective magnetic mercury scavenger would make the entire process much easier and faster as well as enhance the reusability of the chelating agent.

Functionally modified magnetic nanobeads have already been used for the extraction of different metals from aqueous solution such as cadmium,^{13,14} copper,^{13,15} lead,^{13,14} zinc,¹⁵ mercury,^{14,16,17} cobalt^{18,19} and nickel¹⁸ under various conditions. However, concerning mercury,

limitations related to selectivity in the presence of other metals and reusability of the scavengers are being encountered. Iron oxide nanoparticles were primarily considered as an attractive solution for magnetic separation. Recently, Pang *et al.*¹⁷ reported the synthesis of functionalized iron oxide nanoparticles which efficiently remove Hg²⁺ from water samples (380 mg Hg²⁺ extracted per mol adsorbent) but selectivity in combination with other metals or recyclability of this scavenger material was not studied. In addition, Khani *et al.*¹⁶ have developed magnetite nanoparticles functionalized with triazene groups showing selectivity towards mercury in binary systems, which could be used in 2 cycles with an extraction capacity of 10.26 mg Hg²⁺ per gram nanomaterial. Mandel *et al.* have reported that thiol-modified magnetic microparticles are capable of extracting mercury preferentially over other metals. However, co-adsorption of copper and cadmium was also observed in some cases. The release of adsorbed mercury (II) in order to recycle the scavenger was possible to an extent of about 30%, and the estimated extraction capacity was around 74 mg Hg²⁺ per gram microparticles.²⁰ Magnetic Co/C nanoparticles, which exhibit excellent thermal and chemical stability as well as higher magnetization, recently appeared as a promising alternative for improving the extraction capacity and reusability of scavengers.^{13,21} Such nanoparticles provide an additional carbon surface that stabilizes the metal core and allows for functionalization using established diazonium chemistry.^{22,23}

Herein, the potential of Co/C nanomagnets to be used as magnetic scavengers for mercury extraction from water is reported. In addition, the influence of amino functionalities on the nanoparticles to improve the extraction efficiency and selectivity was assessed, providing functional nanomagnets that show an extraction capacity as high as 550 milligrams of Hg²⁺ per gram of nanoparticles.

2.2 Results and Discussion

Carbon-coated nanobeads have proved their effectiveness in a variety of applications such as supports for scavengers, reagents or catalysts.²⁴⁻³⁰ Relevant for this study, this type of nanoparticles was previously used for complexation/extraction of cadmium,¹³ copper,¹³ lead,¹³ arsenic³¹ as well as noble metals like gold^{21,32} and platinum.³² However, no studies for the removal of Hg²⁺ from contaminated water were reported.

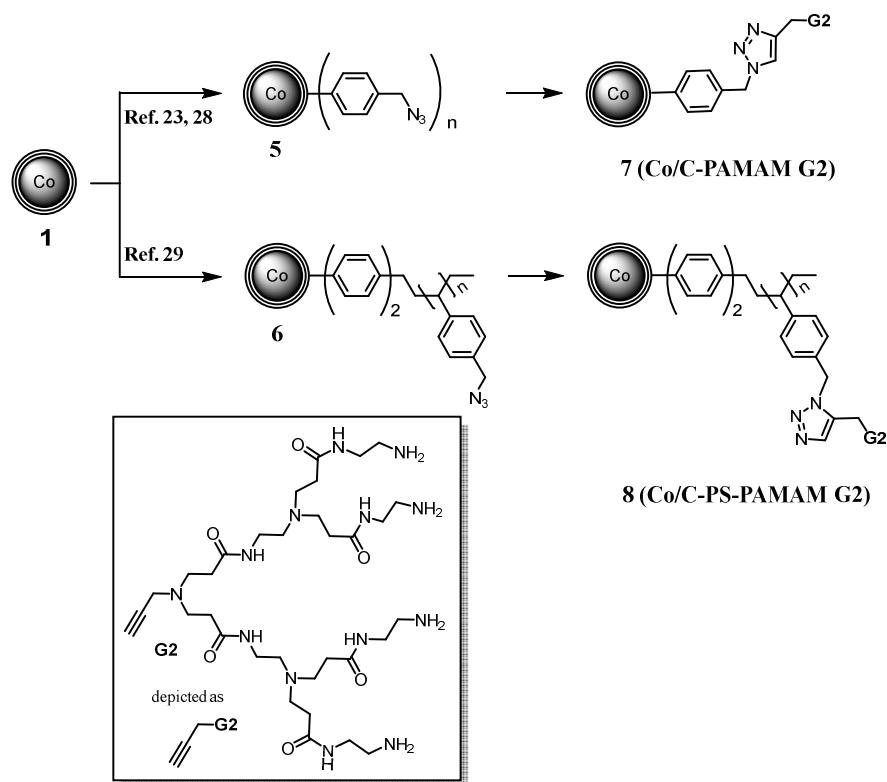
In order to remove Hg²⁺ ions from contaminated water, firstly pristine, commercially available, Co/C nanoparticles (**1**),²² were investigated as a possible scavenger. Two mercury solutions with different concentrations were prepared (15 and 30 mg·L⁻¹) and the progress of extraction was monitored by inductively coupled plasma optical emission spectrometry (ICP-OES) over 10 minutes, aiming at practical decontamination times in real case scenarios, to study the adsorption kinetics and estimate the maximum extraction capacity of the nanobeads. From

these results, using 5 mg of nanoparticles to decontaminate 5 mL of both HgCl₂ solutions, it was concluded that approximately 13 mg Hg²⁺ can be scavenged using 1 gram of nanoparticles within 10 minutes, even at low initial mercury concentrations of 15 mg·L⁻¹. However, also considerable leaching of Co²⁺ ions from the nanoparticle core was observed. The adsorption of Hg²⁺ onto the carbon layer of the nanoparticles was confirmed by X-ray photoelectron spectroscopy (XPS) analysis and is in agreement with the results obtained for multi-walled carbon nanotubes (MWCNTs).³³

Although the extraction of Hg²⁺ ions using unmodified Co/C nanoparticles (**1**) proved to be possible to some extent, there are three major limitations: (1) the occurring cobalt leaching leads to an undesired contamination that needs to be prevented. (2) The extraction capacity (13 mg Hg²⁺ per gram of nanoparticles) is relatively low requiring a high amount of nanoparticles to remove Hg²⁺ on large scale. (3) An efficient release of mercury from the particles, thus allowing their recycling, was not possible under various conditions tried (aqua regia; heating at 150 °C; aqua regia combined with high temperature).

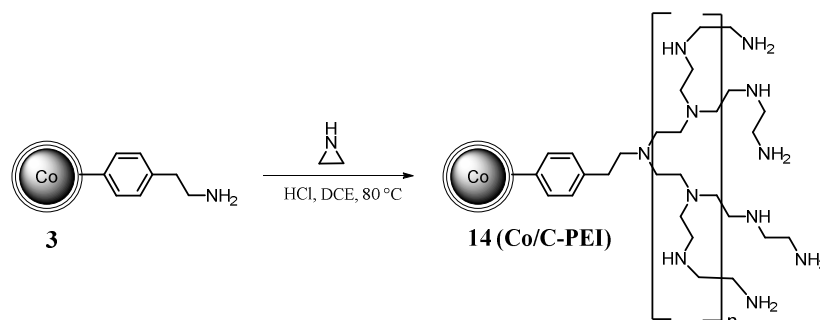
Therefore, the surface of the nanomagnets was functionalized to improve the extraction capacity, also aiming to avoid cobalt leaching and ensuring recyclability. Non-magnetic, amino-functionalized materials have been reported for their extraction capability towards Hg²⁺, and especially Masri and Friedman have demonstrated the high affinity of polyamine derivatives towards Hg²⁺ ions in aqueous solutions.³⁴ Furthermore, amino-functionalized carbon nanotubes have been successfully applied for extracting Hg²⁺ from water samples.³⁵ However, selectivity studies with these materials were either not performed or limited to binary systems. Taken these precedents as a lead, this project focus on the development of high capacity amino-polymers, such as polyethyleneimine (PEI) and poly(amidoamine) (PAMAM), supported on readily recyclable magnetic nanobeads for selective Hg²⁺ removal.

Thus, propargylated PAMAM dendrimer **G2**, having four terminal amino groups was connected in two different ways to the surface of the NPs (Scheme 1): benzyl azide functionalized Co/C nanoparticles (**5**)^{23,28} (0.1 mmol azide per g nanomaterial) or a Wang type resin having azide end groups covalently attached to Co/C nanoparticles (**6**)²⁹ (2.4 mmol azide per g nanomaterial), were found to be suitable platforms to accommodate PAMAM dendrimers via ligation by a copper catalyzed azide/alkyne cycloaddition using conditions previously described in our group.^{23,28} The reaction was conveniently followed by monitoring the characteristic azide peak at 2100 cm⁻¹ with attenuated total reflection infrared spectroscopy (ATR-IR) spectroscopy, to give rise to (**7**) (0.02 mmol PAMAM per gram nanomaterial) and (**8**) (0.57 mmol PAMAM per gram nanomaterial), respectively. Higher magnetization values were observed for Co/C-PAMAM G2 (**7**) (106 emu·g⁻¹) when compared to higher loaded Co/C-PS-PAMAM G2 (**8**) (50 emu·g⁻¹), reflecting the different amounts of non-magnetic material attached to the nanobeads.



Scheme 1 Covalent immobilization of PAMAM dendron G2 on Co/C nanoparticles via click chemistry. Reagents and conditions: i) $\text{CuSO}_4 \cdot 5 \text{H}_2\text{O}$ (10 mol%), sodium ascorbate (30 mol%), THF- H_2O (3:1), 24 h, at room temperature.

PEI-functionalised Co/C nanobeads were prepared starting from Co/C- NH_2 (**3**)²² (0.15 mmol amine per g nanomaterial) following a procedure for the functionalization of carbon nanotubes described by Liu *et al.* (Scheme 2).³⁶ Using 1000 equivalents of aziridine, high loadings of approximately 10 mmol amine per gram nanomaterial (**14**) were obtained, by growing the PEI polymer on the nanoparticle surface. These nanoparticles form stable dispersions in water,³⁷ thus avoiding agglomeration, which is a general problem for unmodified Co/C nanoparticles. The saturation magnetization of this material was found to be still high ($39 \text{ emu} \cdot \text{g}^{-1}$), rivalling that of low-loading magnetite particles.³⁸ Therefore, an easy and effective recovery by magnetic separation is still possible within seconds.



Scheme 2 Synthesis of polyethyleneimine-functionalized nanoparticles (**14**) by ring opening polymerization of aziridine.³⁷

A comparison of the extraction efficiency of all nanobeads (Fig. 1) using 5 mL of an aqueous solution of HgCl_2 ($30 \text{ mg}\cdot\text{L}^{-1}$) and 5 mg of nanomaterial during 10 minutes for benchmarking purposes showed that Co/C-PAMAM G₂ (**7**) was found to extract mercury (50%) comparable to unmodified Co/C nanoparticles, which is attributed to the low loadings of PAMAM, and consequently amine groups, obtained during the functionalization. Improved extraction capacity (73%) was found for Co/C-PS-PAMAM G₂ (**8**), which can be ascribed to increased loadings of terminal amino groups made possible through the additional polystyrene layer on the surface of the nanoparticles.^{26,27,29,31,39} For both materials no significant cobalt leaching was detected. The Hg^{2+} removal efficiency was found to be even better for Co/C-PEI (**14**) ($\geq 98\%$, reaching the detection limit [$100 \text{ }\mu\text{g}\cdot\text{L}^{-1}$] of the ICP-OES), while still avoiding cobalt leaching from the nanoparticles into the solution.

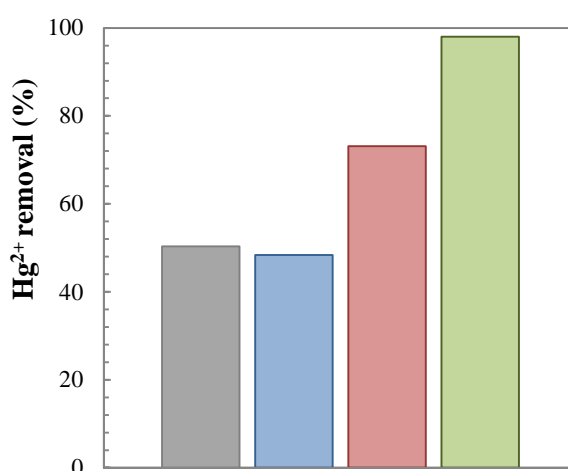


Fig. 1 Comparison of the extraction capacity of the different nanobeads. Reaction conditions: 5 mg of nanoparticles, 5 mL of Hg^{2+} solution ($30 \text{ mg}\cdot\text{L}^{-1}$), 10 min extraction time, solution pH 6.53. The grey bar is for Co/C (**1**), the blue bar for Co/C-PAMAM G₂ (**7**), the red bar for Co/C-PS-PAMAM G₂ (**8**) and the green bar for Co/C-PEI (**14**).

The maximum extraction capacity of Co/C-PEI (**14**) was subsequently estimated by extracting solutions of higher mercury concentration. The removal of mercury from a 5 mL solution containing 580 mg Hg^{2+} per litre was possible using 5 mg of nanoparticles (**14**). The scavenging efficiency was estimated to be 95%, after 10 minutes of reaction. This corresponds to an extraction capacity of 550 mg Hg^{2+} per gram of nanomaterial (**14**), which compares favorably to the results obtained for Co/C (**1**) (15 mg Hg^{2+} extracted per gram of nanoparticles) and for previously reported magnetic mercury scavengers (5.6 – 152 mg Hg^{2+} extracted per gram nanomaterial).^{4,16,40}

Hg^{2+} could also be efficiently removed from much more diluted solutions using Co/C-PEI (**14**). Starting from 100 mL of an aqueous solution containing $1.87 \text{ mg}\cdot\text{L}^{-1}$ Hg^{2+} , 3 mg Co/C-PEI nanoparticles (**14**) are sufficient to bring the mercury concentration down to the detection limit ($100 \text{ }\mu\text{g}\cdot\text{L}^{-1}$) of the ICP-OES analysis again within 10 minutes (Fig. 2).

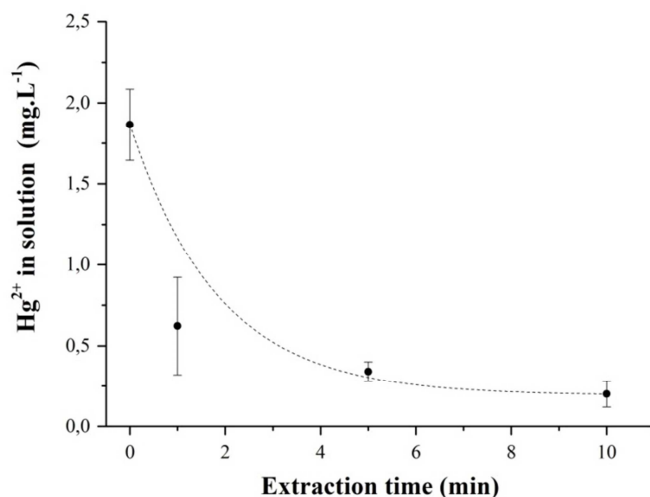
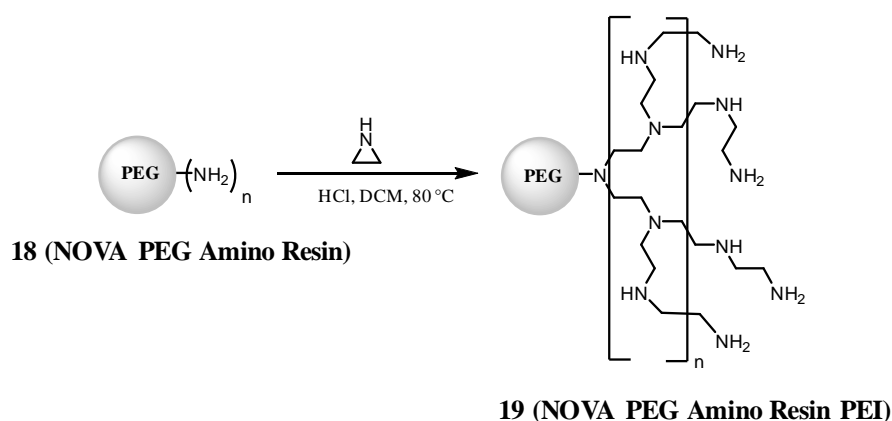


Fig. 2 Hg²⁺ extraction over 10 minutes of reaction. 100 mL of an aqueous solution (1.64 mg·L⁻¹, solution pH 6.71), 3 mg Co/C-PEI nanoparticles (**14**). The dashed curve represents the exponential decay fit of the data set (decay constant: $1.8 \pm 1.2 \text{ min}^{-1}$). After 10 min, the detection limit (100 $\mu\text{g}\cdot\text{L}^{-1}$) of the ICP-OES analysis was reached.

To validate that the Hg²⁺ uptake occurs due to a complexation of the metal ions by the amino groups the extraction capacity of the PEI-polymer itself was tested. A commercially available PEG-resin with terminal amino groups (**18**) was functionalized with PEI in the same manner (Scheme 3) as for the Co/C-NH₂ particles (**3**) described above.



Scheme 3 Synthesis of PEI functionalized PEG-resin (**19**) by ring opening polymerization of aziridin as described for Co/C-PEI (**14**).

The so obtained PEI-resin (**19**) (10.9 mmol of nitrogen per gram of resin) was used for extraction, applying identical conditions as in the previous experiments. A similar extraction capacity for the PEI-functionalized resin (**19**), when compared to the Co/C-PEI nanomagnets (**14**) was determined, while the PEG-amino resin (**18**) itself showed nearly no ability to extract mercury (see Fig. 3). In fact, using PEI-resin (**19**) an extraction efficiency of 90% is achieved, as for the amino-resin (**18**) only 10% of the Hg²⁺ is extracted.

These findings suggest that indeed the amino functionalities on the surface of the nanoparticles are responsible for the removal of mercury, which is in agreement with literature reports for amino functionalized multi-wall carbon nanotubes,³⁵ or chitosan based absorbents⁴⁰ or polyamine derivatives.³⁴

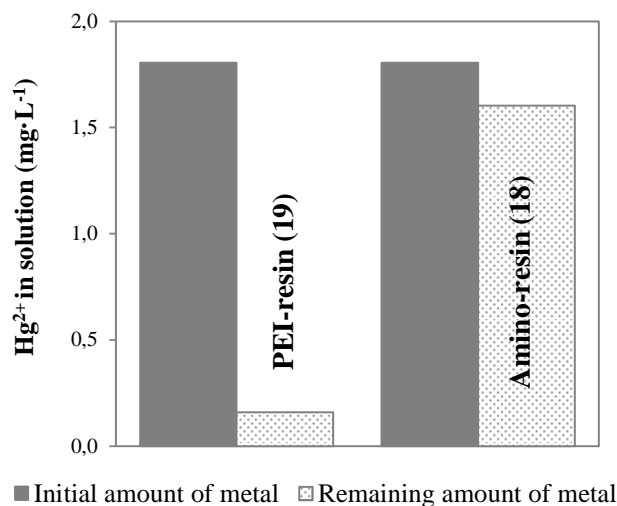


Fig. 3 Hg²⁺ extraction of 100 mL of an aqueous solution (1.8 mg·L⁻¹, solution), using 3 mg of the amino-resin (**18**) and PEI-resin (**19**), within 10 minutes.

It is known that PEI can also chelate metal ions such as Ni²⁺, Cu²⁺, Zn²⁺, Cd²⁺ and Pb²⁺.⁴¹ However, no selectivity studies using PEI for extracting mercury in the presence of other metal ions have been reported up until now. Testing the extraction of Hg²⁺ against other competitive metals in solution at the same time, indeed it was found that Co/C-PEI nanomagnets (**14**) show a high preference for Hg²⁺ (Fig. 4A and 4B). Experiments were done with an extraction time of 10 minutes and 3 hours in a pH range of 5.2 - 6.2, representing the range that is obtained upon dissolving the metal salts in pure water. No significant changes were detected between these two time points indicating that under the conditions applied, the equilibrium time for all tested metals has been reached, after 10 minutes of extraction. The preferential extraction of Hg²⁺ is supported by the selective extraction also shown for the PEI-resin (**19**) (see Fig. 4D). Moreover, XPS analysis on the NPs used to obtain the results in Fig. 4A confirmed the preferential uptake of mercury against the other metals. In addition, an experiment at basic pH 8.3 was performed to evaluate the influence of the pH on the adsorption of the metals (Fig. 4C). Again, a preferential uptake of Hg²⁺ was detected (68%), however absorption Cu²⁺ (51%) and Pb²⁺ (17%) occurred to a significant extent as well.

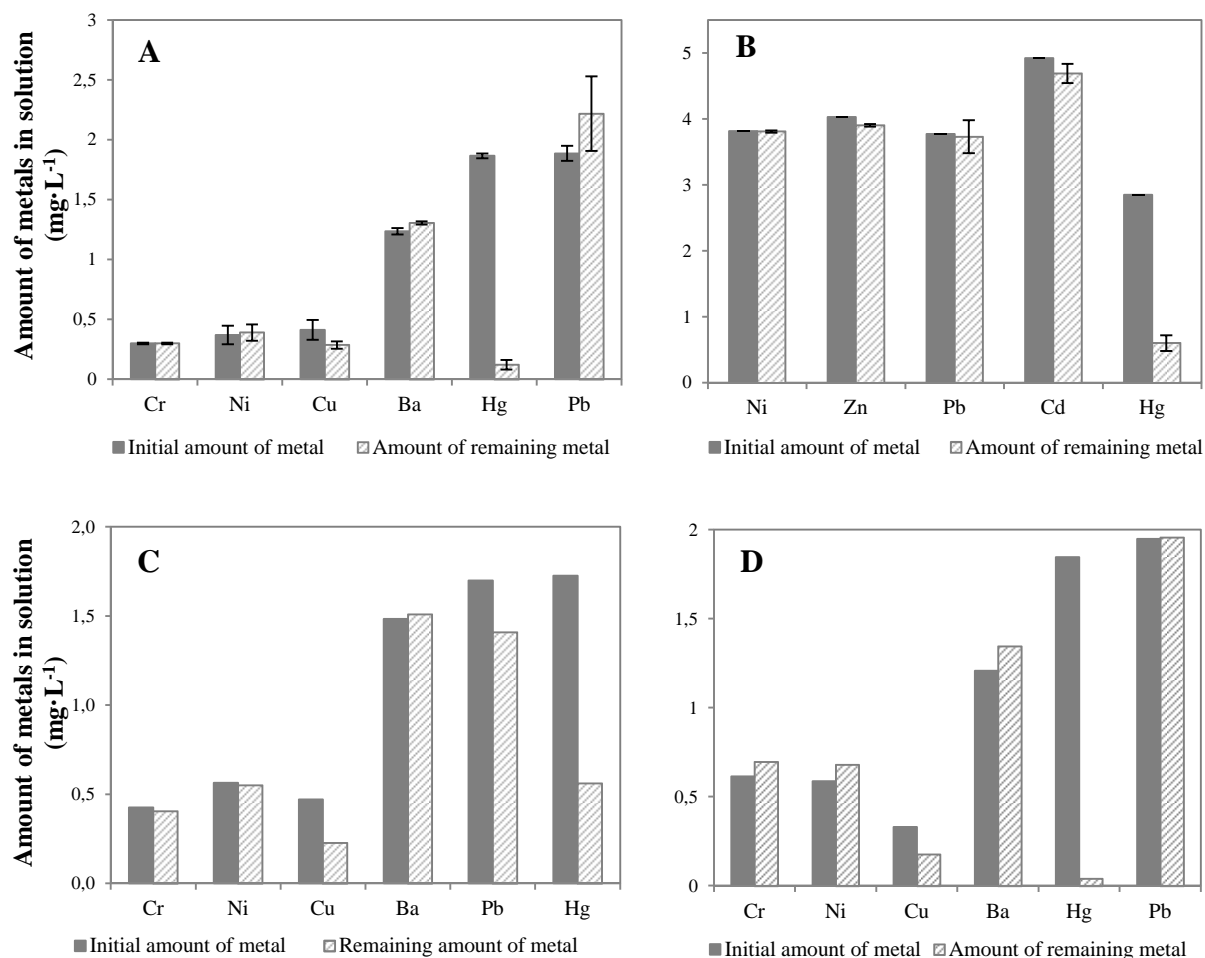


Fig. 4 Selective extraction of Hg^{2+} , within 10 minutes, using Co/C-PEI (**14**) in the presence of competitive metal ions: (A) 3 mg of NPs were used to decontaminate a 100 mL solution containing Hg^{2+} , Cu^{2+} , Pb^{2+} , Ni^{2+} , Ba^{2+} and Cr^{3+} in equimolar amounts ($10 \mu\text{M}$), solution pH 5.59; (B) 3 mg of NPs were used to decontaminate an aqueous 100 mL solution containing Hg^{2+} , Pb^{2+} , Ni^{2+} , Zn^{2+} and Cd^{2+} , solution pH 6.16. (C) 3 mg of NPs were used to decontaminate a 100 mL solution containing Hg^{2+} , Cu^{2+} , Pb^{2+} , Ni^{2+} , Ba^{2+} and Cr^{3+} , solution pH 8. (D) Selective extraction of Hg^{2+} using NOVA PEG amino resin PEI (**18**) in the presence of competitive metal ions: 3 mg were used to decontaminate 100 ml aqueous solution.

Having developed a scavenger that combines the advantages of using a selective adsorbent with the magnetic properties of a solid support, the performance of Co/C-PEI nanoparticles (**14**) was tested in tap water samples. For these experiments water from the facilities of the University of Regensburg was used and artificially contaminated with Hg^{2+} ($2 \text{ mg}\cdot\text{L}^{-1}$). Especially, the water sample was analysed with respect to the content of mercury, magnesium and iron before and after treatment with nanoparticles (**14**). The concentration of Ca^{2+} was also measured to be around $100 \text{ mg}\cdot\text{L}^{-1}$, thus being present in large excess with respect to the extraction capacity of (**14**) used in this experiment. However, the values obtained from ICP measurements for calcium before and after extraction were somewhat erratic, and cannot be taken into consideration. Despite the presence of those other ions that are naturally occurring in drinking water mercury was still efficiently removed (Table 1, Sample 1).

As iron can occur in higher concentrations in water of different areas⁴² an additional experiment was performed in the presence of an excess of iron. Still 90% Hg²⁺ was successfully extracted even if the content of iron was approximately 20 times higher than that of mercury (Table 1, Sample 2).

Table 1 Extraction results in tap water.

	Metal ions before / after extraction (mg·L ⁻¹)		
	Hg ^c	Fe ^c	Mg ^c
Sample 1 ^a - Regensburg drinking water spiked with Hg ²⁺	2.2 / 0.3	≤0.1 / ≤0.1	19.1 / 19.1
Sample 2 ^b - Regensburg drinking water spiked with Fe ²⁺ and Hg ²⁺	2.2 / 0.2	35 / 32.5	-

^a Hg²⁺ artificially added to the tap water samples (the source of mercury used is HgCl₂). In addition, the sample contained approx. 100 mg·L⁻¹ Ca²⁺ (see text). ^b Fe²⁺ and Hg²⁺ artificially added to the tap water samples (the source of iron used is FeCl₂·4H₂O). ^c Values determined for tap water samples from the University of Regensburg. Extraction conditions: 3 mg Co/C-PEI NPs (**14**) were used to decontaminate 100 mL aqueous solution (pH 6.71) within 10 minutes.

Having proven the feasibility of the nanomagnets for extracting mercury in real water samples, a simple recycling methodology of the magnetic scavenger had to be established. More specifically, mercury has to be released after extraction in order to regenerate and reuse the nanomaterial. Considering the fact that the amino groups on the surface of the nanoparticles (**14**) are responsible for scavenging the mercury ions, a logical approach is the protonation of these groups lowering the pH to reverse their complexation ability. For the release the following procedure was established: after the extraction time, the nanobeads were collected with a magnet and the aqueous decontaminated solution was completely decanted, followed by the addition of 20 mL of an acid. In the course of determining the conditions for the release of mercury, different acids (0.01 M) were tested. These experiments showed that strong acids like H₂SO₄, HCl and HNO₃ are suitable for achieving high mercury release, while weak acids like acetic acid are less effective. Further optimizations were performed with H₂SO₄ solutions differing in molarity and thus in the pH. The best conditions were found to be 0.5 M H₂SO₄, corresponding to a pH value of approximately 0.4. Noteworthy, ICP measurements revealed that no significant cobalt leaching from the core of the nanomaterial is detected during the release of mercury.

Thus, a multicycle extraction/recycling protocol was established (Fig. 5) for aqueous solutions (tap water) containing mercury. The Hg^{2+} contaminated water containing the nanomagnets (**14**) was shaken for 10 minutes and then the NPs are recovered applying an external magnet. The decontaminated water is then decanted and the nanoparticles (**14**) were subsequently treated with H_2SO_4 (20 mL, 0.5 M, 20 minutes) in order to release the mercury. Finally, a magnet is used once more to collect the NPs and decant the acidic solution. This was then followed by washing the nanomaterials with a 0.5 M potassium carbonate solution and water to regenerate the amino groups, and the nanoparticles are used in the next cycle.

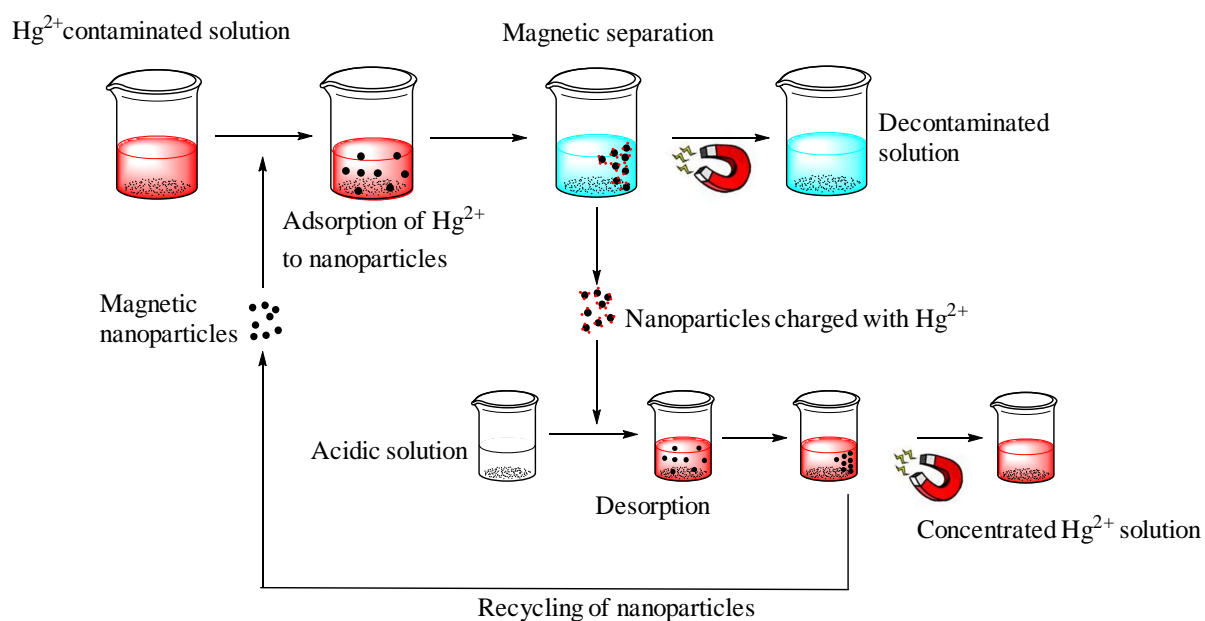


Fig. 5 Graphical representation of the recycling protocol performed for the extraction of mercury in tap water samples. The nanoparticles (**14**) were shaken with the contaminated water for 10 minutes. After completing the extraction time, the magnetic materials are collected by using an external magnet and the Hg^{2+} desorbed by the protonation of the amine groups in H_2SO_4 solution for 5 minutes. The particles (**14**) were regenerated by washing with a 0.5 M potassium carbonate solution and water and re-used for the next adsorption experiment.

Following the scheme in Fig. 5, it was demonstrated that in six consecutive cycles more than 90% of the mercury could be extracted from tap water samples (6x 100 mL spiked with $2 \text{ mg}\cdot\text{L}^{-1} \text{ Hg}^{2+}$ each), after 10 minutes extraction for each single experiment (Fig. 6). Even though the release step was not complete each time, the extraction capacity remained nearly unchanged during the six runs. In some cases the release was observed to be higher than 100%, probably due to incomplete release of mercury at the previous step, which was apparently set free in the next cycle.

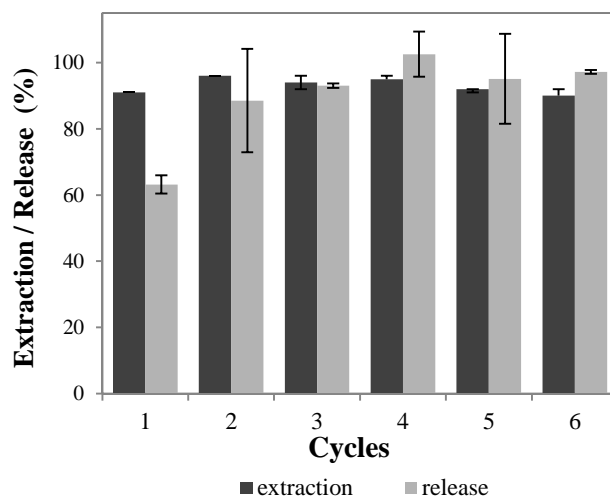


Fig. 6 Reusability of Co/C-PEI (**14**) in six consecutive runs (extraction and subsequent release). Reaction conditions: Co/C-PEI (**14**) (3 mg) were shaken in 100 mL of $2 \text{ mg} \cdot \text{L}^{-1} \text{ Hg}^{2+}$ containing aqueous sample (pH 6.7) for 10 min. Release: 20 mL 0.5 M H_2SO_4 within 20 min.

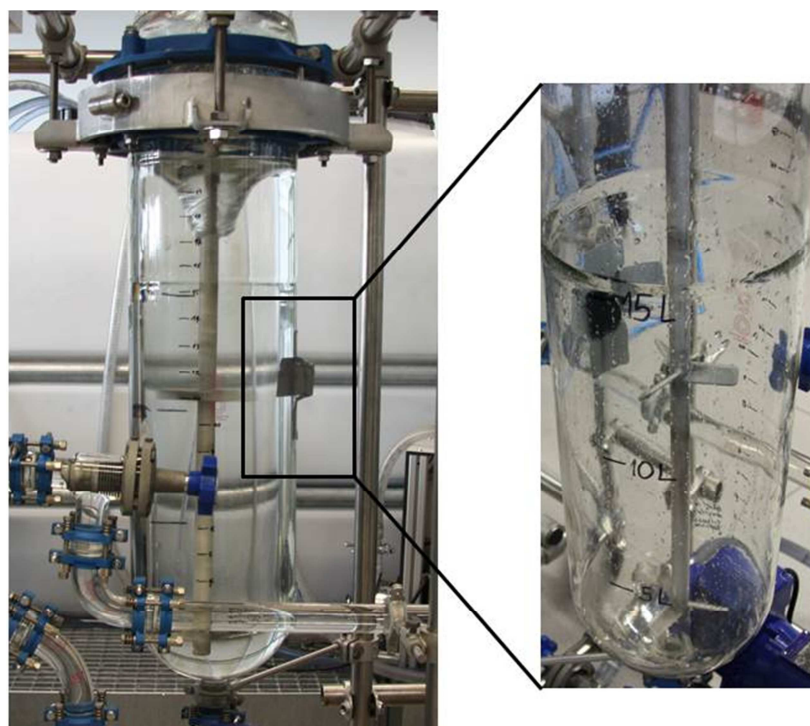


Fig. 7 Large-scale experiment was performed in a reactor containing 20 L of an aqueous mercury solution ($30 \mu\text{g} \cdot \text{L}^{-1}$). The extraction was done at room temperature during one hour using 3 mg of Co/C-PEI (**14**) per liter, which were recovered by an external neodymium magnet (magnification, right picture).

In addition, TEM analysis (see experimental section) proved that there are no significant changes or alterations in the appearance of the nanoparticles visible after the recycling process. Aiming to prove their use in a realistic industrial application, the applicability of these magnetic scavengers in a large-scale experiment was done in cooperation with the group of Prof. Wendelin Stark at the ETH Zurich. For this purpose a 20 liters reactor, from ETH Zurich,

was used (see Fig. 7) and filled with normal Zurich drinking water artificially contaminated with $30 \mu\text{g}\cdot\text{L}^{-1} \text{Hg}^{2+}$. An even lower concentration of particles than in the previous recycling experiments was employed ($3 \text{mg}\cdot\text{L}^{-1}$). Gratifyingly, after one hour reaction time the water was detoxified from mercury to 93%, leaving behind a mercury content of $2 \mu\text{g}\cdot\text{L}^{-1}$ as determined by atomic fluorescence spectroscopy (AFS). This value is within the limit for drinking water according to World Health Organization.⁴² Thus, the simple and efficient scavenger (**14**) developed here has proved its potential to decontaminate water samples from Hg^{2+} poisoning, which also might be applicable in the open environment due to the facile recovery of the magnetic support.

2.3 Conclusion

Unfunctionalized carbon-coated nanobeads (**1**) proved to have potential for mercury removal from water, however, with some major limitations. A significant improvement was achieved with PEI-functionalized nanomagnets (**14**), which showed a very high capacity for extracting toxic Hg^{2+} in a multimetal environment from drinking water samples at relevant concentrations. The extraction occurs through the complexation of Hg^{2+} ions by the amino groups of the functionalized nanoparticles (**14**).

The recyclability of the nanoparticles was ensured for at least 6 consecutive cycles with no loss of extraction capacity. The nanoparticles (**14**) showed as well the ability of extracting from a 20 liters reactor, which proved the potential of (**14**) for the detoxification of drinking water in realistic applications.

In summary, a simple and efficient scavenger has been developed to decontaminate water samples from Hg^{2+} poisoning, which might also be applicable in the open environment due to the facile recovery of the magnetic support.

2.4 Experimental section

Materials and methods

Commercially available chemicals were used without further purification. NovaPEG amino resin Novabiochem® (batch number: S6625326; loading: 0.59mmol/g) was purchased from Merck KGaA. Column chromatography was performed with silica gel (Merck, Geduran 60, $0.063\text{-}0.200 \text{mm}$ particles size) and flash silica gel 60 (Merck, $0.04\text{-}0.063 \text{mm}$ particles size). Attenuated total reflection infrared spectroscopy (ATR-IR) was carried out on a Biorad Excalibur FTS 3000, equipped with a Specac Golden Gate Diamond Single Reflection ATR-System or a Varian FTS 1000 spectrometer. Solid and liquid compounds were measured neatly and the wavenumbers are reported as cm^{-1} . Mass spectrometry was performed using a Finnigan ThermoQuest TSQ 7000 at the Central Analytical

Laboratory (University of Regensburg). Elemental microanalysis was carried out by the micro analytical department of the University of Regensburg using a Vario EL III or Mikro-Rapid CHN apparatus (Heraeus). The inductively coupled plasma optical emission spectrometry (ICP-OES) was measured on a Spectroflame EOP (Spectro) at the University of Regensburg while the atomic fluorescence spectroscopy (AFS) was performed at Bachema AG Switzerland. Thermogravimetric analysis (TGA) was done on a TGA 7 (Perkin Elmer). Magnetization measurements were performed using superconducting quantum interference device (SQUID) at the Physics Department at the University of Regensburg. X-ray photoelectron Spectroscopy (XPS) analysis was performed at SuSoS (Switzerland).

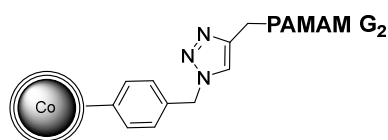
Nomenclature of the magnetic nanoparticles

The nomenclature of the nanoparticles is as follows: Co/C for magnetic nanoparticles with cobalt core and carbon shell. Co/C-R for functionalized Co/C NPs where R indicates the functional groups on the graphene-like layers: PAMAM G2 for the dendrimeric poly(amidoamine) coating of the second generation and PEI for the polyethyleneimine coating. Co/C-PS-PAMAM G2 for polystyrene coated cobalt nanoparticles with an additional dendrimeric functionalization.

Synthesis of the nanoparticles

The ATR-IR spectra and TGA profile of Co/C-PAMAM G2 and Co/C-PS-PAMAM G2 are shown in Chapter 1.

Magnetic Co/C-PAMAM G2 (7)

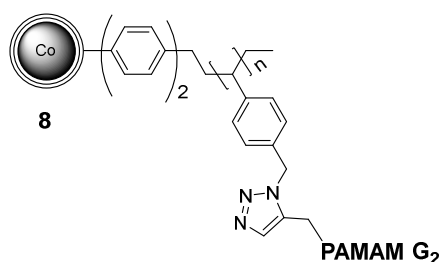


7

In a typical experiment, 100 mg of azide functionalized nanoparticles (0.019 mmol (N₃) per gram nanoparticles, 0.007 mmol) (5) and 5 equivalents (70 mg, 0.095 mmol) of the second generation PAMAM dendron, containing 4 functional groups, were used. The PAMAM was previously dissolved in 5 mL of degassed THF/H₂O (3:1) mixture followed by the successive addition of Co/C- N₃ (5), Na-ascorbate (30 mol%, 0.029 mmol, 5.75 mg) and CuSO₄ (10 mol%, 0.0095 mmol, 2.37 mg). Afterwards the reaction mixture was sonicated for 15 minutes and stirred for 48 hours at room temperature. The magnetic nanoparticles were separated applying an external magnet and washed with acetone (5x 5 mL), H₂O (5x 5 mL) and acetone (3x 5 mL). In the end, the nanobeads were dried under vacuum. The reactions were monitored by ATR-IR, evaluating the attenuation of the azide peak and the loadings estimated by TGA.

Co/C-PAMAM (7): TGA (N₂): 0.02 mmol.g⁻¹; 1.4 % mass loss.

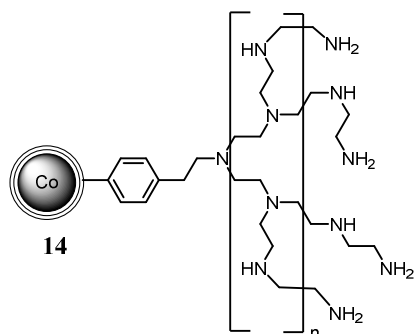
Magnetic Co/C-PS-PAMAM G2 (8)



In a typical experiment, 100 mg of azide functionalized nanoparticles (**8**) (2.42 mmol (N₃) per gram nanoparticles, 0.242 mmol) (**5**) and 5 equivalents (894 mg, 1.21 mmol) of the second generation PAMAM dendron, containing 4 functional groups, were used. The PAMAM was previously dissolved in 5 mL of degassed THF/H₂O (3:1) mixture followed by the successive addition of Co/C-PS-N₃ (**8**), Na-ascorbate (30 mol%, 0.363 mmol, 72 mg) and CuSO₄ (10 mol%, 0.121 mmol, 30 mg). Afterwards the reaction mixture was sonicated for 15 minutes and stirred for 48 hours at room temperature. The magnetic nanoparticles were separated applying an external magnet and washed with acetone (5x 5 mL), H₂O (5x 5 mL) and acetone (3x 5 mL). In the end, the nanobeads were dried under vacuum. The reactions were monitored by ATR-IR, evaluating the attenuation of the azide peak and the loadings estimated by TGA.

Co/C-PS-PAMAM (**8**): TGA (N₂): 0.6 mmol.g⁻¹; 42 % mass loss.

Magnetic Co/C-PEI (14)



For this specific batch, amino-functionalized carbon-coated cobalt nanoparticles (**3**)²² (Co/C-NH₂) (946 mg, 0.1 mmol, 1.0 equiv.) were pre-dispersed in 95 mL DCM using an ultrasonic bath for 15 min. Under stirring, aziridine (5.4 mL, 103.6 mmol, 1000 equiv.) and conc. HCl (141.6 μL) were added to the reaction mixture which then was heated to 80 °C for 48 h. Afterwards the NPs were collected using an external magnet, washed with DCM (2x 50 mL), H₂O (5x 50 mL) and again DCM (3x 50 mL). Then the nanobeads were dried under vacuum at 50 °C. As the degree of polymerization was not satisfactory the whole procedure was repeated using 500 mg of the herein synthesized nanoparticles (1.0 equiv.) in 49 mL DCM, 2.85 mL aziridine (1000 equiv.) and 100 μL conc. HCl. After a reaction

time of 69 h the nanoparticles were washed with DCM (2x 50 mL), H₂O (5x 50 mL) and again DCM (3x 50 mL). The extent of polymerization was estimated by TGA (66 wt%).

IR (v/cm⁻¹): 3417, 2934, 2821, 2362, 1648, 1604, 1458, 1351, 1298, 1014.

Elemental microanalysis [%]: C, 30.46; H, 7.09; N, 14.97; Loading (N): 10.7 mmol·g⁻¹ nanoparticles.

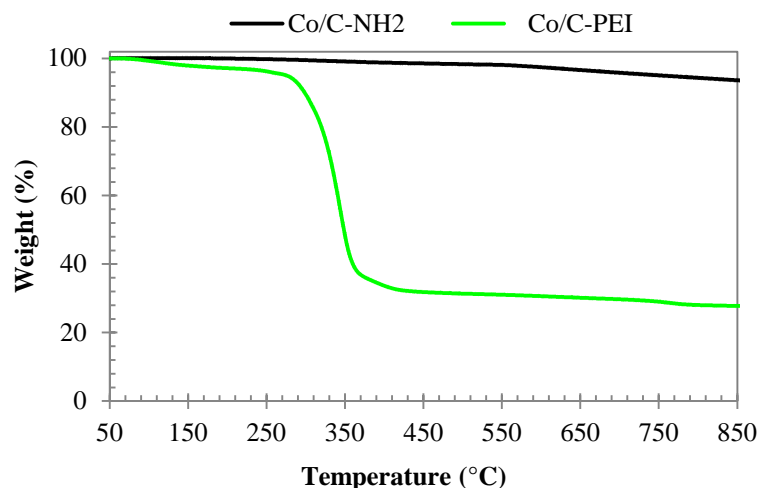
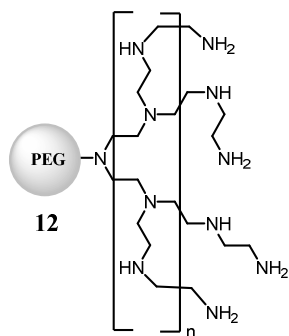


Fig. 8 TGA analysis of the phenylethylamine-coated Co/C nanoparticles (**3**) (black) and PEI-coated MNPs (**14**) (green).

NOVA PEG Amino Resin-PEI (**19**)



The commercially available Nova PEG amino resin (**19**) (50 mg, 29.5 μmol, 1.0 equiv.) was pre-swollen in 5 mL DCM. Then aziridine (775 μL, 14.9 mmol, 506 equiv.) and conc. HCl (15.5 μL) were added under stirring. The resulting reaction mixture was heated to 80 °C for 24 h. Afterwards the resin was filtered off, washed with DCM (2x 20 mL), H₂O (5x 20 mL) and DCM (3x 20 mL) and dried under vacuum at 50 °C.

IR (v/cm⁻¹): 3413, 2936, 2823, 1653, 1614, 1457, 1357, 1292, 1098.

Elemental microanalysis [%]: C, 38.27; H, 8.18; N, 16.24. Loading (N): 10.9 mmol·g⁻¹.

TGA (N₂): 65 wt% PEI.

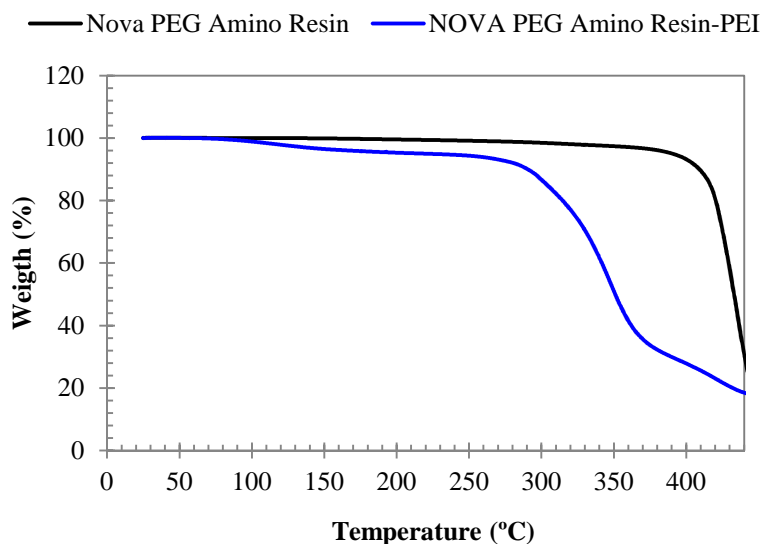


Fig. 9 TGA analysis of the commercially available NOVA PEG Amino Resin (**17**) (black) and the respective PEI-coated resin (**18**) (blue).

Metal extraction experiments

Adsorption of mercury from aqueous solutions

A given amount of the magnetic nanoparticles was added to an aqueous mercury solution with a defined concentration of the heavy metal. The experiment was carried out at room temperature and the pH of the solutions specified at the results section. The metal salts used are HgCl_2 , $\text{BaCl}_2 \cdot 2\text{H}_2\text{O}$, CuCl_2 , $\text{CrCl}_3 \cdot 6\text{H}_2\text{O}$, PbCl_2 , $\text{Ni}(\text{C}_5\text{H}_7\text{O}_2)_2$, $\text{Zn}(\text{ClO}_4)_2 \cdot 6\text{H}_2\text{O}$ and $\text{CdCl}_2 \cdot \text{H}_2\text{O}$.

First, the nanoparticles in solution were dispersed for one minute in the ultrasonic bath and then the dispersion was agitated in a mechanical shaker for 10 minutes. Afterwards the particles were collected with the help of a magnet and the solution was decanted. The remaining mercury in solution was determined by ICP-OES (detection limit: $0.1 \text{ mg} \cdot \text{L}^{-1}$). For the large scale experiment the remaining solution was analyzed by atomic fluorescence spectroscopy (AFS) with a detection limit of $1 \text{ } \mu\text{g} \cdot \text{L}^{-1}$.

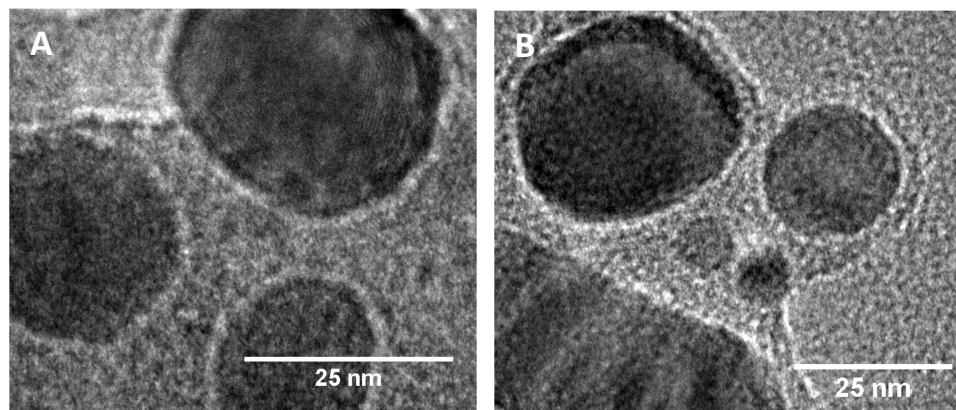
Desorption of mercury and re-usability of the nanomagnets

After extraction, the nanoparticles (**14**) (3 mg) were collected with an external magnet and re-dispersed in 20 mL of H_2SO_4 (0.5 M). The solution was sonicated for 3 min followed by 5 min of mechanical shaking. The nanomagnets were collected once more using by the aid of an external magnet, washed with a 0.5 M potassium carbonate solution (10 mL) and water (10 mL), and re-used for the next extraction experiment. This procedure was repeated six times to study the materials' recyclability.

To determine the amount of mercury desorbed, the acid solution used above was diluted with aqua regia 32% (v/v), filtered and analyzed by ICP-OES.

Transmission electron microscopy pictures

TEM pictures of the Co/C-PEI nanoparticles (**14**) before (A) and after recycling process (B).



X-Ray photoelectron spectroscopy

XPS analysis was performed on three samples of Co/C nanoparticles after extraction of metals:

- Co/C (**1**) after the extraction of HgCl_2
- Co/C-PEI (**14**) after the extraction of HgCl_2
- Co/C-PEI (**14**) after the extraction of HgCl_2 from a mixture of different metal salts (HgCl_2 , $\text{BaCl}_2 \cdot 2\text{H}_2\text{O}$, CuCl_2 , $\text{CrCl}_3 \cdot 6\text{H}_2\text{O}$, PbCl_2 , $\text{Ni}(\text{C}_3\text{H}_7\text{O}_2)_2$)

Results:

- Co/C (**1**): The metallic Co core of the particle can still be detected, indicating, that the C-coating is less than 10 nm thick. Mercury is its oxidized form.
- Co/C-PEI (**14**): The metallic Co core of the particle is not detected anymore on these particles. Hg is detected, in its oxidized form.
- Co/C-PEI (**14**): The metallic Co core of the particle is not detected anymore on these particles. Hg is detected in its oxidized form. Additionally some Cu was detected. Ni, Cr, Pb and Ba could not be detected.

2.5 References

1. Farrukh, A.; Akram, A.; Ghaffar, A.; Hanif, S.; Hamid, A.; Duran, H.; Yameen, B. *ACS Applied Materials & Interfaces* **2013**, 5, (9), 3784-3793.
2. Parham, H.; Zargar, B.; Shiralipour, R. *Journal of Hazardous Materials* **2012**, 205–206, 94-100.
3. Baki, M. H.; Shemirani, F. *Analytical Methods* **2013**, 5, (13), 3255-3263.
4. Zhao, J.; Zhu, B.; Yu, H.; Yan, L.; Wei, Q.; Du, B. *Journal of Colloid and Interface Science* **2013**, 389, (1), 46-52.

5. Zhai, Y.; Duan, S. e.; He, Q.; Yang, X.; Han, Q. *Microchimica Acta* **2010**, 169, (3-4), 353-360.
6. Girginova, P. I.; Daniel-da-Silva, A. L.; Lopes, C. B.; Figueira, P.; Otero, M.; Amaral, V. S.; Pereira, E.; Trindade, T. *Journal of Colloid and Interface Science* **2010**, 345, (2), 234-240.
7. Freyhardt, C. C.; Tsapatsis, M.; Lobo, R. F.; Balkus, K. J.; Davis, M. E. *Nature* **1996**, 381, (6580), 295-298.
8. Inoue, K.; Yoshizuka, K.; Ohto, K. *Analytica Chimica Acta* **1999**, 388, (1-2), 209-218.
9. Kushwaha, A. K.; Gupta, N.; Chattopadhyaya, M. C. *Journal of Chemical and Pharmaceutical Research* **2011**, 807-815.
10. Shannon, M. A.; Bohn, P. W.; Elimelech, M.; Georgiadis, J. G.; Marinas, B. J.; Mayes, A. M. *Nature* **2008**, 452, (7185), 301-310.
11. Khan, A. *Separation Science and Technology* **2006**, 41, (6), 1169-1177.
12. Idris, S. A.; Harvey, S. R.; Gibson, L. T. *Journal of Hazardous Materials* **2011**, 193, 171-176.
13. Koehler, F. M.; Rossier, M.; Waelle, M.; Athanassiou, E. K.; Limbach, L. K.; Grass, R. N.; Gunther, D.; Stark, W. J. *Chemical Communications* **2009**, (32), 4862-4864.
14. Liu, J.-f.; Zhao, Z.-s.; Jiang, G.-b. *Environmental Science & Technology* **2008**, 42, (18), 6949-6954.
15. Zhai, Y.; He, Q.; Han, Q.; Duan, S. e. *Microchimica Acta* **2012**, 178, (3-4), 405-412.
16. Rofouei, M. K.; Rezaei, A.; Masteri-Farahani, M.; Khani, H. *Analytical Methods* **2012**, 4, (4), 959-966.
17. Shen, X.; Wang, Q.; Chen, W.; Pang, Y. *Applied Surface Science* **2014**, 317, 1028-1034.
18. Faraji, M.; Yamini, Y.; Saleh, A.; Rezaee, M.; Ghambarian, M.; Hassani, R. *Analytica Chimica Acta* **2010**, 659, (1-2), 172-177.
19. Wang, Y.; Luo, X.; Tang, J.; Hu, X.; Xu, Q.; Yang, C. *Analytica Chimica Acta* **2012**, 713, 92-96.
20. Mandel, K.; Hutter, F.; Gellermann, C.; Sextl, G. *ACS Applied Materials & Interfaces* **2012**, 4, (10), 5633-5642.
21. Rossier, M.; Koehler, F. M.; Athanassiou, E. K.; Grass, R. N.; Aeschlimann, B.; Gunther, D.; Stark, W. J. *Journal of Materials Chemistry* **2009**, 19, (43), 8239-8243.
22. Grass, R. N.; Athanassiou, E. K.; Stark, W. J. *Angewandte Chemie International Edition* **2007**, 46, (26), 4909-4912.
23. Kainz, Q. M.; Schätz, A.; Zöpfl, A.; Stark, W. J.; Reiser, O. *Chemistry of Materials* **2011**, 23, (16), 3606-3613.
24. Kainz, Q. M.; Linhardt, R.; Grass, R. N.; Vilé, G.; Pérez-Ramírez, J.; Stark, W. J.; Reiser, O. *Advanced Functional Materials* **2014**, 24, (14), 2020-2027.
25. Kainz, Q. M.; Linhardt, R.; Maity, P. K.; Hanson, P. R.; Reiser, O. *ChemSusChem* **2013**, 6, (4), 721-729.
26. Kainz, Q. M.; Reiser, O. *Accounts of Chemical Research* **2014**, 47, (2), 667-677.

27. Kainz, Q. M.; Zeltner, M.; Rossier, M.; Stark, W. J.; Reiser, O. *Chemistry - A European Journal* **2013**, 19, (30), 10038-10045.
28. Schätz, A.; Grass, R. N.; Stark, W. J.; Reiser, O. *Chemistry - A European Journal* **2008**, 14, (27), 8262-8266.
29. Keller, M.; Perrier, A.; Linhardt, R.; Travers, L.; Wittmann, S.; Caminade, A.-M.; Majoral, J.-P.; Reiser, O.; Ouali, A. *Advanced Synthesis & Catalysis* **2013**, 355, (9), 1748-1754.
30. Wittmann, S.; Schätz, A.; Grass, R. N.; Stark, W. J.; Reiser, O. *Angewandte Chemie International Edition* **2010**, 49, (10), 1867-1870.
31. Rossier, M.; Schaez, A.; Athanassiou, E. K.; Grass, R. N.; Stark, W. J. *Chemical Engineering Journal* **2011**, 175, 244-250.
32. Rossier, M.; Koehler, F. M.; Athanassiou, E. K.; Grass, R. N.; Waelle, M.; Birbaum, K.; Günther, D.; Stark, W. J. *Industrial & Engineering Chemistry Research* **2010**, 49, (19), 9355-9362.
33. Tawabini, B.; Al-Khaldi, S.; Atieh, M.; Khaled, M. *Water Science and Technology* **2010**, 61, (3), 591-598.
34. Masri, M. S.; Friedman, M. *Environmental Science & Technology* **1972**, 6, (8), 745-746.
35. Soleimani, M.; Ghahraman Afshar, M.; Sedghi, A. *ISRN Nanotechnology* **2013**, 6, 745-746.
36. Liu, Y.; Wu, D.-C.; Zhang, W.-D.; Jiang, X.; He, C.-B.; Chung, T. S.; Goh, S. H.; Leong, K. W. *Angewandte Chemie International Edition* **2005**, 44, (30), 4782-4785.
37. Kainz, Q. M.; Fernandes, S.; Eichenseer, C. M.; Besostri, F.; Korner, H.; Muller, R.; Reiser, O. *Faraday Discussions* **2014**, 175, 27-40.
38. Tucker-Schwartz, A. K.; Garrell, R. L. *Chemistry - A European Journal* **2010**, 16, (42), 12718-12726.
39. Schaez, A.; Zeltner, M.; Michl, T. D.; Rossier, M.; Fuhrer, R.; Stark, W. J. *Chemistry - A European Journal* **2011**, 17, 10566-10573.
40. Kyzas, G.; Deliyanni, E. *Molecules* **2013**, 18, (6), 6193-6214.
41. Bazzicalupi, C.; Bianchi, A.; Giorgi, C.; Gratteri, P.; Mariani, P.; Valtancoli, B. *Inorganic Chemistry* **2013**, 52, (4), 2125-2137.
42. Iron in drinking water. Guidelines for drinking-water quality, 2nd Ed., Vol. 2, World Health Organization. Geneva, 1996.
43. Lin, Y.-J.; Tsai, B.-K.; Tu, C.-J.; Jeng, J.; Chu, C.-C. *Tetrahedron* **2013**, 69, (7), 1801-1807.

Chapter 3

Development and characterization of suitable antifouling magnetic nanocarriers for RNAi therapy

Herein, the potential of two nanocarriers for RNAi therapy was studied. Two different procedures were followed to coat the different magnetic nanocubes (NCs), composed of iron oxide or manganese ferrite, with positively-charged species that can bind the negatively-charged siRNA simply by electrostatic interaction. Both the cationic nanocubes were fully characterized to assess their physicochemical properties, their behavior in biological environment and the capacity to deliver siRNA to living cells. Iron oxide nanocubes coated with a pH-responsive copolymer containing (dimethylamino)ethyl methacrylate (DMAEMA) and oligoethylene glycol methyl ether methacrylate (OEGMEMA) moieties showed to be quite promising, loading high amounts of siRNA and reducing the non-specific adsorption of proteins, therefore allowing its delivery into the cells without cytotoxic signs.

The functionalization of cationic IONCs (**25**) was performed by my colleague Thanh-Binh Mai and is it is confidential since is not yet published and subject to patenting evaluation.

3.1 Introduction

RNA interference (RNAi) technology is an endogenous pathway for post-transcriptional gene silencing which is triggered by small double stranded RNA (dsRNA) molecules, such as small interfering RNAs (siRNA) and microRNAs (miRNA).¹ By activating this path, RNAs can target and downregulate the expression of specific genes, binding to their complementary messenger RNA (mRNA) sequences.² Thus, the use of synthetic siRNA, endogenous miRNA or oligonucleotides, has emerged as a very promising and revolutionary therapeutic approach for genetic based diseases such as cancer, since they were found to work in mammalian cells.^{1,3}

The RNAi machinery (Fig.1) starts with the binding of the siRNA to the RNA-induced silencing complex (RISC) which separates the two strands of siRNA, allowing the guiding activated-RNA strand to identify, bind and cleave complementary mRNA. As a result, the biosynthesis of the correspondent protein is suppressed. Once incorporated in the RISC, the siRNA can catalyze hundreds of times the gene silencing of identical mRNAs.^{2,4}

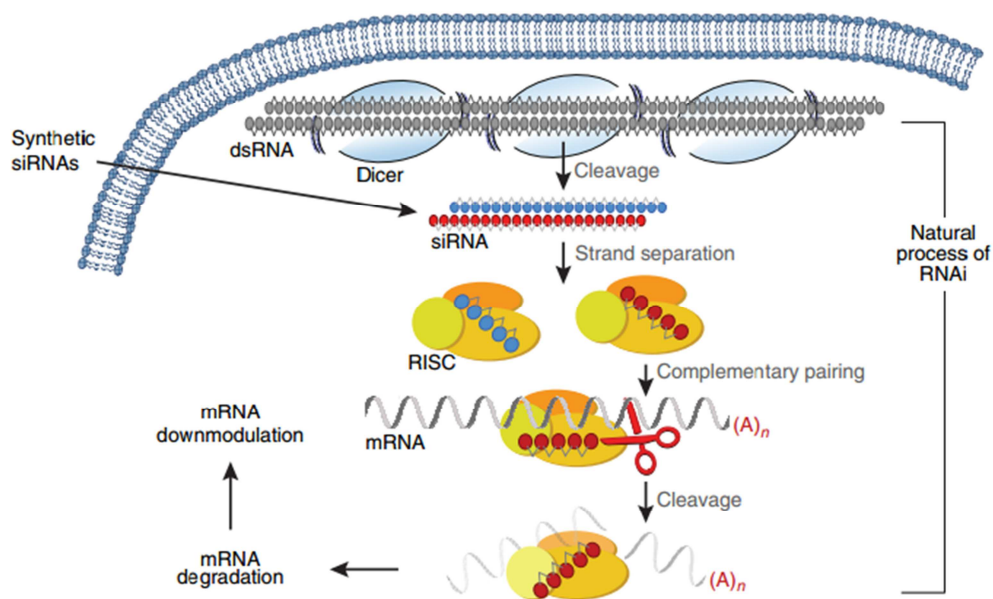


Fig. 1 RNAi machinery scheme. Natural occurring long double-stranded RNAs are introduced into the cytoplasm, where they are cleaved into small interfering RNAs (siRNAs) by the enzyme Dicer. Alternatively, synthetic siRNAs can be introduced directly into the cell. The siRNA is then incorporated into RISC, resulting in the cleavage of the sense strand of RNA. The activated RISC-siRNA complex binds to and degrades complementary mRNA, which leads to the silencing of the target gene. The activated RISC-siRNA complex can then be recycled for the destruction of identical mRNA targets hundreds of times. Scheme adapted with permission from reference 5. Copyright 2006, Nature Publishing Group.

This type of therapy offers some advantages when compared to conventional drugs of synthetic origin: (1) it can target and inhibit mostly any gene, being more than 20 RNAi-based drugs already involved in clinical trials;^{2,5} (2) siRNAs can be easily synthesized in contrast to other biomolecules such as

antibodies or proteins;⁵ (3) siRNAs are highly selective.⁶ However, there are still some limitations on the current siRNA formulations which need to be overcome prior to consider RNAi a valuable alternative therapeutic approach for human diseases. Among them it is possible to distinguish at least four critical issues: (1) the protection from degradation; (2) efficient targeted delivery; (3) silencing specificity; (4) immunogenicity/toxicity. In particular, the delivery of the RNA molecules remains the biggest challenge in clinical applications, for several reasons. It has passed over a decade since Dr. Inder Verma proclaimed “There are only three problems in gene therapy: delivery, delivery and delivery”,^{3,7} but the issue remains an open challenge and opportunity. Also, siRNA by its own has a limited capacity to breakdown the protein expression, due to its instability in the blood stream, the possibility of causing immune responses and the incapacity of diffusing across the cell membrane as a negative, hydrophilic large molecule.⁸ Specifically, when administered in the blood stream, naked siRNA can be degraded very quickly by serum nucleases and stimulate the immune system. Additionally, there were found indications that other factors, involved in the RNAi machinery, can be saturated by over-expressed exogenous siRNAs. This might result in major implications, as reported for the death of mice after PolIII promoter-driven expression of small hairpin RNA (shRNAs) in the liver.⁹ Therefore, research is pushing forward on the development of good delivery systems to bring RNA to its activity site in low effective doses and deprived of any toxic effect.¹⁰

An ideal carrier aiming a successful delivery has to overcome both extracellular and intracellular barriers once administered into the bloodstream (Fig. 2). The carrier must payload and protects the siRNA from degradation and clearance, thus increasing the circulation time in the blood stream by reducing the non-specific interactions with serum proteins (antifouling effect).¹⁰⁻¹³

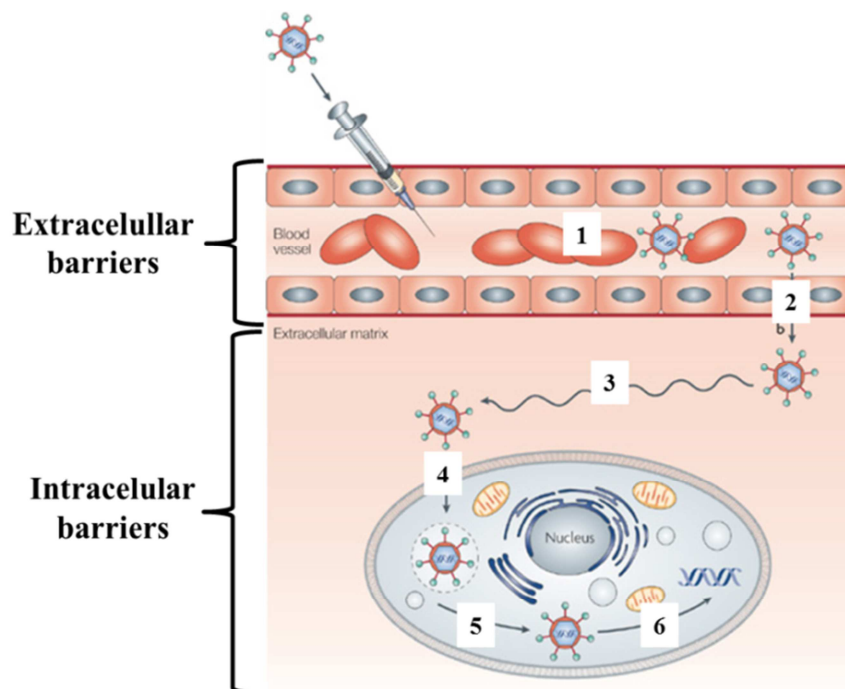


Fig. 2 Schematic trafficking of siRNA-carriers after systemic administration. Both extra and intracellular barriers must be overcome in order to successfully silence target genes. The carriers have to be able to (1) avoid

filtration, phagocytosis and degradation in the bloodstream; (2) be transported across the vascular endothelial barrier; (3) diffuse through the extracellular matrix; (4) enter the cells; (5) escape the endosomal / lysosomal degradation; (6) release the siRNA inside the cell cytosol for RNAi machinery. Scheme adapted with permission from reference 11. Copyright 2009, Nature Publishing Group.

Indeed, the carrier interaction with serum components can cause undesired aggregation with erythrocytes or interaction with other particular proteins, which might tag the delivery vehicles for other cells rather than the target cells for treatment. For instance, the adsorption of opsonins on the carrier promotes its uptake by the mononuclear phagocyte system leading to undesired clearance of the carriers from the bloodstream.^{10,13} In addition, the carrier has to be able to promote cellular uptake, escape the endosomal-lysosomal degradation system and ultimately release the siRNA into the cytosol for entering the RNAi machinery (see Fig. 2).^{11,12}

Considering the endosomal escape, the most commonly used strategy is to induce the so-called “proton sponge” effect. For this purpose, cationic polymers are widely used. However, even though they actually improve the cellular uptake they were proven to induce undesired cytotoxicity and non-specific accumulation in the body.^{8,14} As an alternative, less toxic pH-responsive polymers, which can be protonated under acidic pH to assist endosomal escape, can be used.⁸ The proton sponge effect is directly related with the pH-buffering capacity of the RNA-carrier to retain the protons, during endosomal acidification upon cellular uptake. Alongside, the accumulation of Cl⁻ counter ions disturbs the osmotic pressure inside the endosomal vesicle, eventually leading to its swelling and disruption releasing the nanocarriers into the cell cytoplasm.

The two main strategies in RNAi technology are the delivery of shRNA-encoding genes, by engineering viruses which ultimately generate siRNAs, or the non-viral delivery of synthetic siRNAs.^{1,7,9} No ideal delivery system had been found so far, thus it is important to accurately study the advantages and disadvantages of each of these approaches for clinical translation. Viral vector-dependent delivery systems are generally more effective due to their intrinsic capacity to infect cells. However, they have big constraints concerning immunogenicity. On the other hand, non-viral therapy arises as a less expensive and less immunogenic alternative.^{2,8} It is worth mentioning, that already few years ago, some of the artificial siRNA carriers based on liposomes and siRNA-protein conjugates have been under clinical trial evaluation as siRNA based therapeutics in several human diseases.^{2,15} Compared to naked siRNA sequences the aforementioned carriers showed improved performance in delivery efficiency, targeting specificity and silencing efficacy.¹⁵

Currently, the most commonly studied RNA-carriers are polycations like polyethylene imine^{14,16,17} and poly-L-lysine¹⁸ or lipid-like particles¹⁹ bearing positively charged head groups, such as Lipofectamine[®] 2000. The main benefit of using such carriers is their ability to form polyelectrolyte complexes with the negatively charged-RNAs simply by electrostatic interaction.³ Nevertheless, other nanomaterials such as silica coated nanoparticles, carbon nanotubes and magnetic nanoparticles, are gaining much attention for RNAi therapy.²⁰ Indeed, the proper functionalization of all these nanoscale

materials has the potential to provide a successful dose of siRNAs or miRNAs required for gene delivery, given their high surface to volume ratio (the size range of these nanoparticles is 10-50 nm vs 150-200 nm of liposomes like particles or poly-L-lysine complexes). Magnetic nanoparticles in particular have the advantage of magnetic guidance and accumulation on the desired site of action. They were first introduced for drug delivery purposes late in the 1970s by Widder *et al.*²¹ Here, the authors show the efficacy of magnetic albumin microspheres for tumor therapy and as magnetic resonance contrast agents, in animal experiments. This study prepared the ground to the use of magnetic nanoparticles surrounded by a biocompatible coating in biological systems. Ideally, in a real application, the complex NP-therapeutic agent should be injected into the blood stream, via blood vessels close to the body region where the carrier needs to be delivered. Then a magnetic field is applied at the target site forcing the particles to enter the defective cells.^{21,22}

In the last few years, an increasing attention has been paid to the efficient synthesis of shape-controlled, stable and monodisperse iron oxide nanoparticles (IONPs).²³ Indeed, various studies have proved the potential of magnetic nanoparticles for being used in a variety of biomedical applications like hyperthermia treatment,^{24,25} drug delivery,²⁶⁻²⁸ MRI contrast agents²⁹ and transfection carriers.²⁰ For instance, Boyer *et al.* have shown that IONPs coated with poly(oligoethylene glycol) methyl ether acrylate (P(OEGMA)) and poly(dimethylaminoethyl acrylate) (P(DMAEA)) could be used at the same time as siRNA transfection carrier and be monitored as MRI contrast agents *in vitro*.³⁰ Other studies, have demonstrated the effectiveness of IONPs modified with cationic polymers to yield siRNA-IONPs complexes.^{31,32}

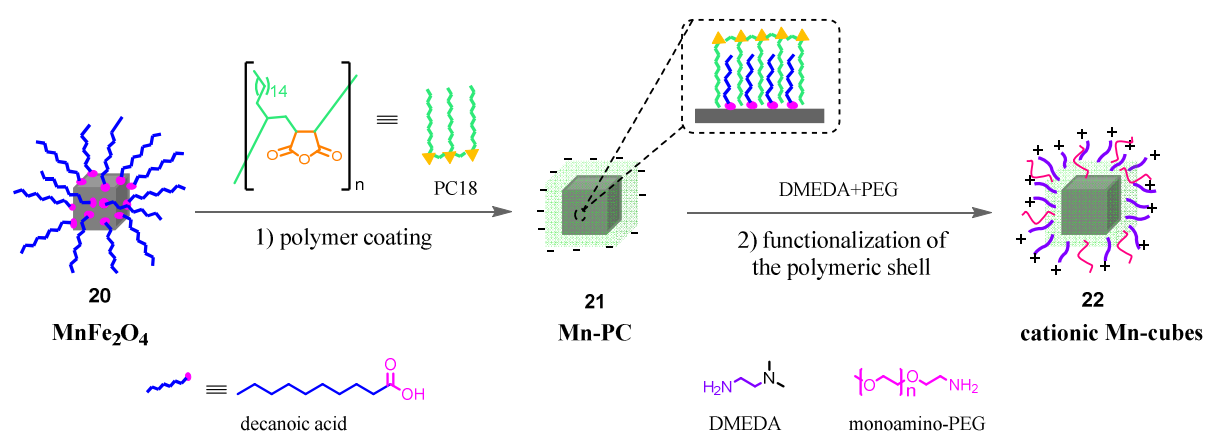
Following the aforementioned evidences, the motivation of this research work was to test new pH-responsive magnetic materials, recently synthesized in Pellegrino's group as magnetic carriers for siRNA molecules. A protocol to obtain controlled colloidal synthesis of monodisperse magnetic iron oxide nanocubes (IONCs)²⁵ and their subsequent transfer in water was recently developed.^{33,34} The possibility to further functionalize these IONCs without compromising their stability and biocompatibility, would enable their use in biological applications such as drug²⁶ or gene delivery.³⁵ In addition, since Pellegrino's group is focused also on the synthesis of new magnetic nanoparticles having available different type of iron oxide or ferrite particles with enhanced features for magnetic hyperthermia, this work explored the possibility to combine heat mediated gene delivery with hyperthermia. Indeed a synergistic therapy reported by Lee *et al.*³⁶ showed that their nanocubes were capable of targeting tumor cells for combined siRNA and hyperthermia-based therapy, resulting in a significant inhibition of proliferation and induction of apoptosis in tumor cells. For this purpose, great efforts were done to synthesize and fully characterize antifouling positively-charged nanocubes of two different chemical natures: manganese ferrite and iron oxide nanocubes. The characterization involved the determination of physicochemical properties but also the biological evaluation of the systems' stability in biological fluids and its interaction with cells including a comparative study of their cytotoxicity. In particular, positive-functionalized IONCs were exploited for the loading of siRNA

molecules. Then, the characterized conjugates IONCs-siRNA were applied for gene silencing therapy studies. Thanks to its suitability, anti-green fluorescent protein (GFP) siRNA was used as a model RNA for validating the effectiveness of nanocarriers as delivery tools for mammalian cells transfection. The carriers' efficiency was evaluated by the downregulation of GFP in human cervical carcinoma cells (HeLa) assessed by fluorescent assay.

3.2 Results and discussion

3.2.1 Preparation and characterization of cationic MnFe_2O_4 cubes by polymer coating and further functionalization of the polymeric shell

The effectiveness of cationic nanocubes (NCs) to load and delivery siRNA, was done by comparing two types of different materials. The first sample was prepared accordingly with the synthesis in Scheme 1. Manganese ferrite nanocubes (here referred as MnFe_2O_4 , **20**), with a size of 13 ± 2 nm, were prepared according to non-hydrolytic wet-chemical protocol, still under development in Pellegrino's group. Then, the as-synthesized nanocubes (**20**), were modified with a positively charged coating (here referred as cationic Mn-cubes, **22**) by a two-step approach: (1) they were first transferred into water enwrapping them in a polymeric amphiphilic shell of poly(maleic anhydride *alt*-1-octadecene) (hereafter referred as PC18);³³ (2) followed by the covalent attachment, via EDC chemistry, of amino bearing tertiary amine named *N,N'*-dimethylethylenediamine (hereafter referred as DMEDA) in order to render them positively-charged and methoxypolyethylene glycol amine (hereafter referred as monoamino-PEG), to improve colloidal stability.



Scheme 1 Sketch of the synthesis of water soluble positively-charged MnFe_2O_4 nanocubes later used for the delivery of siRNA. Starting from hydrophobic MnFe_2O_4 nanocubes (**20**) in CHCl_3 they were first transferred to water by means of polymer coating with poly(maleic anhydride-*alt*-1-octadecene), followed by the covalent linkage of a tertiary amine (DMEDA) and monoamino-PEG molecules to give cationic Mn-cubes (**22**).

Briefly, a large excess of the amphiphilic polymer PC18 was mixed with the as-synthesized MnFe_2O_4 nanocubes (**20**) in chloroform such that a ratio of monomeric polymer units of 500 molecules per nm^2 was set. The development of the polymeric shell is promoted by the intercalation of the hydrophobic alkyl chains of the polymer with the aliphatic chains of the surfactant which coats the nanocubes during solvent evaporation. The hydrophilic region of the polymer is developed during exposure of the maleic anhydride groups at the surface of nanocubes to the water solution added to the dried nanocubes in a second step. The polymer-coated cubes (here mentioned as Mn-PC, **21**) were brought in water by sonication and the excess of polymer was efficiently removed in a sucrose gradient by ultracentrifugation, giving stable monodisperse Mn-PC cubes (**21**) as observed by evaluating their migration band by gel electrophoresis, the hydrodynamic size by dynamic light scattering (DLS) (Fig.3B) and their spectroscopic image by transmission electron microscopy (TEM) analysis (Fig.3A-C). Once transferred into water, Mn-PC (**21**) can be further functionalized by EDC chemistry on the PC18 carboxyl groups exposed on the nanocrystals' surface. Accordingly, a tertiary amine (DMEDA) and monoamino-PEG (750 Da) molecules were covalently attached to the surface of the Mn-PC (**21**). As a result, positively charged and monodisperse Mn-cubes (**22**) were obtained. The comparative measure of the zeta potential confirmed the successful charge conversion from approximately -48 mV to +35 mV, due to the presence of tertiary amines on the surface (Fig. 3). Moreover, the functionalization of the polymeric shell did not compromise the overall size and stability of the nanocubes, as seen by DLS (Fig.3B) and TEM (Fig.3C and 3D). The PEG polymer molecules were employed for stability purposes, particularly to reduce the non-specific protein interaction of the materials when in contact with biological fluids (antifouling ability).³⁰

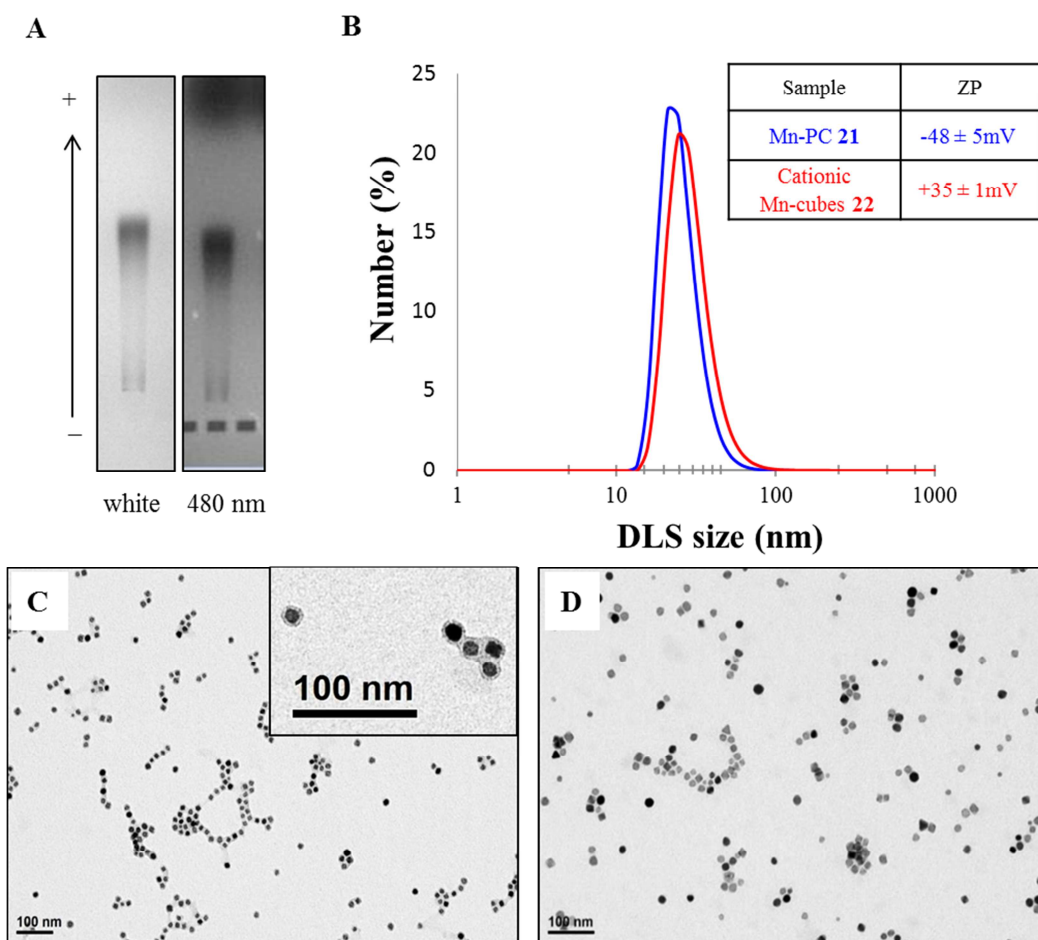


Fig. 3 **A**) Gel electrophoresis of Mn-PC cubes (**21**) after having removed the free polymer by ultracentrifugation. Agarose gel 1% was used and a potential of 100V was applied for 45 minutes. **B**) Average hydrodynamic sizes before and after DMEDA functionalization, inset: zeta potential, in water of the Mn-PC (**21**) and cationic Mn-cubes (**22**). Color code: blue for Mn-PC (**21**) and red for cationic Mn-cubes (**22**). TEM image (scale bars 100 nm) of: **C**) Mn-PC (**21**); cationic Mn-cubes (**22**).

Different types of iron oxide nanocubes have been investigated in Pellegrino's group for their heating ability under an alternating magnetic field.^{24,25} The heating capacity of the magnetic materials is expressed as the specific absorption rate (SAR). Specifically, the SAR provides a measure of the rate at which energy is adsorbed per unit mass (g) of magnetic material when exposed to a radiofrequency. This depends not only on the amplitude of the magnetic field (H) and frequency (f) applied but also on the structure and composition of the NCs.²⁴

SAR measurements were performed on the manganese ferrite Mn-PC (**21**) in order to evaluate their heat performance for hyperthermia applications.

The SAR values, normalized to the iron amount, are calculated according to the equation:

$$SAR \left(\frac{W}{g} \right) = \frac{C}{m} \times \frac{dT}{dt}$$

where $C(\text{J} \cdot \text{L}^{-1} \cdot \text{K}^{-1})$ is the specific heat capacity of water per unit volume and m is the iron concentration in ($\text{g} \cdot \text{L}^{-1}$) of the NCs in solution.³⁷

SAR measurements were performed by introducing an aqueous solution of the magnetic materials in a device consisting of a coil generating magnetic fields of different frequencies and magnetic field amplitudes. The measurements were performed in non-strictly adiabatic conditions, therefore only the first few seconds of the curve temperature vs. time (dT/dt) were used for estimating the slope. A concentration of nanocubes that allows a steep increase of the temperature over few seconds is then necessary.

Fig. 4A displays the SAR values as a function of the magnetic field intensity (H) and Fig 4B the product Hf at two different frequencies (300 and 105 KHz) and for three different fields (12, 16 and 24 $\text{kA}\cdot\text{m}^{-1}$) for both manganese ferrite Mn-PC (**21**) and iron oxide nanocubes of approximated size. The iron oxide cubes²⁵ were transferred to water as described for the manganese ferrite nanocubes, presenting a charge of -45 mV. This set of data shows a decrease in the SAR values for the manganese ferrite NCs (**21**) when compared to the correspondent iron oxide nanocubes of similar size.

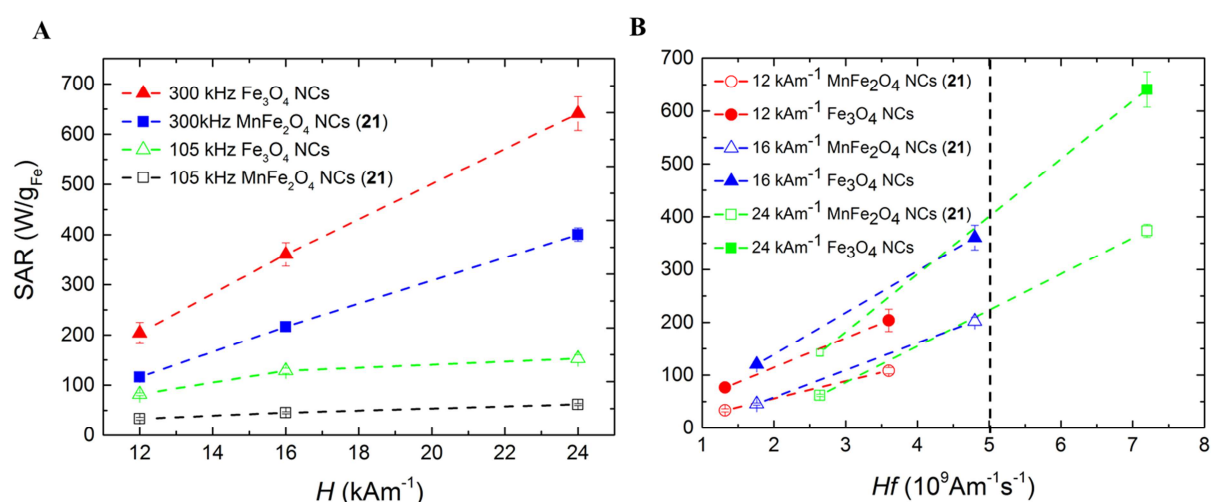


Fig. 4 The graphs show the comparison of the SAR values for Mn-PC (**21**) (13 ± 2 nm) (squares) and the approximately correspondent in size (14 ± 3 nm) standard iron oxide nanocubes (triangles). **A**) SAR values as a function of the magnetic field amplitude H for water soluble Mn-PC (**21**) at 300 (■ blue squares), and 105 kHz (□ black empty squares). Iron oxide nanocubes of the same size were measured as a comparison at 300 (▲ red triangles) and 105 kHz (△ green empty triangles). Each experimental data point was calculated as the mean value of at least 4 measurements and error bars indicate the standard deviation. **B**) SAR values as a function of the product Hf for water soluble Mn-PC (**21**) at 24 (□ green empty squares), 16 (△ blue empty triangles) and 12 $\text{kA}\cdot\text{m}^{-1}$ (○ red empty circles). The corresponding full symbols indicate the SAR values for the standard iron oxide nanocubes at the same field intensities. The vertical dashed line defines the biological limit ($5 \times 10^9 \text{A}\cdot\text{m}^{-1}\cdot\text{s}^{-1}$).³⁸

In Fig. 4A, considering the measurement for the highest applied field intensity and frequency, it is possible to notice a drop in the SAR value from 640 to $374 \text{W}\cdot\text{g}_{\text{Fe}}^{-1}$, being the highest value registered for the iron oxide nanocubes. The same trend is observed for the other frequency-amplitude combinations. In addition from Fig.4B, it is evident that within magnetic fields and frequencies that

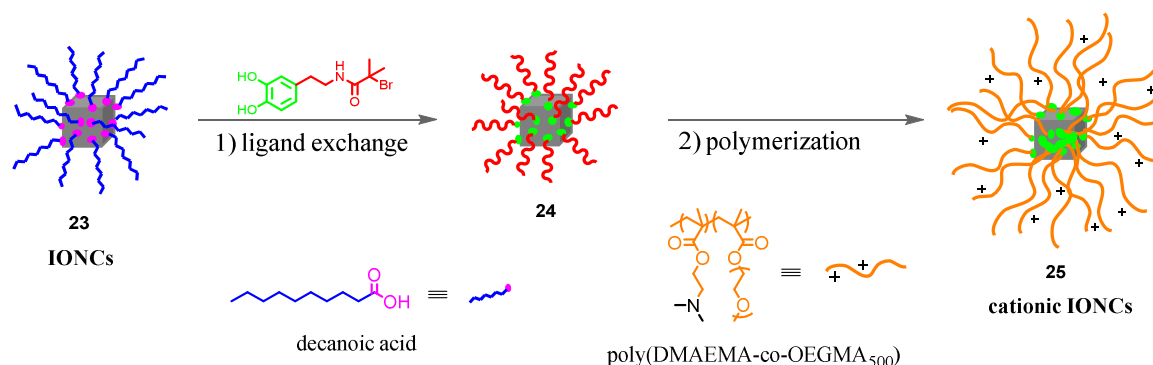
are tolerated by patients (dashed black line) Mn-PC (**21**) have quite low SAR values. Nevertheless, the results shown in Fig. 14 compare well to those obtained by Lee *et al.* who have used nanoparticles with a SAR value of $69 \text{ W} \cdot \text{g}_{\text{Fe}}^{-1}$ (at 334 kHz and $12 \text{ kA} \cdot \text{m}^{-1}$) for the combined therapy of gene delivery with hyperthermia.³⁶

This preliminary data suggests that the manganese ferrite NCs have the potential for being used in hyperthermia treatments, however a better control over shape and size of the nanocubes during the synthesis would be needed to improve the SAR values, as reported before for iron oxide nanocubes by Guardia *et al.*²⁴

3.2.2 Preparation and characterization of cationic IONCs by copolymerization of DMAEMA and OEGMEMA

The second approach followed for preparing water soluble cationic iron oxide nanocubes which were also tested for delivery of siRNA is shown in Scheme 2. In this case, given the very high heating performance of iron oxide nanoparticles of 16 nm in cube edge, this sample was selected. Positive cubes (here referred as cationic IONCs, **25**) were prepared by a two-step approach that involves first a ligand exchange protocol to introduce the macro-initiators on the surface of the iron oxides nanocubes (**23**). Then, in a second step, the polymerization of (dimethylamino)ethyl methacrylate (DMAEMA) and oligoethylene glycol methyl ether methacrylate (OEGMEMA) took place (unpublished procedure). The excess of polymer was removed on a sucrose gradient by ultracentrifugation on the top layer of the gradient, and the resulting water soluble highly positive nanocubes were collected on a different density layer. The cationic IONCs (**25**) were very uniform in size and individual particles with no sign of aggregation could be detected as shown in Fig.5A and 5B.

The DMAEMA moieties act as a pH-responsive block which might trigger endosomal-lysosomal escape and degradation by reinforcing the proton sponge effect, thus being quite attractive for the envisage application in this work.³⁹



Scheme 2 Synthesis of cationic IONCs. The as-synthesized IONCs (**23**) are first subjected to a ligand exchange procedure (1) in order to introduce on the surface the macro-initiators. The copolymerization of DMAEMA and OEGMEMA is then carried out on the nanocubes surface (2) to achieve cationic IONCs (**25**).

Following such a protocol IONCs with charges as high as approximately +50 mV (Fig. 5A) were obtained, thanks to the presence of the DMAEMA block of the co-polymer. On the other hand, the OEGMEMA chains are responsible for retaining the stability and reducing unspecific protein adsorption on the surface in biological medium, thereby improving the antifouling properties of the nanocubes.

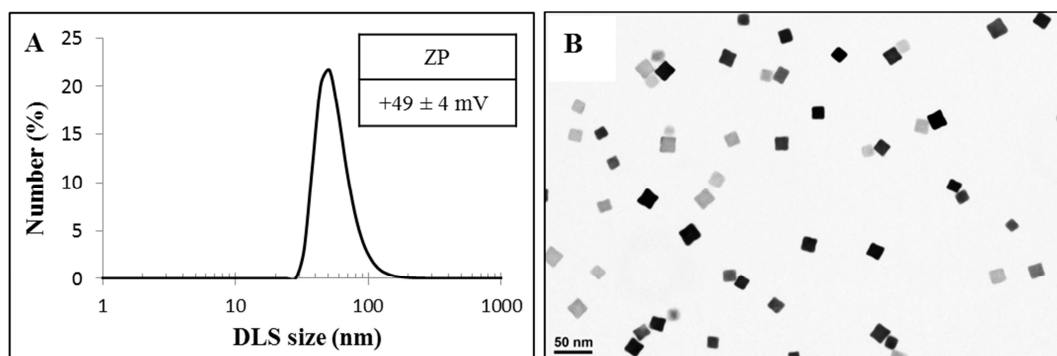


Fig. 5 Average hydrodynamic size (A), zeta potential (inset panel A) and TEM image (B) of cationic IONCs (25) (scale bar 50 nm).

3.2.3 Stability of the synthesized cationic nanocubes in FBS and physiological medium – interaction with serum proteins

The application of nanocubes in the biomedical field is mainly related to their stability, biodistribution and toxicity.⁴⁰ Particularly, the tendency of the nanoparticles to aggregate in high-ionic-strength fluids, as the biological media, is one of the main key limitations for their applications in biomedicine. Particle aggregates can block the blood capillaries and are usually recognized as foreign materials by the immune system being cleared from the blood circulation by the reticuloendothelial system (RES).⁴¹ The key to avoid agglomeration and stabilize the nanoparticles is to overcome magnetic and Van der Waals attraction forces, by engineering their surface, introducing coatings capable of providing steric or electrostatic repulsion at the magnetic nanoparticles surface.⁴¹ Additionally, it is well known that the adsorption of protein onto the surface of nanoparticles occurs immediately upon contact of the magnetic nanoparticles with the physiological environment, forming the so-called protein corona.^{41, 42} The protein corona formation strongly depends on nanoparticle characteristics such as morphology, charge, porosity, crystallinity, roughness, or surface coating. The physical properties of the MNPs are significantly altered after the formation of protein corona, resulting in changes in their size, composition and colloidal stability that might favor particle agglomeration. Thus, the protein layer on the surface provides a new identity of the nanomaterial which determines their behavior and interaction with living cells.^{40,43}

To evaluate the biological impact of the developed magnetic carriers, in particular their antifouling properties, the positive charged NCs were tested for the stability in a 10% fetal bovine serum (FBS) aqueous solution and Dulbecco's Modified Eagle Medium (DMEM) supplemented equally with 10% FBS. The nanocubes were monitored visually over time by checking if precipitation or aggregation occurred. The results in Fig. 6 clearly show that both types of cationic materials, Mn-cubes (**22**) and IONCs (**25**), are stable in the presence of serum proteins (Fig. 6 B, C, E and F) in contrast to the Mn-PC (**21**) which precipitate quite fast (Fig. 6A and 6D).

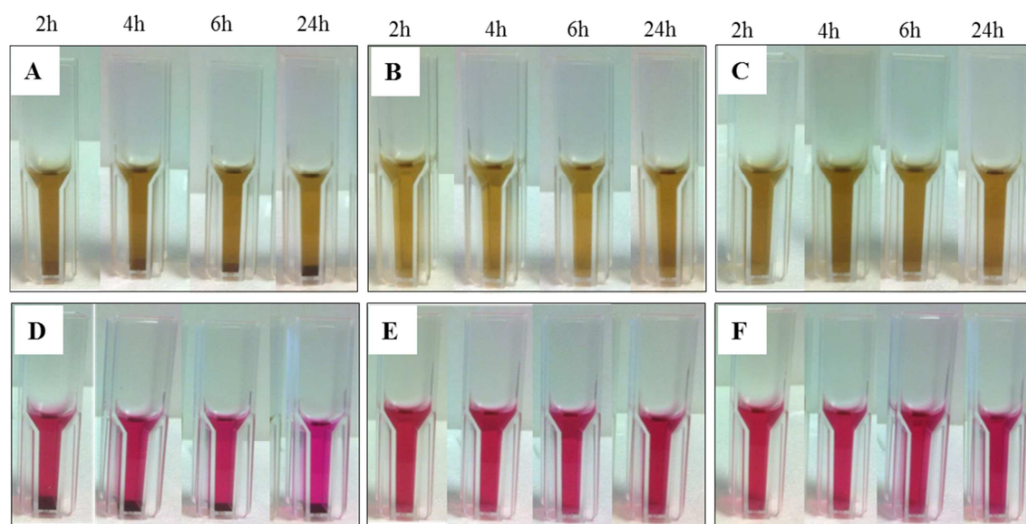


Fig. 6 Stability proof of the nanocubes in 10% FBS aqueous solution (A-C) and DMEM supplemented with 10% FBS (D-F), during 24h of incubation. **A, D** Mn-PC (**20**); **B, E** cationic Mn-cubes (**22**); **C, F** cationic IONCs (**25**).

Furthermore, the protein adsorption on the surface of the cationic Mn-cubes (**22**) and cationic IONCs (**25**) was evaluated by sodium dodecyl sulfate-polyacrylamide gel electrophoresis (SDS-PAGE), which consists on the separation of denatured proteins according to their electrophoretic mobility. Essentially, the SDS detergent linearizes the proteins' charge to negative which then migrate simply according to their molecular weight. The aim of this test was to study and better understand to which extent the protein corona is formed on the surface of these nanocubes and which are the consequences of the different coatings applied on the formation of the corona. Fig. 7 reveals considerably less pronounced bands for both cationic nanocubes (**22** and **25**) compared to the strong bands detected for Mn-PC (**21**). This indicates a much lower amount of adsorbed proteins on the cationic NCs that is most likely due to the presence of the PEG molecules in the polymeric shell which provide antifouling features.

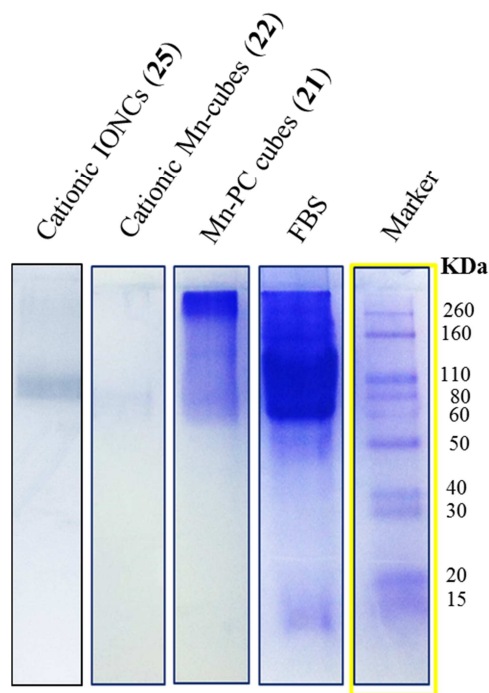


Fig. 7 Comassie stained SDS-PAGE gel of NCs-PC (**21**), cationic Mn-cubes (**22**) and cationic IONCs (**25**) after 90 minutes of incubation in FBS solution. The electrophoresis was run at 120 V for 60 minutes on a 12% acrylamide gel. After, the gel was stained with Comassie for visual evaluation of the protein bands.

Nonspecific protein adsorption on the surface of nanoparticles, forming the protein corona, is commonly defined as a negative effect, once it can compromise the fate of the nanoparticles. However, it is well known that the formation of coronas is also relevant to help on the stabilization of the nanoparticles in biological systems.^{41,44} The advantages and disadvantages of protein corona formation strongly depend on the nature of the protein-nanoparticle interaction, considering the amount and type of proteins adsorbed.⁴¹

From the results obtained for our positive charged materials, one can assume that the protein corona occurs to an extent in which it doesn't compromise the colloidal stability of the nanocubes in biological environment (see Fig. 6). Less clear results were found for Mn-PC (**21**), which precipitated early after incubation with the serum. To better comprehend the effect of the corona formation in these cationic magnetic nanocubes, the time evolution of the hydrodynamic diameter of cationic IONCs (**25**) was measured for 24h, to assess their stability in biological medium in the presence or absence of FBS.

As depicted in Fig. 8, in the presence of FBS the nanocubes show an excellent stability over an incubation of 24h in biological medium, while in the non-supplemented medium the nanocubes reveal significant aggregation. These results proved that the corona effect is favorable and greater stability of the nanohybrids is achieved, allowing a safe application of these NCs for biological studies.

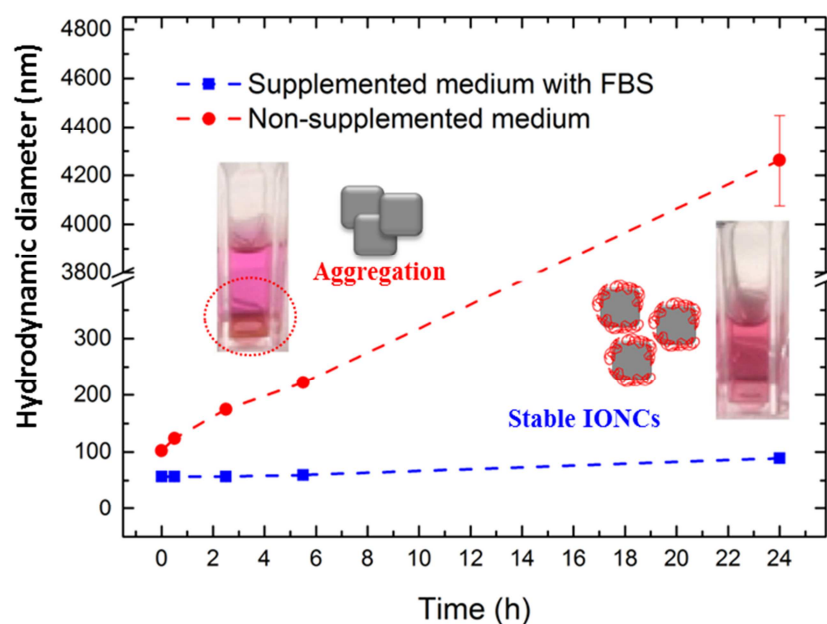


Fig. 8 Hydrodynamic diameter (intensity average) monitoring study of cationic IONCs (**25**) in biological medium in the presence or absence of 10% FBS, over a total incubation period of 24h. The red curve indicates the hydrodynamic size of the IONCs incubated in non-supplemented medium, while the blue curve indicates the hydrodynamic diameter for the IONCs incubated with FBS supplemented medium.

3.2.4 Cell cytotoxicity and intracellular iron concentration estimation

The cytotoxicity and uptake of nanoparticles by cells depends mainly on the materials properties like size, shape, composition, surface charge and surface hydrophobicity.⁴⁵

Firstly, the cytotoxicity of cationic Mn-cubes (**22**) was studied at different incubation times (24, 48 and 96h) and at various Fe concentrations in a range from 6 to 50 $\mu\text{g}\cdot\text{mL}^{-1}$ on human cervical carcinoma cell line (HeLa) cells. HeLa cells were chosen here due to the possibility to be used also for the protein downregulation experiments in a later stage. The cellular viability was assessed by PrestoBlue (PB) assay which consists on the change in color of the PB reagent once reduced by metabolic active living cells. The percentage of viable cells was estimated by monitoring the absorbance of the PB solution after incubation with the cells. As shown in Fig. 9, no significant signs of toxicity were detected, even after an incubation time of 96h. The viability results higher than 80% for all the concentrations of iron administered, proved the feasibility of the materials for being used in biological applications.

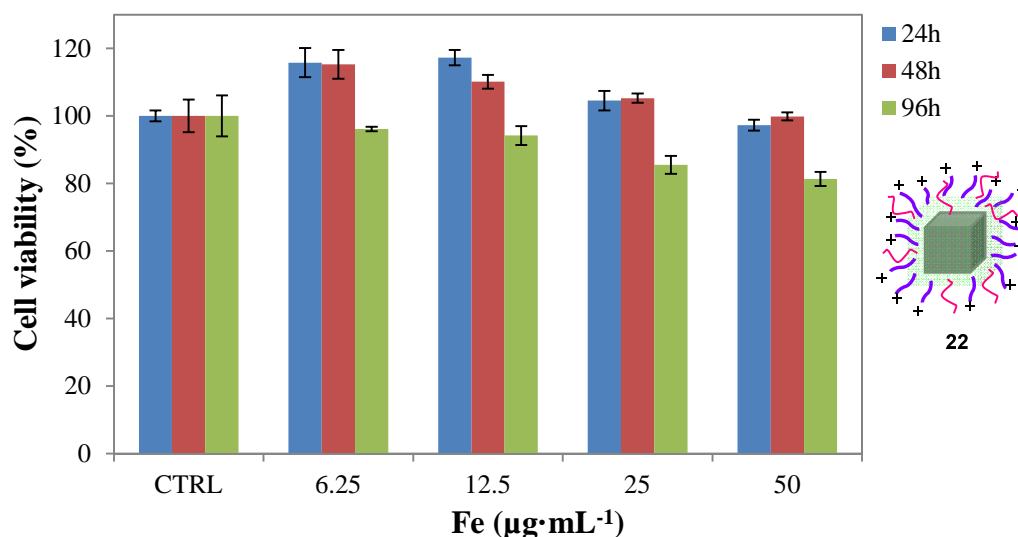


Fig. 9 HeLa GFP cell viability assessed by PrestoBlue for cationic Mn-cubes (**22**). Fe concentrations ranging from 6 up to 50 $\mu\text{g}\cdot\text{mL}^{-1}$, after 24, 48 and 96 hours of incubation, were analyzed. The percentage of viable cells is normalized with respect to the non-treated control cells.

Similarly, the cytotoxicity of cationic IONCs (**25**) was also studied. For this Ovarian-carcinoma cells (IGROV-I) were incubated with Fe concentrations from 6 to 50 $\mu\text{g}\cdot\text{mL}^{-1}$, for 24, 48 and 72h. In this case, IGROV-I cells which naturally overexpress epidermal growth factor receptor (EGFR) were used since they are also a good target for protein downregulation experiments due to the opportunity to delivery anti-EGFR siRNA. Again, no significant toxicity was noticed for all the concentrations tested, especially for the highest one, in which more than 80% of viability is still achieved after 3 days of incubation with the magnetic nanocubes.

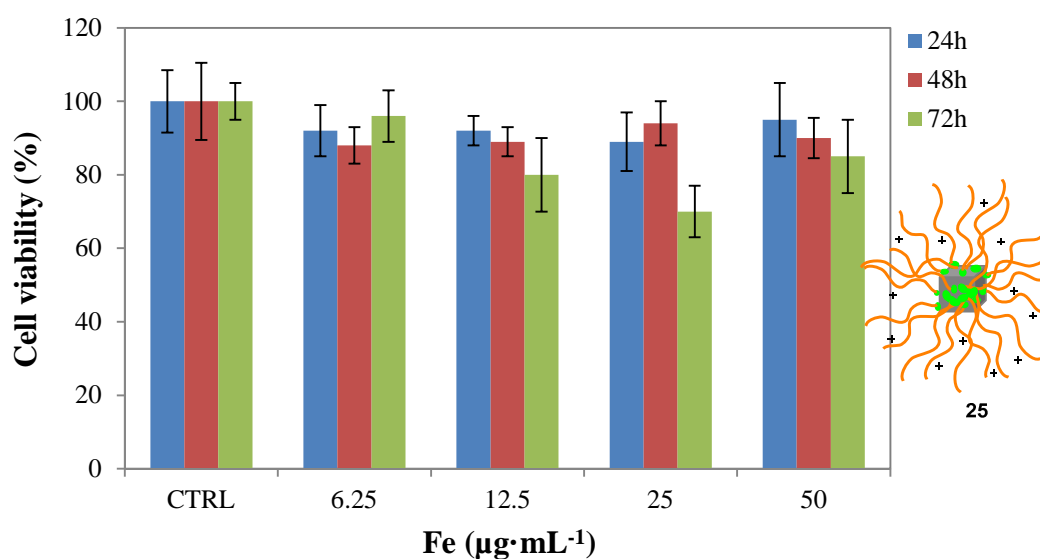


Fig. 10 IGROV-I cell viability accessed by PrestoBlue for cationic IONCs (**25**) at Fe concentrations ranging from 6 up to 50 $\mu\text{g}\cdot\text{mL}^{-1}$, after 24, 48 and 72 hours of incubation. The percentage of viable cells is normalized with respect to the non-treated control cells.

Generally, highly positive charged nanoparticles are associated with enhanced cytotoxic responses.⁴⁵ Indeed, cationic nanoparticles are known for causing more pronounced disruption of plasma membrane as well as stronger mitochondrial and lysosomal damage.⁴⁵ However, the interference of the nanoparticles on intrinsic cellular signaling pathways does not depend exclusively on surface charge but on a variety of factors, and it varies also with the type of cells used.⁴⁴⁻⁴⁶ In this case, the obtained results reveal that, despite the high positive charge of the particles, no real cellular damage is detected, most likely due to the presence of PEG molecules. Indeed, PEGylation is a well-known strategy to decrease cytotoxicity of the nanoparticles.^{30,45} Though, it has to be applied in a suitable manner because it affects as well the uptake of the materials and indeed it can lead to a reduction in the amount of nanoparticles internalized. Giving that the final efficacy of the nanoparticles as a delivery agent depends on the amount of particles which can be taken up by the cells, a compromise has to be found, in order to decrease cytotoxic effects but retaining the charge high enough to load the negative charged siRNA and ensure higher uptake by the cells.⁴⁴⁻⁴⁶

As shown before, the designed cationic Mn-cubes (**22**) and IONCs (**25**), present high surface charge, but they do not induce cytotoxic effects at the maximum iron dosage administered ($50 \mu\text{g}\cdot\text{mL}^{-1}$).

The performance of the nanocarriers for any biomedical studies, such as hyperthermia or delivery systems, strongly depends on the amount of nanocubes capable of entering the cells. Similarly to the cytotoxicity, the uptake depends also on the nanoparticles size, shape, composition and surface charge.⁴⁵ The intracellular uptake of the positive charged nanocubes was measured by administering an iron dosage of $50 \mu\text{g}\cdot\text{mL}^{-1}$ to HeLa GFP cells. After 24h of incubation, the Fe content internalized was measured by elemental analysis after digesting the cells in an acidic solution.

Both types of nanocrystals, cationic Mn-cubes (**22**) and IONCs (**25**), were taken up by the cells in comparable amounts which corresponds to about 14 and 12 picograms (pg) of iron per cell, respectively. By optical microscopy, (Fig. 11) one can observe the incorporation of the both kinds of NCs. Slight agglomeration is detected for Mn-cubes (**22**), although no signs of cytotoxicity are registered.

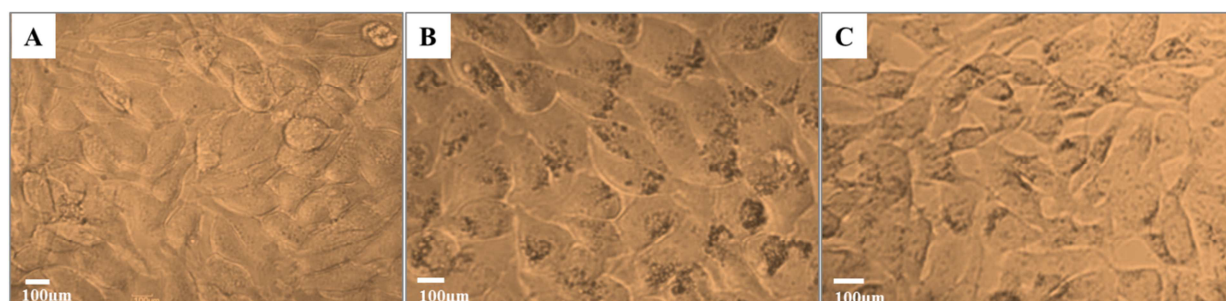


Fig.11 Optical microscope imaging of HeLa GFP cells exposed (24h) to cationic Mn-cubes (**22**) (**B**) and cationic IONCs (**25**) (**C**) at an iron content of $50 \mu\text{g}\cdot\text{mL}^{-1}$. (**A**) Control untreated HeLa GFP cells. The scale bar is $100\mu\text{m}$.

3.2.5 siRNA loading onto cationic nanocubes

The ability of the positive charged nanocarriers to complex siRNA was evaluated by agarose gel electrophoresis and photoluminescence (PL) measurements. For detection purposes, a siRNA sequence bearing a terminated a fluorescent marker (herein referred as Alexa488-siRNA) was chosen. For the loading, increasing amounts of siRNA were added (Table 1), while keeping fixed the amount of nanocubes at a Fe concentration of 25 μg . The volume of all solutions was adjusted to keep the concentration of Fe at 0.38 $\text{g}\cdot\text{L}^{-1}$

Table 1 Ratio of siRNA tested, keeping the amount of Fe constant at 25 μg for cationic cubes **22** and **25**.

Sample	Cationic Mn-cubes (22)			Cationic IONCs (25)					
	1	2	3	4	5	6	7	8	9
Ratio pmol siRNA / μg Fe	1	5	10	2	4	8	16	32	100

The reactions were mixed for 30 minutes, in RNase-free water. The formation of the conjugates is expected to happen simply by electrostatic interaction between the positive charged NCs and the negative charged siRNA molecules. To confirm it, after washing away unbounded siRNA molecules, the conjugates NCs-siRNA were loaded into a 1% agarose gel and the electrophoresis ran for 45 minutes at 100 V. The washing solutions were monitored by measuring the photoluminescence of the of free siRNA molecules. As shown in the two examples given in Fig. 12 it was found that two washing steps were sufficient to ensure the clearance of siRNA from the solution, resulting in a spectrum without the peak at 519 nm associated to the presence of Alexa488-siRNA.

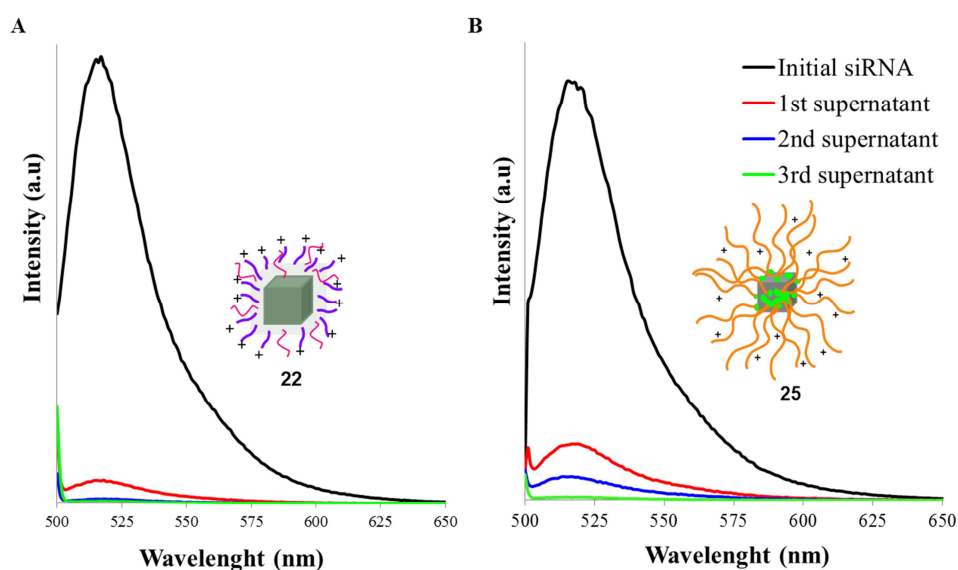


Fig. 12 Photoluminescence measurements (excitation wavelength: 495 nm) of the initial siRNA solution and the washing solutions after conjugation of siRNA with cationic nanocubes. Washing solutions from the conjugation of siRNA with (A) cationic Mn-cubes (**22**) and (B) with cationic IONCs (**25**).

After conveniently washed, one can see from the results obtained for the electrophoresis in Fig. 13 that both the materials have the ability to load siRNA given the presence of fluorescent siRNA molecules co-localized with the nanocubes bands in the gels. Although, there is a significant difference in the manner by which siRNA is loaded and complexed to the positive NCs. For instance, when applying the voltage for running the gel, the siRNA complexed with the cationic Mn-cubes (**22**) is detached from the magnetic materials, which remain inside the well, and runs along the gel in accordance with the control free siRNA molecules (see Fig. 13A). Oppositely, as shown in Fig. 13B, for all complexes formed using cationic IONCs (**25**) the siRNA remains in the well attached to the magnetic nanocubes. These results not only confirm the formation of the siRNA-loaded nanocubes for both nanocarriers but also reveal a very strong interaction, in the case of cationic IONCs (**25**). In fact, the siRNA does not segregate from the nanocubes even when applying the high voltage used to run the gel (100 V). Increasing the amount of siRNA (sample 9 in Fig.13B) one can detect loosely bounded molecules which start to detach from the IONCs and run accordingly to the free siRNA control, towards the positive pole. However, most of the genetic material remains attached to the nanocubes. This set of data suggests that for the cationic Mn-cubes (**22**) siRNA is adsorbed more on the surface of the cationic nanocubes by interacting with available tertiary amines, whereas for cationic IONCs (**25**) the siRNA is encapsulated inside the polymeric layer which is developed around the particles. Considering that an optimal nanocarrier must protect the siRNA from degradation when entering the cells, IONCs (**25**) might present a greater potential for the expect application since the siRNA molecules are not completely exposed to the surrounding environment.

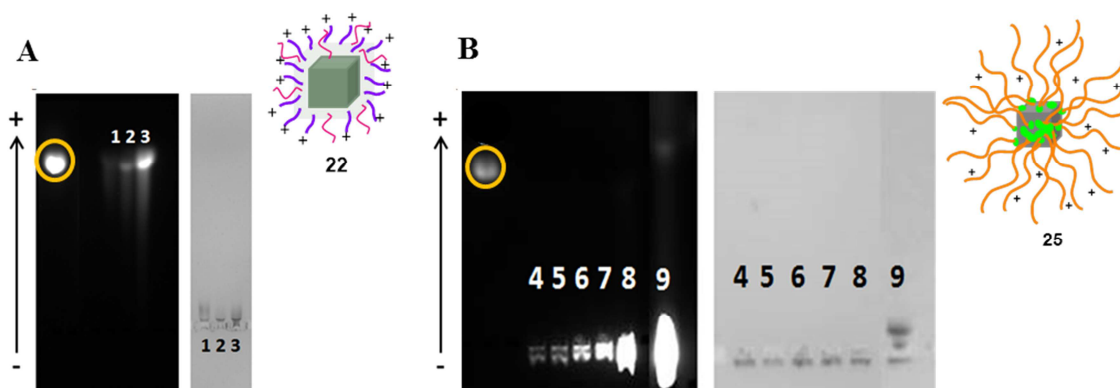


Fig. 13 Gel electrophoresis of NCs-siRNA conjugates for Mn-cubes **22** (A) and IONCs **25** (B). The gel was run at 100 V for 45 minutes. For number code see Table 1. The points highlighted with the yellow circles are the free siRNA molecules.

Once confirmed the loading of siRNA on the surface of the cationic NCs, by electrophoresis, a more detailed analysis was carried out to better understand the properties of the as-formed nanocarriers. Cationic Mn-cubes (**21**) showed a limited capacity for loading the siRNA cargo, losing the stability and precipitating already when using a ratio of 5 pmol siRNA to microgram of iron, as it is shown in Fig. 14A. This phenomenon might be attributed to the loss of electrostatic repulsion between

neighboring Mn-cubes (**22**) when partially “covered” with RNA molecules. Nevertheless, sample number 1 in Fig. 14A, having a ratio of 1pmol of siRNA per microgram of iron, was further characterized exhibiting good stability after conjugation with the genetic material as observed from the picture in Fig. 14A and the TEM micrographs in Fig. 14B. Additionally, the zeta potential on this sample reveals a decrease of the surface charge from +35 mV to +24mV due to the adsorption of the negatively-charged RNA on the surface.

In order to assess the amount of siRNA adsorbed onto cationic Mn-cubes (**22**) a different experiment using 2 pmol siRNA per microgram iron was performed. The total amount of siRNA adsorbed onto Mn-cubes (**22**) was roughly estimated by photoluminescence measurements of Alexa488-siRNA. The loading estimation was done by subtracting the signal of the remaining siRNA in solution, after loading magnetic decantation, to the signal of the initial siRNA solution used to form the conjugates, as reported by Curcio *et al.*³⁵ From the graphic depicted in Fig. 14C, 95 % of the siRNA binds to the nanocubes giving an overall loading of approximately 1.9 pmol siRNA per microgram of iron. Although it looks that saturation is not yet achieved, the concentration of siRNA could not be increased as this would compromise the stability of the cationic Mn-cubes (**22**) and lead to precipitation, as shown in Fig. 14A for sample 2 and 3.

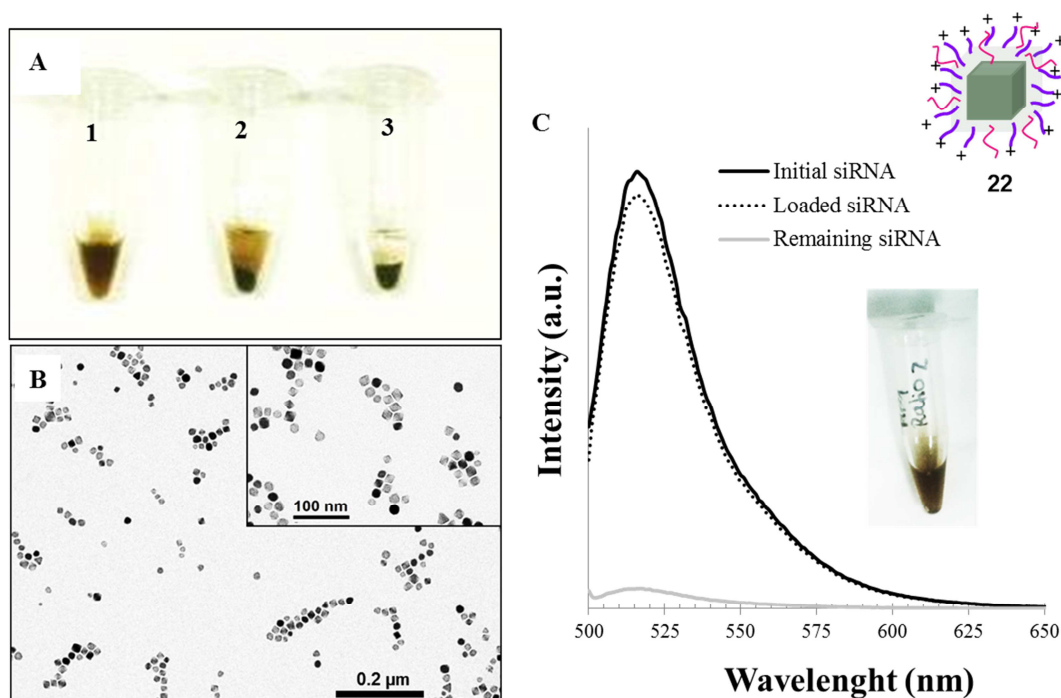


Fig. 14 A) Stability in solution of siRNA-NCs conjugates using cationic Mn-cubes (**22**). B) TEM image of the siRNA-NCs conjugates and C) PL spectra of siRNA solutions used to prepare the conjugates (excitation wavelength: 495 nm). The siRNA loaded was calculated from the difference of the remaining solution of siRNA (after performing 2 washing cycles with RNase-free water) when compared to the initial one, giving a loading of 95%. For this particular experiment 25 μg Fe were used to load 50 pmol of siRNA.

Differently, the positive charged cationic IONCs (**25**) can load much higher amounts of siRNA without losing the stability of the complex siRNA-NCs (Fig. 15). The formation of the conjugates and the increase in siRNA loaded was confirmed by zeta potential measurements (Fig. 15A). According to the obtained results, for the lowest ratios of siRNA studied, no significant difference in the surface charge was detected. This outcome confirms the hypothesis that the siRNA is encapsulated inside the polymeric shell rather than adsorbed on the surface. Oppositely, when the ratio of siRNA increases substantially one can see a decrease in surface charge, most likely due to the adsorption of siRNA on the surface of the nanocubes once the inner polymeric shell is saturated.

The loading of siRNA onto cationic IONCs (**25**) was also estimated by measuring the PL of the siRNA in solution.³⁵ In this case, 25 μg of Fe were reacted with 625 pmol siRNA (ratio of 5) revealing 75% of siRNA complexation to the nanocubes from the results obtained in Fig. 14B. From this data the loading saturation seems to be achieved at roughly 19 pmol siRNA per picogram of Fe, which is 10 times higher than the loading obtained for Mn-cubes (**22**).

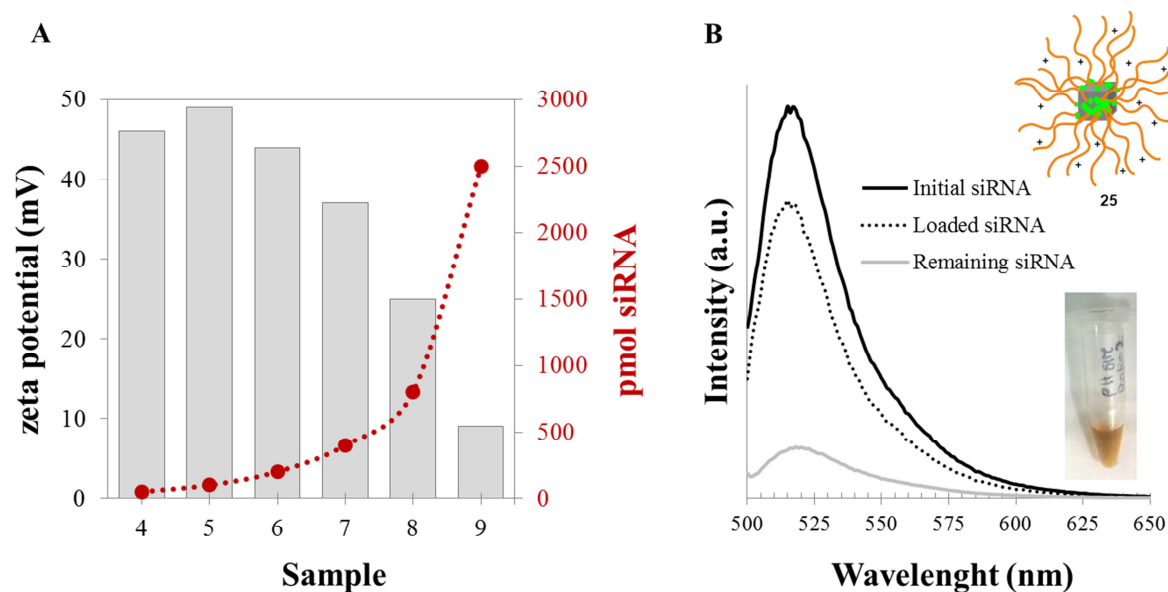


Fig. 15 **A**) siRNA-IONCs (**25**) conjugates charge variation (grey bars) in respect to the amount of siRNA used (red dashed line); **B**) PL spectra of siRNA in solution (excitation wavelength: 495 nm) before and after reaction with cationic IONCs (**25**). The amount of loaded siRNA was calculated from the difference of the initial and the remaining siRNA in solution after performing 2 washing cycles with RNase-free water.

From these data, given the fact that siRNA could successfully be loaded on for both cationic Mn-cubes (**22**) and IONCs (**25**) and considering their different behavior when loading the siRNA, the materials were then studied in a biological model for protein expression downregulation, and their potential for protecting and delivery the genetic material was compared.

3.2.6 GFP knockdown on HeLa cells using siRNA-NCs conjugates

In order to evaluate *in vitro* the transfection efficiency of the developed carriers, and thus understand the biological activity of the NCs- siRNA conjugates, HeLa GFP transfected cells were used as a model. Briefly, as shown in Fig. 16, the complexes were formed simply by mixing the positive NCs with siRNA for 30 minutes in reduced serum media Opti-MEM. Then, the as prepared conjugates with no further purification were administered to the cells and the culture was maintained for 96 hours, with a medium exchange after the first 24h of incubation. These conditions were chosen because by previous group work on the same cell line using other types of siRNA carrier vector, the most effective incubation time required for the silencing was found to be at 96h.³⁵

Lipofectamine® 2000, which is a well-known transfection agent, was used for comparison. A control containing only siRNA was also performed in order to confirm the incapability of transfection by the siRNA itself. After treating the cells for 96h the fluorescence of GFP protein was assessed by fluorescence activated cell sorting (FACS) which records the fluorescent signal of single cells. The results were normalized to the percentage of GFP signal measured for HeLa GFP non-treated cells (control).

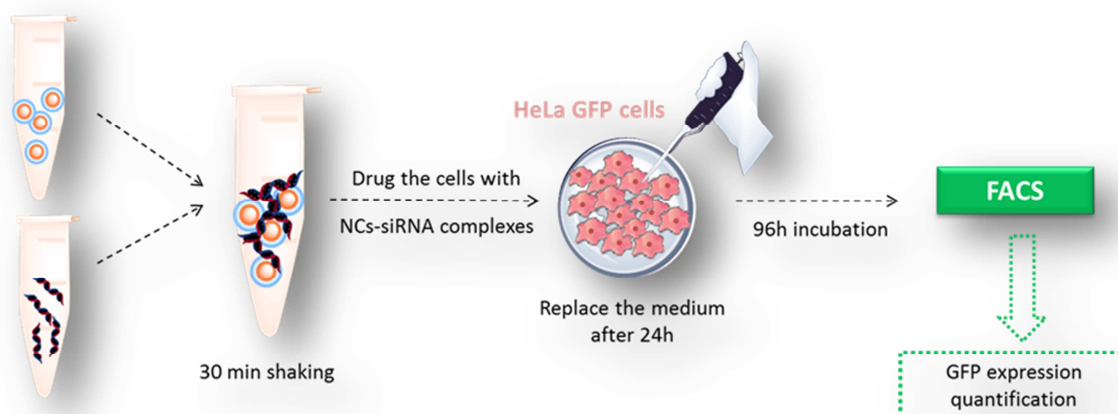


Fig. 16 Schematic protocol for the GFP knockdown analysis in HeLa cells. The culture was always done in 24-MW plate seeded with 10 000 cells one day before starting the incubation with the NCs.

Fig. 17 clearly shows the incapability of siRNA itself to penetrate the cell membrane, as stated before. Additionally, a control containing only cationic Mn-cubes (**22**) ($50 \mu\text{g}\cdot\text{mL}^{-1}$) was done, as a negative control, to ensure that the presence of the nanocarriers themselves, had no interference with the intrinsic detected cell fluorescence. For the siRNA-Mn-cubes (**22**) conjugates tested, a decrease in GFP expression was detected when increasing the amount of iron used to load the same amount of siRNA (250 nM). At the lower dosages of iron, little effect was noticed on the downregulation of GFP protein, which was estimated to be around 20%. Indeed, even at an iron administered dosage of

80 $\mu\text{g}\cdot\text{mL}^{-1}$ 30% of knockdown was registered. Although, regarding their cytotoxicity, the applicability of such materials is quite limited. From an iron concentration of 80 $\mu\text{g}\cdot\text{mL}^{-1}$ the effects on cell death were considerably high, reducing their potential for the desired application.

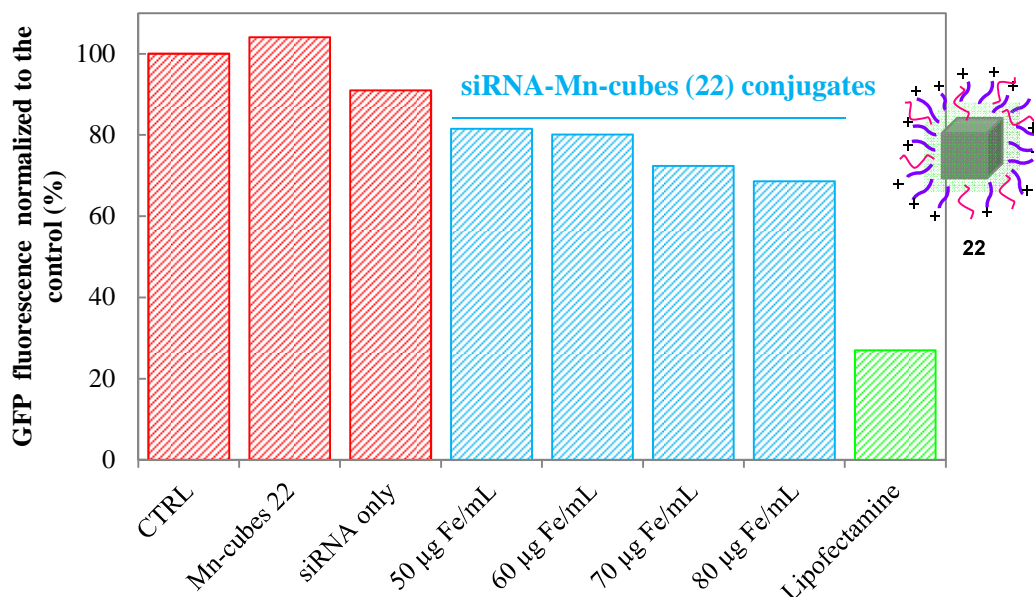


Fig. 17 FACS normalized data for GFP downregulation on HeLa cells using cationic Mn-cubes (**22**) as the nanocarriers for siRNA delivery. The red coloured bars represent the control for untreated HeLa GFP cells, NCs (**22**) only (50 $\mu\text{g}\cdot\text{mL}^{-1}$) and siRNA only; the blue bars represent the knockdown results obtained when using different concentrations of the conjugates siRNA_NC (**22**) to treat the cells; the green bar is the positive control performed with Lipofectamine. For all experiments, the concentration of siRNA was kept constant as 250 nM).

On the contrary, as revealed in Fig. 18 and Fig. 19, when cationic (**25**) were used to load the siRNA and subsequently treat the cells, 40 % of gene knockdown was achieved at the lowest level of Fe dosage (50 $\mu\text{g}\cdot\text{mL}^{-1}$) tested also for cationic Mn-cubes (**22**). Compared to the results discussed in Fig. 17 (for cationic Mn-cubes, **22**), for the same concentration of iron used (50 $\mu\text{g}\cdot\text{mL}^{-1}$) the efficiency of the RNAi therapy increases by a factor of 2 using cationic IONCs (**25**). Noteworthy, this downregulation occurred without cytotoxic side effects as it was shown before in Fig. 10. Moreover, the percentage of gene knockdown achieved was found to be directly related with the amount of materials used to treat the cells, as shown by the results obtained when using half the amount of the conjugates (25 $\mu\text{g}\cdot\text{mL}^{-1}$) in Fig. 18. Even though, lower percentage of knockdown was obtained comparing to the commercial available Lipofectamine, it is worth to note that siRNA loaded onto Lipofectamine is easily internalized via direct diffusion within the cell membrane and it is quite toxic, as described in previous studies.^{30, 35} On the contrary, the cationic-polymeric coated nanoparticles bind the plasma negatively-charged cellular membrane and are transported inside the cell via endosomal-lysosomal system. The presence of amines buffers H^+ and cause lysosomal Cl^- accumulation likely leading to osmotic swelling and lysis of endosomes, thereby preventing the degradation of the siRNA.

This mechanism has been reported for other types of pH-sensitive carriers and it would need a further microscopy cellular study to confirm it.³⁵

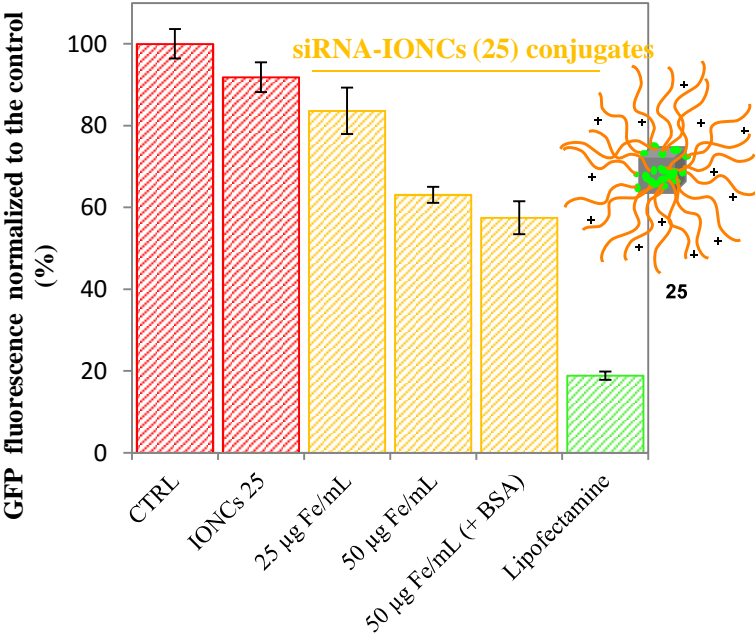


Fig. 18 FACS normalized data for GFP downregulation on HeLa cells using cationic IONCs (25) as the nanocarriers for siRNA delivery. The red bars represent the control for untreated HeLa GFP cells and cell treated with IONCs (25) only ($50 \mu\text{g}\cdot\text{mL}^{-1}$); the blue bars represent the knockdown results using conjugates siRNA_IONCs (25) as siRNA carriers; the green bar is the positive control performed with Lipofectamine.

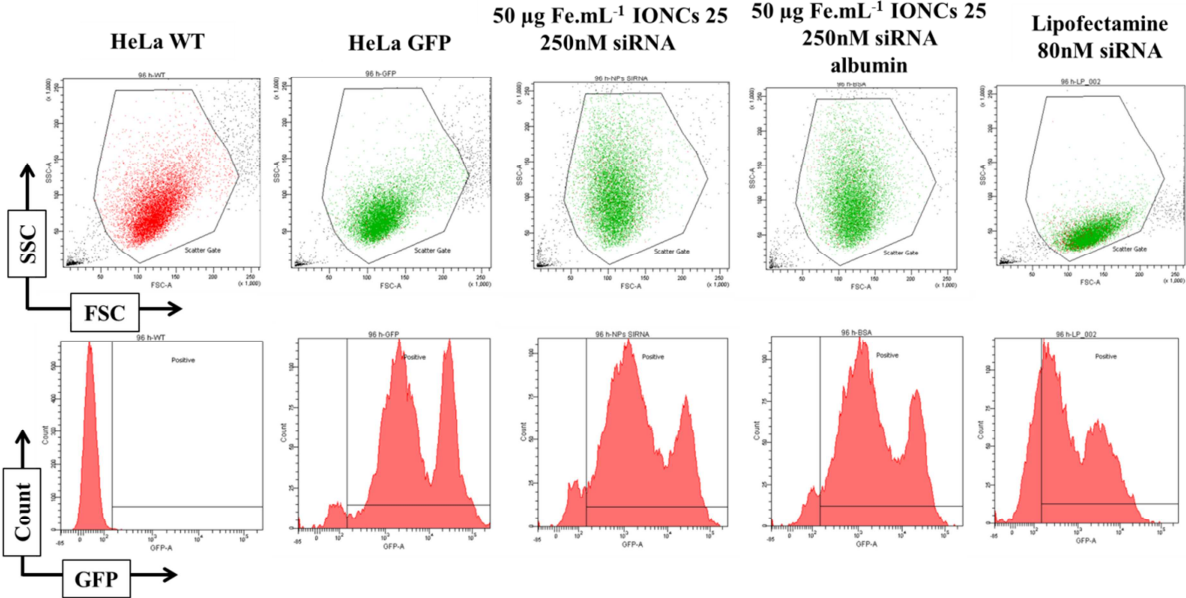


Fig. 19 FACS data for GFP downregulation on HeLa cells using cationic IONCs (25) as the nanocarriers for siRNA delivery.

The obtained results were in good agreement with the measured capacity of loading the siRNA. For cationic Mn-cubes (22) which can load a limited amount of siRNA, it was necessary to increase the

amount of Fe used to knockdown the GFP expression to a comparable extent when using the cationic IONCs (**25**). Moreover, the strongest interaction assumed for nanocarrier (**25**) and the siRNA, which is encapsulated in the polymeric shell, offers a better protection mechanism to avoid the degradation of the genetic material once in physiological environment. For this reason it would be also interesting to study the dissociation kinetics of the siRNA from the nanocubes in order to adapt the time of incubation and enhance the downregulation efficiency of the nanocarriers. The protective feature of these nanocarriers was confirmed by performing an additional experiment in which BSA was used to pre-coat the IONCs-siRNA conjugates before administration to the cells. This approach is reported for enhancing gene silencing effect by increasing cell uptake and protecting siRNA from degradation.⁴⁷⁻⁴⁹ However, the outcome downregulation percentage was comparable to the one observed when no BSA was used (see Fig. 18). This data corroborated the above stated assumption that the encapsulation of the siRNA inside the polymeric shell is enough to efficiently prevent its degradation. On the other hand having a protein serum, such as human albumin, absorbed on the siRNA/nanocarriers might better camouflage the carrier and thus enable a longer blood circulation time, with enhanced accumulation at the tumor. Additional tests by confocal imaging will be performed in the future in order to better understand the mechanism of nanocarrier uptake and siRNA release once inside the cell. Furthermore, the delivery efficiency will be also studied under a magnetic field, which has been reported to enhance the transfection efficiency by increasing the dosage of iron taken up by the cells.³⁰

3.3 Conclusions

Herein, I present the *in vitro* study of two potential nanocarriers for siRNA delivery. In the first part of this chapter, two different procedures were followed to obtain cationic water-soluble nanocubes. Cationic Mn-cubes (**22**) were prepared using manganese ferrite nanocubes which were transferred in water, functionalized and fully characterized to assess their heat performance, protein adsorption and colloidal stability. Cationic IONCs (**25**) were prepared starting from iron oxide nanocubes (**23**) that were already known to have optimal heat performance proving ideal candidates for combining heat-mediated siRNA delivery and magnetic hyperthermia.^{24,25,36} Both types of cationic nanocubes were successfully transferred in water without losing stability while presenting very high positive surface charge. This feature was required for complexing negatively-charged siRNA molecules. More specifically, cationic Mn-cubes (**22**) were obtained by first developing a polymeric coating around the as synthesized IONCs using the amphiphilic polymer PC18. This gives negatively water soluble Mn-PC (**21**) which are then further functionalized with DMEDA and PEG molecules for obtaining stable cationic Mn-cubes (**22**) (+30 mV). Differently, a new unpublished procedure was set by another member of the group to obtain highly cationic and stable IONCs (**25**) (+50 mV).

Then, in a second part of the project, a biological characterization of the magnetic nanocubes was done. Firstly, the nanocubes were tested for their stability in biological medium, by incubating them in

FBS containing media and confirming the positive influence of protein corona on their colloidal stability. Then, the different cationic NCs were tested on cell lines showing a high degree of internalization by HeLa GFP cells. Moreover, no cytotoxicity was found at an iron concentration range from 6 to 50 $\mu\text{g. mL}^{-1}$.

Finally, the last part of this work describes and compares the use of the cationic nanocubes as delivery tools of siRNA into cells by evaluating protein downregulation in HeLa GFP cells. In theory, the positive surface charge of these IONCs allows them to easily bind siRNA molecules by simple electrostatic interaction. This was confirmed for both cationic Mn-cubes (**22**) and cationic IONCs (**25**) by gel electrophoresis and photoluminescence measurements. Although significant differences were observed on the binding forces between the genetic material and the differently functionalized nanocarriers. Cationic IONCs (**25**) showed a much stronger interaction with siRNA, which is encapsulated inside the polymeric shell, when compared with cationic Mn-cubes (**22**), which adsorbs the siRNA on their surface. Indeed, in the latter case siRNA is more exposed to enzyme degradation. Additionally, the pH-responsive block DMAEMA³⁹ (from cationic IONCs, **25**) might prompt endosomal-lysosomal escape by reinforcing the proton sponge effect, preventing in a more efficient way lysosomal degradation.

In conclusion, a promising nanocarrier for siRNA delivery was developed. Noteworthy, this nanotool is able to ensure the three main requirements need for transfection applications. Cationic IONCs (**25**) composed of a copolymer of DMAEMA and OEGMEMA are (1) capable of loading the siRNA, (2) efficiently protect it against degradation and (3) release it into the cell cytoplasm for binding the RISC complex and finally interrupt specific protein's expression. However, further experiments must be carried out in order to increase the knockdown effect and understand how the siRNA is released and its mechanism of action once inside the cell. This study represents the proof of concept for using other siRNAs sequences against tumor targeting proteins (e.g. the anti-EGFR siRNA sequence to be tested on IGROV-I cells) as the next target in order to have a more relevant impact in gene therapy for cancer treatment.

3.4 Experimental section

Materials and methods

Unless specified, chemicals were purchased from Sigma-Aldrich and used as received without further purification. Poly (maleic anhydride-alt-1-octadecene), MW 20.000 - 25.000 was purchased from Polyscience. The HPLC purified α GFP-siRNA oligonucleotide (target sequence 5'-GCAAGCTGACCCTGAAGTTC-3') and siRNA modified at the 5'end of the sense stand with the AlexaFluor488 (target sequence 5'-GGCAAGCUGACCCUGAAGUUC-3') were purchased from Qiagen. Lipofectamine 2000 was purchased from Invitrogen. All suspensions for working with siRNA were diluted using RNase free milli-Q water (18.2 M Ω).

Preparation and characterization of cationic MnFe₂O₄ cubes by polymer coating and further functionalization of the polymeric shell

Water transfer by polymer coating of single MnFe₂O₄ NCs

MnFe₂O₄ NCs (**20**) were prepared accordingly to a non-hydrolytic wet-chemical protocol set up in our laboratory by another group member and not yet published. The as-synthesized MnFe₂O₄ NCs (**20**), with an average size of 13 ± 2 nm, were first transferred into water by using a previously reported method.^{21,22} Specifically, 1.28 mL of nanocubes in chloroform (0.2 μ M) were mixed with 6.3 mL of a 137 mM solution of amphiphilic PC18 in a total volume of 10 mL, keeping a ratio of polymer monomers per nm² of nanocrystal surface equal to 500. The solvent was slowly evaporated, overnight, inside the oven at 65°C under slow shaking. When solvent evaporation was completed, the nanocrystals formed a film that was re-dissolved in 15 mL of sodium borate buffer (50mM, pH 9) in an ultrasonic bath, until all the polymeric film was completely dissolved in the aqueous phase. The solution was then concentrated on a centrifuge amicon tube (cut off: 100 KDa Amicon, Millipore) and purified by ultracentrifugation to remove the excess of polymer in solution. The concentrated Mn-PC (**21**) were loaded on the top of a continuous sucrose gradient (20% - 40% -66%), at a maximum volume of 1 mL per tube and ultracentrifuged at 20000 rpm for 1h30, using a Beckman Coulter Optima LE-80 K ultracentrifuge equipped with a SW41 Ti rotor. During the ultracentrifugation, the NCs moved along the gradient until they reached a phase with comparable density while the polymer excess, which had a clear blue fluorescent signal under UV light, remained on top of the sucrose gradient (20%). Then, the nanocubes were collected with a syringe and washed in an amicon centrifuge tube, at 2500 rpm, to remove the sucrose. Depending on the batch of nanocubes, time and speed of ultracentrifugation needed to be slightly adjusted. To confirm the removal of the free polymer the NCs were loaded in a 1% agarose gel and the electrophoresis ran for 45-60 minutes at 100V. The analysis of the gel, under at 480 nm, provided a feasible measure of the successful removal of PC18 when no fluorescent band was detected on the front of the gel. The resulting water soluble magnetic nanocubes were also characterized by DLS, zeta potential and TEM for size, surface charge and morphology evaluation.

Hyperthermia measurements of Mn-PC (21)

To evaluate the SAR of Mn-PC (**21**) a commercially available DM100 Series (nanoScale Biomagnetics Corp.) set up was used. 300 μ L of IONCs in water, at a Fe concentration of 3 g.L⁻¹, were introduced into the sample holder and exposed to an AC magnetic field at two different frequencies (110 kHz and 300 kHz) and at three magnetic field amplitudes (12, 16 and 24 kA.m⁻¹). All reported SAR values and error bars were calculated from the mean and standard deviation respectively of at least four experimental measurements. SAR values were calculated according to the Equation 1 and taking into account only the first few seconds of the curve dT/dt. The specific heat capacity of the water is 4185 J.L⁻¹.K⁻¹.

Functionalization of the polymer shell of Mn-PC (21)

Once transferred to water, the Mn-PC (21) were further functionalized with DMEDA and monoamino-PEG by EDC chemistry on the exposed carboxylic groups on the polymeric shell. After optimizing the reaction conditions, a solution of 1 mL of Mn-PC nanocubes (21) ($0.5 \mu\text{M}$, 1.7 mg Fe) in borate buffer was reacted with an equal volume of DMEDA (1 mL, 100 mM, molar ratio DMEDA/NCs equal to 2×10^5), mono-amine-PEG molecules (750 Da, 1 mL, 100 μM , molar ratio PEG/NCs equal to 200) and 2M solution EDC (1 mL, molar ratio EDC/NCs equal to 2×10^6) in borate buffer. The mixture was shaken for 3h at room temperature. To remove the unreacted molecules several washes in Amicon centrifuge tubes were performed at no more than 2500 rpm, in RNase free water. Once again, the resulting cationic Mn-cubes (22) were analyzed for surface charge, size and morphology by zeta potential measurement, DLS and TEM respectively.

Electrophoretic characterization

Each sample was mixed with a solution of gel-loading buffer (Orange G and 30 % glycerol) corresponding to 20% of the total sample volume. Gel electrophoresis was done on 1% agarose gel for 45-60 minutes at 100V. The gel was observed in bright field or under 480 nm filter using a BIO-RAD Gel DocTM XR imaging system.

Dynamic light scattering measurements and zeta potential

The measurements were carried out using a Zeta Sizer Nano ZS90 (Malvern Instruments, USA) equipped with a 4.0 mW He-Ne laser operating at 633nm and Avalanche photodiode detector. At least three replicate measurements were made for each sample dissolved in water, at 25°C with the pH adjusted to 7.

Elemental analysis

The concentration of Fe was determined by elemental analysis using the inductively coupled plasma optical emission spectrometer (ICP-OES iCAP 6500, Thermo). The samples were digested in 3:1 HCl/HNO₃ (v/v) solutions.

Transmission electron microscopy

Conventional TEM images were obtained using JEOL JEM 1011 electron microscope, working with an acceleration voltage of 100 kV and equipped with a W thermionic electron source and a 11Mp Orius CCD Camera (Gatan company, USA). Samples were prepared by placing a drop of sample onto a carbon coated copper grid which was then left to dry before imaging.

Stability of the synthesized cationic nanocubes in FBS and physiological medium – interaction with serum proteins

The stability of the cationic nanocubes was assessed by pouring 100 µg Fe inside 1 mL of a 10% FBS aqueous solution and DMEM physiological medium, monitoring it visually during 24h to see if precipitation occurred. For that purpose pictures were taken every two hours for the first 6 hours of incubation and then again when 24h incubation was completed. The stability of the two types of cationic NCs (**22** and **25**) was compared with the unstable Mn-PC (**21**) monitored under the same conditions.

To better investigate the interaction with serum proteins, a SDS-PAGE analysis was done. For that, the nanocubes were incubated at a concentration of 0.2 mg Fe·mL⁻¹ in 10% FBS for 2h. Then, they were collected by centrifugation at 14000 rpm for 30 minutes. The pellet was re-suspended and washed in PBS three times through gentle pipetting to remove non-bounded proteins. After, the proteins were eluted by re-suspending the samples in sample buffer (containing 0.002% bromophenol blue, 10% sodium dodecyl sulfate, 5% β-mercaptoethanol and 30% glycerol) and denatured at 100°C for 5 minutes. The separation was done on a 12% polyacrylamide gel at 120 V. Control sample of FBS was prepared in the same way and loaded to the gel. Novex® Sharp Pre-stained Protein Standard from Invitrogen was used as a molecular ladder. The same volume of all samples was added to allow a direct comparison of the results. The gel was stained with comassie for one hour and after washed in destained solution for another hour followed by water overnight. Finally, it was analyzed using a BIO-RAD ChemiDOC™ MP equipment.

siRNA loading onto cationic nanocubes

The loading of Alexa488-labelled siRNA molecules on the positively charged NCs was done by simply mixing together the siRNA with the NCs. Different ratios of siRNA, reported in Table 2, were loaded on the nanocubes according to the following formula:

$$ratio = \frac{pmol\ siRNA}{\mu g\ Fe}$$

In a typical experiment, 25 µg Fe of NCs, previously washed with RNase-free milli-Q water, were used to react with different amounts of siRNA (see Table 2), keeping the iron concentration in solution at 0.38 g·L⁻¹. After 30 minutes shaking, the siRNA-loaded NCs were washed and analyzed by agarose gel (1%) electrophoresis (using a BIO-RAD ChemiDOC™ MP imaging system) and measured for size and charge determination at the DLS. In addition, since an Alexa488 tagged siRNA was used, the estimation of loaded siRNA was done by measuring its emission spectra at an excitation wavelength of 495 nm, using a Cary Eclipse Varian photoluminescence spectrometer.³⁵ The initial loading solution of siRNA and the final solution, which contains the non-bounded siRNA molecules after NCs collection by magnetic decantation, were analyzed. The loading efficiency was calculated by the difference of the fluorescent intensity peak at 519 nm of both solutions.

Table 2 Conditions tested for siRNA loading on the cationic NCs.

	Cationic Mn-cubes 22			Cationic IONCs 25					
Sample	1	2	3	4	5	6	7	8	9
$\mu\text{g Fe}$	25			25					
$\text{pmol siRNA} / \mu\text{g Fe}$	1	5	10	2	4	8	16	32	100
siRNA (pmol)	25	125	250	50	100	200	400	800	2500

Cellular studies for cationic nanocubes

Cell culture

HeLa (ATCC, UK) (here referred as HeLa WT) and IGROV-I cells (ATCC, UK) were cultured in DMEM (Gibco, UK) and RPMI-1640 (Gibco, UK), respectively, in T75 flasks. Both physiological media were supplemented with 10% Inactivated Fetal Bovine Serum (FBS), 1% Penicillin Streptomycin (PS) and 1% Glutamine at 37 °C, in 95% humidity and 5% CO₂. Cells were split every 3-4 days before reaching 90 % confluence.

GFP over-expressing HeLa cells (HeLa GFP) were obtained by lipofectamine transfection of pAcGFP1-N1 vector (ClonTech). After three days of transfection the cells were treated with neomycin antibiotic at increasing concentrations until 1mg·mL⁻¹ to select the positive GFP over-expressing cells. This cell line was grown in the same conditions described for HeLa Wild Type (WT) with the addition of 10% G418 disulfate salt solution (50 mg·mL⁻¹ in H₂O, Sigma Aldrich) to the complete DMEM culture medium.

Cytotoxicity by PrestoBlue

For testing cell viability PrestoBlue (PB) assay was used according to the manufacturer's protocol (Invitrogen, Carlsbad, CA, USA). HeLa GFP cells were seeded in a 24 multiwell plate, 24 hours before starting the nanocubes exposure treatment at the following cell densities: 5x10⁴, 3x10⁴ and 1x10⁴. Then, the cells were incubated with cationic Mn-cubes (**22**) and the cytotoxicity assessed at 24, 48 and 96 h. IGROV-I were plated at 10x10⁴, 6x10⁴ and 3x10⁴. After letting the cells adhere in the bottom of the well for a day, a Fe dose of 50 $\mu\text{g}\cdot\text{mL}^{-1}$ of cationic IONCs (**25**) was added to the media and incubated for 24, 48 and 72 h, at 37°C. After the incubation time was complete, the medium was exchanged by a 10% solution of PB reagent in complete DMEM, and the cells incubated for additional 2h at 37 °C with 5% CO₂. The cell viability was detected by reading the absorbance for each well at 570 and 600 nm. All the values for the different nanocubes conditions were normalized with respect to the cell viability values obtained for not treated cells (control).

Intracellular Fe uptake

HeLa GFP cells were seeded, at a concentration of 12×10^4 cells per well, in 12 multiwell plate one day before the experiment, and incubated at 37°C with 5% CO_2 . 24 hours after, the adherent cells were treated with cationic NCs (**22**) and (**25**) dissolved in $800\mu\text{L}$ of complete DMEM at an iron concentration of $50\ \mu\text{g}\cdot\text{mL}^{-1}$. After 24h of incubation at 37°C , the cells were washed with PBS three times, trypsinized/detached and centrifuged. The pellet was re-suspended in 1mL of complete fresh medium. Then, the cells were counted, centrifuged again and the obtained pellet digested in Aqua Regia overnight. The acidic solution was diluted with water and the intracellular Fe concentration determined by ICP-OES. For the imaging of the internalized nanocubes, a Motic AE31 inverted microscope equipped with a Moticam 2500, in a True-color phase contrast mode, was used to acquire cell images.

GFP knockdown on HeLa cells using siRNA-NCs conjugates

For the siRNA downregulation assay, HeLa GFP cells (1×10^4) per well were seeded in 24 multiwell plates, in $500\mu\text{L}$ of complete DMEM, one day before the injection of the magnetic nanocubes. Immediately before starting the treatment, $\alpha\text{GFP-siRNA}$ was loaded on the magnetic nanocubes by simply mixing the two components. An iron amount ranging from $25\text{-}100\ \mu\text{g Fe}$, depending on the experiment, was reacted with $125\ \text{pmol}$ of siRNA in Opti-MEM reduced serum media (Gibco, UK). For the formation of the conjugates the nanocubes concentration was maintained at $0.38\ \text{g}\cdot\text{L}^{-1}$ of iron. After shaking for 30 minutes, the as-prepared conjugates were administered to the cells at iron dosages of $50\text{-}200\ \mu\text{g}\cdot\text{mL}^{-1}$ and siRNA concentration of 250nM , adjusting the total volume to $500\mu\text{L}$ with complete DMEM. After 24h incubation, the medium was exchanged and the culture maintained for 72h more, thus completing a total incubation time of 96h. As a positive control, $1.5\mu\text{L}$ of Lipofectamine 2000 (Invitrogen) was used to load $125\ \text{pmol}$ of siRNA, in Opti-MEM[®], by shaking it 15 minutes, and then given to the cells at a total concentration of 250nM siRNA per well. Once the 96h of culture were finished, the medium was collected, the cells washed once with PBS and detached from the growing substrate by trypsinization. After washing two times in $500\ \mu\text{L}$ of PBS, the cell pellet was re-suspended in $200\ \mu\text{L}$ of PBS and analyzed 2-3h later by FACS (FACSARIAII, BD). FACS is a specialized flow cytometry method which provides a fast, objective and quantitative recording of fluorescent signals from individual cells. Particularly for this application, the cell suspension enters a narrow rapid stream flow which is arranged in such a way that forces the passage of single cells per droplet. Each droplet is crossed by a laser light source giving information on the granularity and size of the cells, as well as the fluorescent characteristic of each single cell. FACS analysis was performed on the following samples: (1) non-fluorescent wild-type HeLa, (2) untreated HeLa GFP (control), and HeLa GFP treated with (3) $\alpha\text{GFP-siRNA}$ alone ($250\ \text{nM}$), (4) siRNA-Lipofectamine, (5) cationic nanocubes (**22**) and (**25**) alone, (6) siRNA-NCs (**22**) and (7) siRNA- IONCs (**25**) conjugates. The fluorescent signal of each cell suspension tested was normalized with respect to the result obtained for HeLa GFP untreated cells.

3.5 References

1. Dykxhoorn, D. M.; Palliser, D.; Lieberman, J. *Gene Therapy* **2006**, 13, (6), 541-552.
2. Kanasty, R.; Dorkin, J. R.; Vegas, A.; Anderson, D. *Nature Materials* **2013**, 12, (11), 967-977.
3. Choi, K. Y.; Silvestre, O. F.; Huang, X.; Hida, N.; Liu, G.; Ho, D. N.; Lee, S.; Lee, S. W.; Hong, J. I.; Chen, X. *Nature Protocols* **2014**, 9, (8), 1900-1915.
4. Fujita, Y.; Takeshita, F.; Kuwano, K.; Ochiya, T. *Pharmaceuticals* **2013**, 6, (2), 223.
5. Bumcrot, D.; Manoharan, M.; Kotliansky, V.; Sah, D. W. Y. *Nature Chemical Biology* **2006**, 2, (12), 711-719.
6. Petrocca, F.; Lieberman, J. *Journal of Clinical Oncology* **2011**, 29, (6), 747-754.
7. Green, J. J.; Langer, R.; Anderson, D. G. *Accounts of Chemical Research* **2008**, 41, (6), 749-759.
8. Ma, D. *Nanoscale* **2014**, 6, (12), 6415-6425.
9. Castanotto, D.; Rossi, J. J. *Nature* **2009**, 457, (7228), 426-433.
10. Tseng, Y.-C.; Mozumdar, S.; Huang, L. *Advanced Drug Delivery Reviews* **2009**, 61, (9), 721-731.
11. Whitehead, K. A.; Langer, R.; Anderson, D. G. *Nature Reviews Drug Discovery* **2009**, 8, (2), 129-138.
12. Gujrati, M.; Malamas, A.; Shin, T.; Jin, E.; Sun, Y.; Lu, Z.-R. *Molecular Pharmaceutics* **2014**, 11, (8), 2734-2744.
13. Oliveira, A. C. N.; Raemdonck, K.; Martens, T.; Rombouts, K.; Simón-Vázquez, R.; Botelho, C.; Lopes, I.; Lúcio, M.; González-Fernández, Á.; Real Oliveira, M. E. C. D.; Gomes, A. C.; Braeckmans, K. *Acta Biomaterialia* **2015**, 25, 216-229.
14. Buchman, Y. K.; Lellouche, E.; Zigdon, S.; Bechor, M.; Michaeli, S.; Lellouche, J.-P. *Bioconjugate Chemistry* **2013**, 24, (12), 2076-2087.
15. Burnett, J. C.; Rossi, J. J.; Tiemann, K. *Biotechnology Journal* **2011**, 6, (9), 1130-1146.
16. Abbasi, S.; Paul, A.; Prakash, S. *Cell Biochemistry and Biophysics* **2011**, 61, (2), 277-287.
17. Malek, A.; Merkel, O.; Fink, L.; Czubayko, F.; Kissel, T.; Aigner, A. *Toxicology and Applied Pharmacology* **2009**, 236, (1), 97-108.
18. Inoue, Y.; Kurihara, R.; Tsuchida, A.; Hasegawa, M.; Nagashima, T.; Mori, T.; Niidome, T.; Katayama, Y.; Okitsu, O. *Journal of Controlled Release* **2008**, 126, (1), 59-66.
19. Kozielski, K. L.; Tzeng, S. Y.; Hurtado De Mendoza, B. A.; Green, J. J. *ACS Nano* **2014**, 8, (4), 3232-3241.
20. Sokolova, V.; Epple, M. *Angewandte Chemie International Edition* **2008**, 47, (8), 1382-1395.
21. Widder, K. J.; Senyei, A. E.; Ranney, D. F. *Adv Pharmacol Chemother* **1979**, 16, 213-271.
22. McBain, S. C.; Yiu, H. H. P.; Dobson, J. *International Journal of Nanomedicine* **2008**, 3, (2), 169-180.

23. Lu, A.-H.; Salabas, E. L.; Schüth, F. *Angewandte Chemie International Edition* **2007**, 46, (8), 1222-1244.
24. Guardia, P.; Di Corato, R.; Lartigue, L.; Wilhelm, C.; Espinosa, A.; Garcia-Hernandez, M.; Gazeau, F.; Manna, L.; Pellegrino, T. *ACS Nano* **2012**, 6, (4), 3080-3091.
25. Guardia, P.; Riedinger, A.; Nitti, S.; Pugliese, G.; Marras, S.; Genovese, A.; Materia, M. E.; Lefevre, C.; Manna, L.; Pellegrino, T. *Journal of Materials Chemistry B* **2014**, 2, (28), 4426-4434.
26. Deka, S. R.; Quarta, A.; Di Corato, R.; Riedinger, A.; Cingolani, R.; Pellegrino, T. *Nanoscale* **2011**, 3, (2), 619-629.
27. Chomoucka, J.; Drbohlavova, J.; Huska, D.; Adam, V.; Kizek, R.; Hubalek, J. *Pharmacological Research* **2010**, 62, (2), 144-149.
28. Mattingly, S. J.; O'Toole, M. G.; James, K. T.; Clark, G. J.; Nantz, M. H. *Langmuir* **2015**, 31, (11), 3326-3332.
29. Bruns, O. T.; Ittrich, H.; Peldschus, K.; Kaul, M. G.; Tromsdorf, U. I.; Lauterwasser, J.; Nikolic, M. S.; Mollwitz, B.; Merkel, M.; Bigall, N. C.; Sapra, S.; Reimer, R.; Hohenberg, H.; Weller, H.; Eychmuller, A.; Adam, G.; Beisiegel, U.; Heeren, J. *Nature Nanotechnology* **2009**, 4, (3), 193-201.
30. Boyer, C.; Priyanto, P.; Davis, T. P.; Pissuwan, D.; Bulmus, V.; Kavallaris, M.; Teoh, W. Y.; Amal, R.; Carroll, M.; Woodward, R.; St Pierre, T. *Journal of Materials Chemistry* **2010**, 20, 255.
31. Pan, B.; Cui, D.; Sheng, Y.; Ozkan, C.; Gao, F.; He, R.; Li, Q.; Xu, P.; Huang, T. *Cancer Research* **2007**, 67, (17), 8156-8163.
32. Wang, X.; Zhou, L.; Ma, Y.; Li, X.; Gu, H. *Nano Research* **2010**, 2, (5), 365-372.
33. Di Corato, R.; Quarta, A.; Piacenza, P.; Ragusa, A.; Figuerola, A.; Buonsanti, R.; Cingolani, R.; Manna, L.; Pellegrino, T. *Journal of Materials Chemistry* **2008**, 18, (17), 1991-1996.
34. Quarta, A.; Curcio, A.; Kakwere, H.; Pellegrino, T. *Nanoscale* **2012**, 4, (11), 3319-3334.
35. Curcio, A.; Marotta, R.; Riedinger, A.; Palumberi, D.; Falqui, A.; Pellegrino, T. *Chemical Communications* **2012**, 48, (18), 2400-2402.
36. Park, J. K.; Jung, J.; Subramaniam, P.; Shah, B. P.; Kim, C.; Lee, J. K.; Cho, J.-H.; Lee, C.; Lee, K.-B. *Small (Weinheim an der Bergstrasse, Germany)* **2011**, 7, (12), 1647-1652.
37. Rosensweig, R. E. *Journal of Magnetism and Magnetic Materials* **2002**, 252, 370-374.
38. Hergt, R.; Dutz, S. *Journal of Magnetism and Magnetic Materials* **2007**, 311, (1), 187-192.
39. Tayo, L. L.; Venault, A.; Constantino, V. G. R.; Caparanga, A. R.; Chinnathambi, A.; Ali Alharbi, S.; Zheng, J.; Chang, Y. *Journal of Applied Polymer Science* **2015**, 132, (32), n/a-n/a.
40. Sakulkhu, U.; Mahmoudi, M.; Maurizi, L.; Coullerez, G.; Hofmann-Antenbrink, M.; Vries, M.; Motzacker, M.; Rezaee, F.; Hofmann, H. *Biomaterials Science* **2015**, 3, (2), 265-278.
41. Wiogo, H. T. R.; Lim, M.; Bulmus, V.; Yun, J.; Amal, R. *Langmuir* **2011**, 27, (2), 843-850.

42. Pelaz, B.; del Pino, P.; Maffre, P.; Hartmann, R.; Gallego, M.; Rivera-Fernández, S.; de la Fuente, J. M.; Nienhaus, G. U.; Parak, W. J. *ACS Nano* **2015**, 9, (7), 6996-7008.
43. Aires, A.; Ocampo, S. M.; Cabrera, D.; Cueva, L. d. l.; Salas, G.; Teran, F. J.; Cortajarena, A. L. *Journal of Materials Chemistry B* **2015**, 3, (30), 6239-6247.
44. Hauck, T. S.; Ghazani, A. A.; Chan, W. C. W. *Small* **2008**, 4, (1), 153-159.
45. Fröhlich, E. *International Journal of Nanomedicine* **2012**, 7, 5577-5591.
46. Arvizo, R. R.; Miranda, O. R.; Thompson, M. A.; Pabelick, C. M.; Bhattacharya, R.; Robertson, J. D.; Rotello, V. M.; Prakash, Y. S.; Mukherjee, P. *Nano Letters* **2010**, 10, (7), 2543-2548.
47. Kummitha, C. M.; Malamas, A. S.; Lu, Z.-R. *International Journal of Nanomedicine* **2012**, 7, 5205-5214.
48. Yogasundaram, H.; Bahniuk, M. S.; Singh, H.-D.; Aliabadi, H. M.; Uluda; #x1e7; , H.; Unsworth, L. D. *International Journal of Biomaterials* **2012**, 2012, 10.
49. Piao, L.; Li, H.; Teng, L.; Yung, B. C.; Sugimoto, Y.; Brueggemeier, R. W.; Lee, R. J. *Nanomedicine: Nanotechnology, Biology and Medicine* **2013**, 9, (1), 122-129.

List of abbreviations

AcOH	acetic acid
AFS	atomic fluorescence spectroscopy
ATR-IR	attenuated total reflection infrared
BCN	((1R,8S,9s)-bicyclo[6.1.0]non-4-yn-9-yl)methyl 4-nitrophenyl carbonate
CNTs	carbon nanotubes
Co/C	carbon-coated cobalt nanoparticles
CTAB	cetyltrimethylammonium bromide
CuBr ₂	copper bromide
DCM	dichloromethane
DLS	dynamic light scattering
DMA	dimethylacetamide
DMAEMA	(dimethylamino)ethyl methacrylate
DMEDA	N,N'-dimethylethylenediamine
DMEM	Dulbecco's Modified Eagle's Medium
DMF	dimethylformamide
DMSO	dimethylsulfoxide
DNA	deoxyribonucleic acid
DOPA BiBA	dopamine 2-bromoisobutyramide
DVS	divinyl sulfone
EDC	1-ethyl-3-(3-dimethylaminopropyl)carbodiimide
equiv.	equivalent
Et ₃ N	triethylamine
EtOH	ethanol
FACS	fluorescence activated cell sorting
FBS	fetal bovine serum
G2	second generation
GFP	green fluorescent protein
H ₂ SO ₄	sulfuric acid
HCl	chloridric acid
HeLa	human cervical carcinoma cell line
HNO ₃	nitric acid
ICP-OES	inductively coupled plasma optical emission spectrometry
IGROV-I	ovarian-carcinoma cells
IONCs	iron oxide nanocubes

IONPs	iron oxide nanoparticles
i-PrOH	isopropanol
MACS	magnetically assisted chemical separation
Me ₆ TREN	tris[2-(dimethylamino)ethyl]amine
MNPs	magnetic nanoparticles
MRI	magnetic resonance imaging
mRNA	messenger RNA
M _s	saturation magnetization
MWCNTs	multiwalled carbon nanotubes
NCs	nanocubes
IONCs	iron oxide nanocubes
NMP	<i>N</i> -Methyl-2-pyrrolidone
OEGMEMA	oligoethylene glycol methyl ether methacrylate
Opti-MEM	reduced serum Modified Eagle's Medium
PAMAM	poly(amidoamine)
PB	presto blue
PBS	phosphate-buffered saline
PC18	poly(maleic anhydride <i>alt</i> -1-octadene)
PEG	polyethylen glycol
PEI	polyethylenimine
PL	photoluminescence
RISC	RNA-induced silencing complex
RNA	ribonuclei acid
RNAi	RNA interference technology
RPMI	Roswell Park Memorial Institute medium
SAR	specific absorption rate
SDS-PAGE	sodium dodecyl sulfate polyacrylamide gel electrophoresis
siRNA	small interfering RNA
SPIONs	superparamagnetic iron oxide nanoparticles
TEM	transmission electron microscopy
TEOS	tetraethyl orthosilicate
TGA	termogravimetric analysis
THF	tetrahydrofurane
UB	ultrasonic bath
UV	ultraviolet light
XPS	x-ray photoelectron spectroscopy

Curriculum Vitae

Soraia Margarida da Silva Teixeira Fernandes

Date of birth: 27-05-1989

Nationality: Portuguese

Email: Soraia.margarida.fernandes@gmail.com

Education

02.2013 - 01.2016	PhD in the Marie Curie Initial Training Network - Mag(net)icFun
04.2015 - 01.2016	PhD project with <i>Dr. Teresa Pellegrino</i> (Italian institute of technology, Genova)
03.2015	Internship at NOVARTIS with <i>Dr. Peter Meier</i> (Basel, Switzerland)
02.2013 - 02.2015	PhD project with <i>Prof. Oliver Reiser</i> (University of Regensburg, Germany)
21.10.2013 - 31.10.2013	Secondment at the group of <i>Prof. Wendelin Stark</i> (ETH, Zurich)
09.02.2015 - 13.02.2015	Secondment at the group of <i>Prof. Yurii G'unko</i> (Trinity College, Dublin)
2012	Master degree in Bioengineering - Biomedical engineering
02.2012 - 07.2012	Master thesis in the group of <i>Prof. José Domingos dos Santos</i> (University of Porto, Portugal)
02.2011 - 07.2011	Erasmus period with <i>Prof. Elzbieta Pamula</i> (AGH University of Science and Technology, Poland)
09.2009 - 02.2012	Advanced studies in Biomedical engineering
09.2007 - 08.2009	Studies in Bioengineering (University of Tras-os-Montes e Alto Douro, Portugal)

List of publications

- *Synthesis of functionalized, dispersible carbon-coated cobalt nanoparticles for potential biomedical applications*

Kainz, Q. M.; **Fernandes, S.**; Eichenseer, C. M.; Besostri, F.; Korner, H.; Muller, R.; Reiser, O. *Faraday Discussions* 2014, 175, 27-40.

- *Reversible magnetic mercury extraction from water*

Fernandes, S.; Eichenseer, C. M.; Kreitmeier, P.; Rewitzer, J.; Zlateski, V.; Grass, R. N.; Stark, W. J.; Reiser, O. *RSC Advances* 2015, 5, (58), 46430-46436.

- *Novel cerium doped glass-reinforced hydroxyapatite with antibacterial and osteoconductive properties for bone regeneration*

Morais, D. S.; **Fernandes, S.**; Gomes, P. S.; Fernandes, M. H.; Sampaio, P.; Ferraz, M. P.; Santos, J. D.; Lopes, M. A.; Hussain, S. H. *Biomedical Materials* 2015, 10, (5), 055008.

- *Synthesis of Thermo-responsive Iron Oxides Nanoparticles with High Specific Absorption Rates as Platform for Cancer Treatment*

Than Binh Mai *et al.* – manuscript in preparation.

Conferences and workshops

- 20-22 of February, 2013 - Magnifico workshop, Barcelona. Poster contribution: “Magnetic nanoparticles as recyclable supports for synthesis, purification and biomedical applications.”
- 22-24 of February, 2013 - Mag(net)icFun kick-off meeting, Barcelona. Oral presentation: “Carbon-coated cobalt magnetic nanoparticles for biomedical applications”.
- 02-03 of September, 2013 - Mag(net)icFun workshop, ETH Zurich. Oral presentation: “Magnetic nanoparticles for biomedical applications”.
- 02-04 of June, 2014 – Mag(net)icFun mid-term meeting, IIT Genoa. Oral contribution: “Dual covalent / non covalent functionalized carbon coated nanoparticles for biomedical applications”.
- 19-20 of June, 2014 - Marie Skłodowska-Curie Conference, ESOF 2014. Copenhagen. Contribution: Poster contribution: “Magnetic Nanoparticles as Recyclable Support for Catalysis and Scavengers for Water Treatment”.
- 17-19 of September, 2014 - Faraday Discussion 175: Physical Chemistry of Functionalised Biomedical Nanoparticles. Bristol, UK.

- 27-28 of October, 2014. Mag(net)icFun workshop, University of Regensburg. Oral presentation: “Co/C magnetic nanobeads as: a) antimicrobial nanobeads and b) supports for enzyme immobilization and further use in catalysis”.
- 23-24 of March, 2015. Mag(net)icFun workshop, Univeristy of Keele. Oral presentation: “Magnetic enzymes for biodiesel production; Surface functionalization of Co/C magnetic nanobeads for chemical applications”.
- 16-20 of August, 2015 - ACS Meeting. Boston. Oral contribution: “Biodiesel production using magnetic-lipase”.
- 21.09.2015 - Nanomedicine Symposium CEN@Regione Lombardia. Milano
- 03-04 of March, 2016 - Mag(net)icFun workshop, Trinity College Dublin. Oral presentation: “Magnetic nanoparticles as carriers for siRNA delivery into cells”.

Professional References

Prof. Dr. Oliver Reiser
 Institut für Organische Chemie
 Universität Regensburg, Universitätsstr. 31
 93053 Regensburg, Germany
 oliver.reiser@ur.de

Dr. Teresa Pellegrino
 Istituto Italiano di Tecnologia
 via Morego 30, Genoa,
 16163 Italy
 teresa.pellegrino@iit.it

Dr. Peter Meier
 Novartis International AG
 Postfach
 CH-4002 Basel
 Schweiz
 peter.meier@novartis.com

Acknowledgments

I would like to show my gratitude to everyone that somehow contributed or made part of this work during the last three years.

- **University of Regensburg**

First of all, for the tutoring and interesting discussions throughout my doctoral work I thank my supervisor Prof. Dr. Oliver Reiser. I am thankful also for his support and encouragement for all the collaborations I did abroad during my PhD.

For preparation and characterization of the materials I would like to thank Dr. Peter Kreitmeier for the synthesis of aziridin, Joachim Rewitzer for the ICP-OES measurements, Dr. Rainer Muller for the TGA analysis, Prof. Dr. Josef Zweck for the TEM analysis and Helmut Koerner for the SQUID characterization.

I need to thank also Antje Weigert for the help with all the bureaucracy and advice for specific personal situations.

I must show my gratitude to Dr. Quirin Kainz for the help he gave me in the beginning of my PhD to get the knowledge necessary to work with magnetic nanoparticles.

For proofreading any parts of this thesis I am grateful to Dr. Roland Linhardt and Martin Hofmann (Jimmy). A special thanks to Jimmy also for the countless times that he helped me on work related issues. I know I was annoying sometimes but you also know that's part of the deal! You don't get to have my friendship just for the good things! But also for the great ones!

For providing a cheerful environment at the workplace I thank all my colleagues from the organic chemistry department at the UR, in particular Francesca, Lu, Jimmy, Sharom, Roland, Nanaji, Paul, Matze, Benni, Daniel Rackl, Berni, Roxy, Mischo, Viktor, Okun and Carina. To all of you thanks for the great moments!

I am also grateful to my flat mate Lamprini who was always supportive during the difficult periods and very pleasant during the good times. I had a really great time with you!

- **Istituto Italiano di Tecnologia**

For the guidance and supervision during the 10 months of PhD work at the IIT, I am grateful to Dr. Teresa Pellegrino who provided interesting topics of research and fruitful discussions.

For helping on the materials synthesis and analysis I must thank Simone Nitti and Giammarino Pugliese for the synthesis of the nanocubes, Thanh Binh Mai for the preparation of some samples and Filippo Drago for the ICP analysis (Grazie mille Pippo!). I thanks also to Dr. Alberto Curcio for showing me essential techniques and procedures to carry out my work at the IIT.

Thanks also to Iulia Manolache Orlatan for the great help with both bureaucratic and personal issues.

For proofreading of any parts of this thesis I am grateful to Dr. Tommaso Avellini, Dr. Alessia Petrelli, Dr. Maria Elena Materia and Marco Cassani.

A special thanks to Marco, Graziella, Alessia, Maria Elena, Tommaso, Filippo, Simone, Francesco, Niccolò, Carmine, Markus, Aidin, Giammarino and Gabriele for making our workplace so hospitable and stimulating. Thanks for all the help I got from you guys workwise and most importantly thanks for your friendship. I really enjoyed the time we spent together! C'è già la saudade!

I could not finish without leaving a special word also to my very good friends Irene and Nawid with whom I have lived wonderful moments in Genoa!

- **NOVARTIS, Basel**

I am grateful to Dr. Peter Meier for giving me the possibility to work with him during my internship period at NOVARTIS. It was really a pleasure to share science in such a friendly and welcoming environment.

- **ETH, Zurich**

For allowing me to use their facilities and perform essential tests of a part of my work there I thank Dr. Robert Grass and Prof. Dr. Wendelin Stark. Thanks also to my colleague Vladimir Zlateski for the help given to handle the equipment and perform the experiments.

- **TCD, Dublin**

For letting me use his laboratories and equipment to get important data for this work I thank Prof. Dr. Yurii G'unko as well as my colleague Raquel Serrano for helping me in the studies I performed there.

- **Financial support**

For the financial support I am thankful to the Marie Skłodowska-Curie actions, in particular to the EU-ITN network Mag(net)icFun in which this PhD work was developed.

For being always by my side in the most stressful period of this work I am really thankful to Marco Cassani. Even though you came along in my life just in the last period of this journey, you were one of the most supportive and influent persons at the conclusive phase of this work. Thanks for being so patient and most of all for encouraging me when motivation was lost! Grazie per esserci...

A very special thanks to Francesca Besostri for all the time we spent together. Thanks for supporting me even in the moments that I could not stand myself! Thanks for the extra baggage of motivation you gave me anytime I needed it. It was not always easy but somehow together we made it through the end. She was my nearest pillar for everything and my best mate for the good moments. Thanks for the great time we had together and most of all thanks for your friendship!

Last but not least I want to show my gratitude to the most important people of all: my family! Without them this work would have never been possible. For all the comprehension, patient and love I am grateful to my parents who have always encouraged me to follow my ideas and supported my decisions. Thanks for all the trust you deposited on me! Thanks also to my brother and sister for the admiration shown along these years. Vocês foram sem dúvida a maior motivação que poderia ter para a realização deste trabalho e é a vocês que o dedico em primeiro lugar! Obrigada por tudo família!

Um muito obrigada a todos que de alguma forma contribuíram para o desenvolvimento deste trabalho direta ou indiretamente, sem esquecer obviamente todos os meus amigos e familiares não referidos anteriormente.

Declaration

Herewith I declare that the present thesis is a presentation of my original doctoral work. Wherever contributions from others are involved all of them are clearly marked with reference to the literature, licence and acknowledgment of collaborative research.

Regensburg, 11 April 2016

Soraia Fernandes